Experimental Investigation & Data-Driven Modeling of Mechanical Properties of Particulate Polymer Composites

Thesis submitted for the award of the degree of

Doctor of Philosophy

by

Aanchna Sharma

भारतीय प्रौद्योगिकी संस्थान जम्मू
INDIAN INSTITUTE OF TECHNOLOGY JAMMU
विद्याधनं सर्वधन प्रधानम्

Department of Civil Engineering

Indian Institute of Technology Jammu

Jammu-181221

September 2022

Declaration

I hereby declare that the matter embodied in this thesis entitled **"Experimental Investigation & Data-Driven Modeling of Mechanical Properties of Particulate Polymer Composites"** is the result of investigations carried out by me in the Department of Civil Engineering, Indian Institute of Technology Jammu, India, under the supervision of Dr. Vinod Kushvaha, Assistant Professor, Indian Institute of Technology Jammu and it has not been submitted elsewhere for the award of any degree or diploma, membership etc. In keeping with the general practice in reporting scientific observations, due acknowledgements have been made wherever the work described is based on the findings of other investigators. Any omission that might have occurred due to oversight or error in judgment is regretted. A complete bibliography of the books and journals referred in this thesis is given at the end of the thesis.

September, 2022

Aanchna Sharma (2018RCE0035)
Indian Institute of Technology Jammu

I dedicate this thesis to my late brother, Dixant Sharma who has always been my constant source of inspiration and motivation, and played a very significant role in shaping me into the person that I am today.

Abstract

Particulate polymer composites are an emerging class of composites that have many potential applications in aerospace, automotive, marine and electronic industries due to the synergistic combination of mechanical characteristics like high strength and lightweight. These composites are of great interest because of the manufacturing ease and their macroscopically isotropic nature. The industrial applications demand for prior knowledge of the fracture and fatigue behaviour due to the inherent brittle nature of these composites. The nature of the particulate fillers such as the geometric properties (size, and shape), volume fraction, filler dispersibility and interfacial bonding significantly influence the stress distribution within the composite. Additionally, the crack growth of such composites is loading rate-dependent. Therefore, for the appropriate use of these materials in various engineering applications, understanding the effect of the mentioned parameters on ultimate mechanical response of the resulting particulate polymer composite is critical.

In this view, this thesis is divided into three major parts where the first part of the thesis is dedicated to develop a machine learning based predictive modeling framework to predict the dynamic fracture toughness of glass-filled epoxy composites with limited experimentation. Two computationally efficient and reliable artificial neural network models are developed to individually predict the effect of filler aspect ratio and loading rate on the dynamic fracture toughness of these composites.

Further, in the second part, the developed predictive model has been appended with an efficient framework of uncertainty quantification for the investigation of stochastic effects. Three different shapes of glass particles are considered including rod, spherical and flaky shapes with coupled stochastic variations in aspect ratio, dynamic elastic modulus and volume fraction. An artificial neural network based surrogate assisted Monte Carlo simulation is carried out to quantify the uncertainty and sensitivity associated with the dynamic fracture toughness of composites under dynamic impact. This study reveals that the pre-crack initiation time regime shows the most prominent effect of uncertainty. Additionally, rod shape and the aspect ratio are the most sensitive filler type and input parameter respectively for characterizing dynamic fracture toughness.

Furthermore, to ensure the structural integrity of the components involving the usage of these composites, the last part of this thesis presents a comprehensive experimental investigation of the crack initiation behavior and the progressive failure of these composites under cyclic loading. Here the particulate polymer composites are prepared by reinforncing the epoxy matrix by rod-shaped glass particles in a volume fraction of 0% (neat epoxy), 5%, 10% and 15%. This study has suggested that the particulate fillers act as crack nucleation sites that result in coalescing the micro-cracks developed at the filler-matrix interface and within the filler itself. Epoxy composite with 10% volume fraction of rod-shaped glass fillers is found to exhibit the maximum fatigue life under the applied loading.

Acknowledgements

Praise to the Almighty for granting me the capability to successfully complete this research work.

I would like to express my sincere gratitude to my Ph.D. supervisor, *Dr. Vinod Kushvaha*, Assistant Professor, Department of Civil Engineering, IIT Jammu, India for his constant guidance and motivation. I am grateful to him for his dedication, deep intereset, meticulous scrutiny, timely advice and scholarly instruction. Also, I profusely thank *Dr. Tanmoy Mukhopadhyay*, Assistant Professor, Department of Aerospace Engineering, IIT Kanpur, India for his scientific perspective and invaluable research feedback. Further, I extend my gratitude to the members of my research committee, *Dr. Rahul Salunkhe* and *Dr. Rimen Jamatia* for their constructive feedback and encouragement. The financial support received from the Ministy of Education (MoE) India during the entire Ph.D. is gratefully acknowledged.

I am deeply grateful to the technical staff in the central workshop specially *Mr. Arun*, *Mr. Naveen*, *Mr. Arul* and *Mr. Mayur* who have helped me immensly for machining the fabricated samples. My sincere thanks also goes to *Dr. G. Balaganesan* for providing me the opportunity to work at the Composite Technology Center, IIT Madras and gave me the access to the research facilities there.

I would like to offer my special thanks to my colleagues and friends, special mention to *Sudhanva Kusuma Chandrashekhra* for all the stimulating discussions and the constant encouragement.

Lastly, I would like to thank my family who is accountable for setting up the pillars on which my working persona is based. I am deeply grateful to my parents, *Mr. Dinesh Sharma* and *Mrs. Nindu Sharma* for their unwavering love, support and belief in me. A heartfelt thanks for always being so empathetic and patient with me.

I can not close these acknowledging remarks without expressing deep reverence and recognition to my parents-in-law, *Mr. Suneel Gupta* and *Mrs. Shobha Gupta* who believed in me throughout this journey. Their blessings and hope in me have been the constant source of optimism and enthusiasm throughout my research period. I feel extremely glad to offer a deep and sincere appreciation to my spouse, *Mr. Naman Gupta* for standing by me through all my travails, my absences, my fits of pique and impatience. A heartfelt gratitude for the constant support, understanding, care and cheering.

Table of contents

List of figures

List of tables

List of abbreviations

PPC	Particulate polymer composite
CNT	Carbon nano tube
SIF	Stress intensity factor
DIC	Digital image correlation
SEM	Scanning electron microscopy
FEM	Finite element method
ANN	Artificial neural network
ANFIS	Adaptive neuro fuzzy inference system
ML	Machine learning
RoI	Region of interest
LCF	Low cycle fatigue
MCS	Monte carlo simulation
DOS	Degree of stochasticity
PDF	Probability density function
MAPE	Mean absolute percentage error
UTS	Ultimate tensile strength
SiC	Silicon carbide

List of symbols

K_{IC}	Critical stress intensity factor in mode-I/fracture toughness
G_{IC}	Fracture energy
µm	Micronmeter
s	Second
µs	Micro-second
mm	Millimeter
GPa	Giga Pascal
MPa	Mega Pascal
KN	Kilo Newton
Hz	Hertz
R	Strain ratio
AR	Aspect ratio
V_f	Volume fraction
t	Time
E_d	Dynamic elastic modulus
LR	Loading rate
C_s	Shear wave speed
C_l	Longitudinal wave speed
%	Percentage
R^2	Coefficient of determination

Chapter 1

Introduction

Modern industrial applications demand for multi-functional nature of the materials to be used to have the advantage of synergistic properties that are easily tailorable and achieve the desired performance. Polymer composites are found to have many such muti-functional charecteristics like high strength, lightweight, corrosion resistance, thermal insulation, acoustic damping along with aesthetic features. Additionally, it is also advantageous in terms of rapid and easy manufacturing process. Generally, polymer composite is made of two phases: the matrix phase (continuous) and the reinforcement phase (dispersed). Usually, a thermosetting or thermoplastic organic polymer serves as the matrix, the basic purpose of which is to bind the reinforcement and transfer the load uniformly to the embedded reinforcement. Different types of materials are used to strengthen the polymeric matrix and are known as reinforcing agents. These materials can be in the form of natural or man-made fibers, particles, whiskers and fragments. When in the polymeric matrix, reinforcements are provided in the form of particles, the resulting composite is known as the Particulate Polymer Composite (PPC). Alumina, silica, zirconia, mica, carbon etc. are a few examples of particulate fillers which are used to reinforce the polymeric matrix. The principal advantage of these particulate polymer composites lies in the fact that they are structurally simpler, easy to manufacture and macroscopically isotropic [1].

The excellent mechanical properties and high resistance to corrosion of fiber reinforced polymer composites make them a suitable material to be used by the marine and medical industry. Due to their high specific strength and impact resistance, these materials have also found applications in wind turbine blades and aircraft components. Particulate polymer composites are relatively at a nascent stage and are presently being utilized in medical, marine, automotive and electronic industries. These composites are extensively used by the electronic packaging industry wherin particle reinforced epoxy composites are used to reduce the thermal expansion. Some of the examples are the chip scale packages, ball grid arrays and flip chip on board assemblies that make use of thermoset polymers filled with different inorganic particles to enhance their working consistency by improving the mechanical and thermal properties. Figure 1 is an illustration of some of the applications where particulate polymer composites are extensively used.

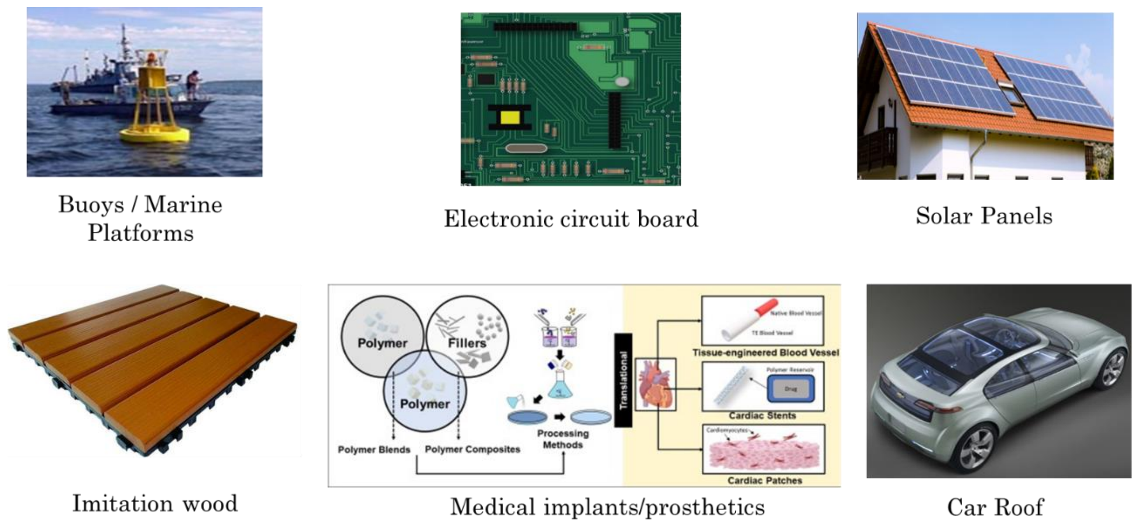

Figure 1 Applications of particulate polymer composites

1.1 Background

Epoxy resin is one of the most widely used thermoset polymers for manufacturing polymer composites owing to it's high specific strength, low shrinkage and great adhesion properties. However, it has a brittle nature and lacks damage tolerance which is a critical attribute for advanced engineering applications. This adversely affects the resistance of the resulting composite material to crack growth. A secondary phase is usually introduced in the epoxy matrix to improve the strength, stiffness and the overall mechanical behaviour of the composite. Dispersing particles of different sizes, shapes and stiffness in the epoxy matrix is the most common and economical way of improving it's mechanical properties. In real life applications, structural members are exposed to different loading conditions, ranging from static to highly transient which significantly impact the material's mechanical behaviour specially in terms of crack-growth. Resistance to crack growth is governed by the fracture toughness and material's response to dynamic loading is of prime importance in aerospace, automotive and defense industries. Therefore, studying the material deformation in terms of fracture toughness under loading conditions where inertial effects play a significant role is a critical research area. In addition to this, material's response to different loadings is strain rate sensitive. The failure mechanisms that a material undergoes in response to the rapidly changing loads are very different and complex compared to the deformation process observed under quasi-static loading conditions. Time varying loads are one of the main reason for the material failure in different components. Fatigue is one such phenomena where load changes with respect to time in a cyclic manner and leads to a progressive failure at stresses lower than the ultimate tensile strength of the material. Hence, it is crucial to investigate the effect of adding particulate fillers in epoxy resin on the fracture and fatigue properties of the resulting composite.

1.2 Motivation and challenges

Shape, size, chemical composition, and the amount of the particulate reinforcement added along with its degree of dispersion are the key parameters that greatly affect the overall resulting properties of the composite material [2]. Another influencing parameter on the mechanical behaviour of composite materials is the residual stress and strain [3]. Stress transfer from the continuous phase to the dispersed phase is a very important phenomenon that critically affects the strength and stiffness of the composites [4].

Therefore for the appropriate use of these materials in various engineering applications, understanding the effect of the mentioned parameters on the macromechanical properties such as stiffness, strength and toughness of the resulting composite is critical. As mentioned in the previous section, studying the aspect of fracture toughness under dynamic loading conditions holds great importance. A fairly good amount of investigation in this regard has been done by many researchers on the conventional fiber reinforced composites [5–11]. However, a very limited literature is available for such investigations on the particulate polymer composites. An adequate and proper knowledge of strength, toughness and crack initiation is very much essential for exploring the possible applications of PPCs. Therefore the present work bridges this gap and provides a deeper insight into the fracture and fatigue behaviour of PPCs.

Also, it is important to study the combined effect of all the process parameters (mentioned earlier) to explore the broader efficacy of such composites, so that an optimized material design can be achieved. However, modeling the complex relationships between the governing parameters is extremely strenuous. Despite the availability of large experimental setups and computational tools, it is laborious and time-consuming to investigate the significance of each of the governing parameters experimentally. For instance, determining the fracture toughness of composites under dynamic loading conditions involves a very complex experimental setup based on stress wave propagation. Also, considering the multiphase nature of polymer composites, conventional modeling techniques require too much of computational effort.

In this view, the approach of machine learning can be effectively used to build predictive models and determine the significance of the process parameters for an optimal design [12–15]. It provides a wider scope for efficiently investigating the behaviour of resulting composites with limited experimentation or computationally intensive realizations of expensive models. Exploitation of different machine learning algorithms have resulted in unprecedented insights and exploration of the composite properties beyond the capability of traditional computational and experimental analyses.

The fact that modeling complex phenomena like fracture toughness of such composites under dynamic loading conditions is theoretically demanding but holds a large practical relevance, has motivated us to make tangible contribution by developing a reliable and computationally efficient framework to predict the same.

1.3 Objectives

Though there is a plethora of literature on the mechanical characterization and application of other types of composites, studies concerning PPCs are very limited despite its favorable properties reported in some initial studies. Also, the scope of development of high performance composite using particulate fillers remains unexplored due to the limited data on fracture and fatigue properties of PPCs. In addition to that, a realistic analysis and design framework for particulate composites should account for the possible uncertainties considering the multiphase nature of the PPCs. Moreover, the unavoidable variation in process parameters due to the varying physical properties of matrix and reinforcement, degree of polymerization, environmental conditions and filler dispersion can significantly affect the ultimate response of PPCs. To ensure the accurate assessment of the ultimate composite performance and to avoid the deviation from the expected material behaviour, uncertainty quantification is another critically important aspect.

Based on the introduction and the brief discussion above, the objectives of this research are:

1. Predictive modeling of glass-filled polymer composites for determining the dynamic fracture toughness with limited experimentation and its validation.

2. Uncertainty quantification of the dynamic fracture toughness of particulate polymer composites.

3. To examine the robustness of the predictive model and evaluate the effect of individual or joint contribution of the parametric uncertainties on the model response.

4. Experimental investigation of fatigue response of glass filled epoxy composites and exploring the plausible applications.

1.4 Organization of thesis

The subsequent chapters are outlined as follows:

Chapter 2 presents the state of the art that gives an idea of previous research done in this area. Chapter 3 discusses the methodology adopted for developing predictive models of glass-filled polymer composites for determining the dynamic fracture toughness with limited experimentation. Also, the influence of aspect ratio and loading rate on the dynamic fracture toughness of the composites is highlighted. Chapter 4 presents a machine learning based uncertainty quantification approach to quantify the stochastic variability in the dynamic fracture toughness of glass-filled epoxy composites due to the inevitable random stochasticity in the material and geometrical properties. Also, to quantitatively characterize the importance of each input parameter along with the consideration of parametric interactions, a global sensitivity analysis is presented. Chapter 5 presents the experimental findings of the crack initiation and propagation study performed on glass filled epoxy composites under cyclic loading. A detailed description of material fabrication is also given in this chapter. Chapter 6 summarizes the contributions, conclusions and the future scope.

Chapter 2

State of the art

For any material to be utilized in the engineering applications, fracture and fatigue are two very critical attributes. Specially for particulate polymer composite which is the material of interest in this research, it is imperative to investigate the behaviour of PPCs in fracture and fatigue owing to its brittle nature. The relative ease in the manufacturing of these composites at lower cost has motivated researchers to study the mechanical properties of PPCs. However, most of these investigations unfold the behaviour of these composites under quasi-static loading conditions but the studies concerning the dynamic responses of PPCs are very limited. Some of the reported literature in this context is discussed in subsequent sections.

2.1 Fracture toughness

Dittanet et al. [16] studied the effect of particle size on the toughening mechanisms of PPCs. They used epoxy composites filled with nano-silica particles in a size range of 23-170 nm and used a single-edge notch bend test to determine the fracture toughness of the composite material. This study indicated that the addition of nano-silica particles improved the fracture toughness but the particle size did not have any significant effect on its toughness. Another research group [17] studied the fracture toughness of CNT reinforced epoxy composites under quasi-static and dynamic loading conditions. It was found that the critical stress intensity factors were improved after performing a non-ionic surface treatment on the CNT fillers. Sandeep et al. [18] prepared a hybrid composite by adding micron-sized alumina particles in the glass fiber reinforced epoxy composite and evaluated it for the fracture toughness using a single-edge notch bend test. As a result, an enhancement was observed in alumina-filled epoxy composites in terms of mode-I stress intensity factor. Kawaguchi et al. [19] investigated the static fracture toughness of epoxy filled with three different types of glass particles. They treated the surface of each glass filler and examined the effect of moisture exposure on the fracture toughness of epoxy composite. Microscopic studies were performed and it was observed that due to the surface treatment of glass fillers, the matrix-filler adhesion was affected. One of the interesting findings of this study was that in the case where poor adhesion was observed due to the surface treatment, exposure to moisture resulted in improved fracture toughness. In another study [20], izod impact test was performed on composites prepared by reinforcing hollow glass beads in the polypropylene matrix. The impact strength of the composite was found to increase with increase in the volume fraction of glass beads upto 15%. The main reason for this improvement was suggested to be the shear yielding of the polymeric matrix around the glass fillers. The nature of the fillers such as the geometric properties (size, and shape), volume fraction, filler dispersibility and interfacial bonding significantly influence the stress distribution within the composite [21–24].

Determining the fracture toughness under dynamic loading conditions is typically achieved by using a drop tower, split Hopkinson pressure bar or gas gun setup [25–27]. The onset of crack propagation is captured using a high-speed camera and a technique known as digital image correlation (DIC) is often used to determine the parameters of dynamic fracture [28]. Jajam and Tippur [26] conducted a study to compare the effects of nano and micron-sized silica particles on the static and dynamic fracture toughness of epoxy composites. The test setup of three point bending and drop tower was used to measure the quasi static and dynamic fracture toughness of the composites respectively. While the static measurement of fracture toughness (K_{IC}) was straightforward, dynamic measurement involved the correlation of deformed and undeformed images captured with a high speed camera using the technique of DIC. This correlation was done to compute the in-plane displacement components which were further used to extract the mode-1 stress intensity factor histories. It was found that irrespective of the filler scale, the fracture toughness was improved with the particle reinforcement in the epoxy matrix under both the loading conditions. However, under dynamic loading, micron-sized fillers showed more improvement in the fracture toughness compared to the nano-sized fillers while the nano fillers performed better under the quasi-static loading conditions.

One more research group [29] investigated the fracture toughness of rubber filled polymer composites under quasi-static and dynamic loading conditions. Dynamic fracture toughness was characterized using a new experimental approach wherein the magnetic field is generated using a magnetic impulse installation and converted into mechanical loading. In this study, data was obtained in terms of crack length corresponding to the applied pulse amplitudes. Specific fracture energy was found to be higher in dynamic process compared to the quasi-static loading conditions. In another study [30], the effect of filler size and the filler-matrix interfacial strength on the dynamic fracture toughness of epoxy composites was investigated. In this study, spherical glass particles of different sizes (7-200 µm) were used with two different interfacial strengths. Interferograms were used to extract the information regarding the stress intensity factor and the crack velocity. Reinforced epoxy samples showed higher dynamic fracture toughness compared to the unfilled ones corresponding to both the interfacial strength conditions. The effect of the particle size was found to be more prominent in the case of weakly bonded fillers. There are a few more studies that indicate that the size, shape and interfacial strength of the reinforcing agents play a major role in deciding the dynamic fracture toughness of PPCs [31–38]. Bie et al. [39] studied the effect of strain rate on the dynamic fracture toughness of CNT reinforced epoxy composites. They used three different types of multi-walled CNT (randomly dispersed, functionalized and pristine) to reinforce the epoxy matrix and subjected the resulting composite to a loading of very high strain ($10^5 – 10^6$ /s). The highest fracture toughness was exhibited by the functionalized CNT filled epoxy composites owing to the underlying failure mechanisms. A few more studies also suggest that increasing strain rate results in increasing value of fracture toughness for different PPCs [2,40–42].

A detailed experimental investigation was performed by Kushvaha and Tippur [43] to qualitatively characterize the effect of using different shapes and volume fraction of glass particles on the dynamic fracture toughness of epoxy composites. The setup of gas-gun based long bar impactor was used to experimentally simulate the fracture of composite samples under dynamic loading conditions. The composite samples were prepared by reinforcing rod, flake and spherical shaped glass fillers in the epoxy matrix, each in a volume fraction of 5, 10 and 15%. Different pulse shapers were used during the experiment to control the rate of dynamic loading. DIC was used to measure the fracture parameters and comparison of fracture toughness was made between the neat epoxy and the reinforced samples. Epoxy reinforced with rod-shaped fillers was found to exhibit the highest crack initiation toughness followed by flake and spherical fillers. Another finding was that with increasing loading rate an increased fracture toughness was observed. This study holds a great significance as it forms the basis of the current research work. While it is evident that such elaborate investigations are done experimentally, there is a huge need of developing a reliable computational model to reduce the experimental effort.

2.2 Computational methods

Various researchers have relied on computational methods to evaluate or predict the mechanical properties of different PPCs to get a hint of their application potential while reducing the experimental effort. Hutar et al. [44] modelled a polypropylene based particulate composite as a three phase system (matrix, particle and the interphase) and predicted the overall response of the composite in terms of stiffness. Another research group [45] also made use of a Finite Element Model (FEM) to predict the flexural properties of PPCs used for dental applications. They assumed that the polymeric matrix and the filler particles were homogeneous, isotropic and linear elastic, and also assumed the filler-matrix interface to be continuous. This finite element analysis facilitated with a stress distribution map under the given loading. The predicted values of flexural strength of the composite were validated against the experimental findings. Cho et al. [46] presented an experimental investigation along with numerical analysis on the effect of particle size on the interfacial fracture properties of the glass/alumina reinforced polymer composite. They used the model of an axisymmetric representative volume element and subjected the uniaxial tensile stress to it and the subsequent particle-matrix debonding was reported. Zhang and Chen [47] used a numerical model with the consideration of cohesive force to compute the critical interfacial strength using the particle size and the matrix properties. Extended finite element method was also used to model the fracture behaviour of poly-sulfone composites and the displacements, stress intensity factor along with the energy release rate were computed [48]. They used enrichment functions to incorporate the discontinuities in the considered elements.

Yang et al. [49] used Finite Element framework to analyse the mechanical behaviour of polymer composites heavily filled with fillers. In conjunction with the implicit framework of the FEM, a cohesive zone model was used for capturing the deformations and the undergoing failure modes. They considered the matrix to be viscoelastic and used the traction constitutive law to simulate delamination. Another research group [50] utilized a FEM to model the micro-mechanical behaviour of the PPCs. They used such obtained information regarding the highest stress concentration and its distribution to further predict the mechanisms of crack growth under the applied loading. A computational approach based on cohesive zone modeling was used to investigate the interaction of the embedded particles with the crack by taking into consideration the mismatch between the elastic properties of the matrix and the reinforced particles [51]. Ju and Lee [52] developed a micromechanical model to predict the damage response of the elasto-plastic polymer composites. Their formulation resulted in successful predictions of the effective elastic modulus of the resulting composite. Lee et al. [53] proposed a computational model for the prediction of microstructural damage by using the approach of voronoi cell finite element and a displacement based finite element model for the microscopic and macroscopic analysis respectively. In another study [54], a method based on the discrete element approach was used to model the mechanical behaviour of PPCs and information regarding the ultimate tensile strength and toughness was obtained. Individual discrete elements were clustered to model the entire volume of the composite. The contact forces were evaluated in accordance with coulomb's friction law and the time integration scheme adopted for the dynamic analysis was based on conditionally stable central difference method. While such an effective approach was adopted, the results largely depended on element size which also directly influenced convergence of the adopted numerical method. Wolff et al. [55] used the concept of 2-radii to generate filler polymer composites and performed parametric studies on the elastic modulus of the resulting composite. Many others have utilized the three-phase computational modeling techniques to evaluate the damage behaviour of different particulate composites [56–62]. Msekh et al. [63] used phase field modeling to predict the tensile strength and the J-integral, a fracture parameter in case of clay/epoxy nanocomposites. They replaced the discontinuities with a damage field to represent the topology of the crack using a regularization parameter. Another research group [64] also used the approach of phase field modeling to predict the macroscopic mechanical behaviour of clay nanocomposites.

As discussed above, the finite element, phase field modeling, molecular dynamics and cohesive zone modeling have been used to model the material behaviour of polymer composites for the longest time [65–72]. However, these methods involve assumptions regarding the interphase properties, particle arrangement, and the bonding between the matrix and the reinforcement. Also, the existing numerical frameworks for modeling of cracks largely rely upon adaptive mesh refinement, localized enhancements of interpolation functions and artificial regularization parameters to solve the ill-posed problem [73–78]. Additionally these techniques require proper determination of parameters associated with internal length scales for different materials. Therefore, the complexity and computational intensiveness of these methods have encouraged the research community to look for other alternatives.

In this view, many researchers have relied on the Machine Learning (ML) approach to predict the mechanical properties and also determine the significance of the process parameters for an optimal design. In the last few years, machine learning has been recognized as a powerful tool used for efficient predictive modeling in the field of polymer composites that could lead to unprecedented insights and exploration of the system properties beyond the capability of traditional computational and experimental analyses. There are various machine learning algorithms that are being utilized in material science depending upon the type of problem and the dataset available. Wiangkham et al. [79] used the framework of Artificial Neural Network (ANN) and Adaptive Neuro Fuzzy-Inference System (ANFIS) to predict the fracture toughness of poly-methyl methacrylate based composite. They used the ratio of crack length to sample width, sample thickness, width of the sample and the angle of mode mixity as the predictor variables to accurately predict the fracture toughness. Another group [80] made use of the data obtained from the Charpy impact test and finite element simulations to predict the fracture toughness of poly-propylene based composites using the algorithm of decision tree regression and the adaptive boosting. Cidade et al. [81] used the ANN framework to accurately predict the dynamic fracture toughness of carbon reinforced epoxy composites by utilizing the data obtained from the full field digital image correlation measurements. A few more successful attempts can be found in the literature where ML algorithms have been used to predict the mechanical properties of PPCs under different exposure conditions [82–85]. Over the last two decades, material science has undergone a steady shift from the phase of developing purely computational techniques for the discovery and design of new and complex materials to the phase of developing coupled methods that increase the reliability of results by making use of computational predictions and experimental validation.

2.3 Fatigue

One of the most critical attributes for a material to be utilized for structural applications is its ability to resist crack under different loading conditions. To ensure the long-term serviceability of these materials, a few of the researchers have studied the behaviour of particulate polymer composites under cyclic loading. Blackman et al. [86] prepared a particulate polymer composite by blending nano-sized silica particles in the epoxy resin and introduced a notch in the final specimen. This specimen was then subjected to sinusoidal loading and the corresponding fatigue behaviour was studied. It was found that with the presence of nano-silica particles in the epoxy matrix, the fatigue response improved the threshold values of stress intensity factor.

Another research group [87] performed a fatigue crack growth study on epoxy reinforced with crushed silica particles under different stress ratios. The major finding of this study was the improved resistance to crack growth as the crack was observed to get deflected by the reinforced silica particles. Another observation was that the threshold value of the stress intensity factor reduces with an increasing stress ratio. The effect of particle morphology on the fatigue response of epoxy-alumina composite was also studied and spherical alumina particles were found to have better resistance to the crack-initiation and propagation nano-scaled rod-shaped particles and the unfilled epoxy [88]. Another important observation from a study on the fatigue investigation of alumina-filled particulate composites was that fatigue life of any polymer composite can be controlled by controlling the interfacial bonding between the matrix and the reinforcing particles [89]. In another study, Bellemare et al. [90] investigated the fatigue crack initiation and propagation in polyamide composites reinforced with nano-sized clay particles. They considered the composite specimens with and without notch and generated stress with respect to the number of cycles to failure curves as well as the rate of crack propagation versus stress intensity factor curves respectively. They concluded that addition of nano-particles changed the mechanism of cracking and resulted in reducing the resistance to crack propagation which was contradicting to the previously reported literature. Also, the incorporation of even small quantities of carbon nano fibers in the polymeric matrix resulted in significant improvement in the fatigue response of the resulting composite owing to the underlying toughening mechanisms [91]. The main failure mechanism in particulate polymer composites under cyclic loading was observed to be the filler matrix debonding which resulted in the growth of subcritical cracks and consequently a sudden failure occured [92].

The literature concerning the fatigue response of particulate polymer composites is very limited. Most of the existing work focuses on the investigation of the fatigue response of composite materials in terms of crack propagation where a pre-existing notch is introduced in the sample [93–96]. Thus, leaving a wide gap in understanding the phenomena of crack initiation during cyclic loading conditions without the presence of a sharp notch. Therefore, it is a logical progression to investigate the crack initiation behaviour and the progressive failure of particulate polymer composites under cyclic loading. Since it has been indicated in a few recent studies that the dynamic fracture toughness of epoxy composites significantly improves when reinforced with micron-sized glass particles, the fatigue response of the same needs to be investigated in sufficient detail [1,28].

Chaper 3

Predictive modeling

This chapter presents the methodology adopted to predict the dynamic fracture toughness of glass-filled epoxy composites. Artificial Neural Network (ANN), a supervised machine learning framework is used to develop two different predictive models for the dynamic fracture toughness corresponding to two different datasets available. One dataset focuses on the material properties, while the other dataset represents the loading conditions in terms of loading rate and wave speed. The problem background, methodology of the proposed solution and the obtained results are discussed in the subsequent sections of this chapter.

3.1 Background

The PPC under consideration in this study was an epoxy composite reinforced with micron-sized glass particles in three different shapes viz. spherical, flake and rod (refer to Figure 2). The epoxy system comprised of a Bisphenol-A resin and an amine-based hardener, purchased from Buehler, U.S.A. The composite sheets were cast using glass particles in a volume fraction of 5%, 10% and 15%. Further, these sheets were machined into rectangular specimens of size 60 mm × 30 mm × 9 mm with a notch of length 6 mm at the center of each specimen. The physical properties of these composite specimens were measured using pulse-echo techniques and are given in Table 1. The shear (*Cs*) and longitudinal wave speed (C_l) were determined at discrete locations using stress wave transducers.

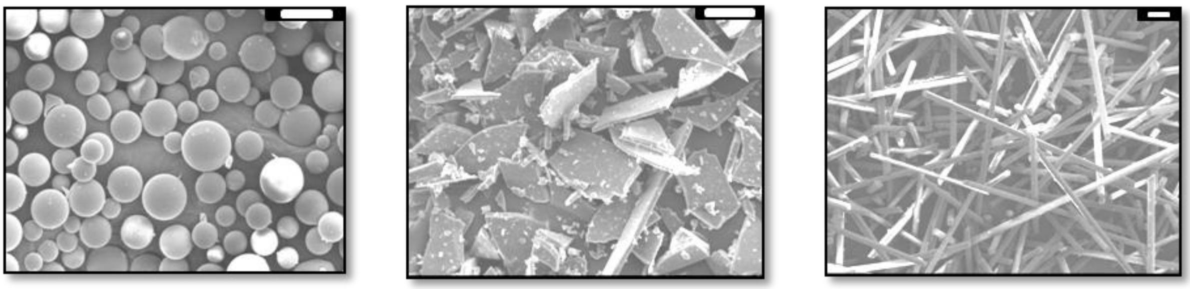

Figure 2 Sphere, flake and rod shaped glass fillers (scale bar: 50 μm) [43]

Table 1 Properties of the glass particles used

Particle type	Aspect Ratio	Dynamic elastic modulus (GPa)		
		V_f = 5 %	V_f = 10 %	V_f = 15 %
Sphere	1	4.62	5.08	5.67
Flake	6	4.69	5.40	6.16
Rod	80	4.68	5.33	6.08

Each specimen was then subjected to dynamic loading using the setup of long bar impactor which works on the principle of stress wave propagation. The schematics of the dynamic fracture test are given in Figure 3. A gas gun setup with high pressure cylinder was used for launching the projectile. The impact of the striker (diameter, 25.4 mm; velocity ~16 m/s) onto the specimen generated a compressive stress wave that propagated through the specimen. The stress wave upon reaching the free edge of the specimen, reflected back in the form of tensile wave which resulted in opening the pre-notch and started the growth of crack in mode-I. This stress wave was responsible for the in-plane deformation in the specimen, which was measured using the technique called, Digital Image Correlation (DIC). A black and white random granular pattern was created on the specimen surface and a high-speed digital camera (Cordin 550) was used to capture the images of the specimen before and after the event of impact. The camera was triggered by delay generator through the completion of the electrical circuit with the impact of the long bar. The images were taken at a frame rate of 3.33 microseconds (300,000 frames /s). Each image in the deformed state had its counterpart in the set of undeformed images.

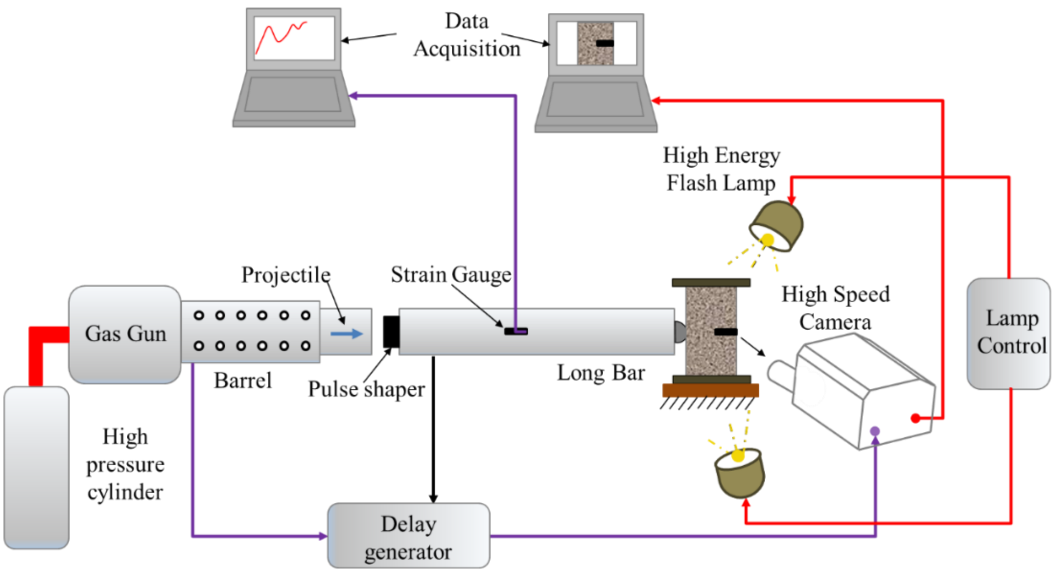

Figure 3 Schematic diagram of the experimental setup used for determining the dynamic fracture toughness

Further using DIC, these sets of images were correlated, and the in-plane displacement components namely crack opening (u_y) and crack sliding (u_x) were obtained using the following asymptotic expressions [28]

$$u_x = \sum_{n=1}^{N} \frac{(K_I)_n}{2\mu} \frac{r^{\frac{n}{2}}}{\sqrt{2\pi}} \left\{\kappa\, cos\left(\frac{n}{2}\theta\right) - \frac{n}{2} cos\left(\frac{n}{2} - 2\right)\theta + \left\{\frac{n}{2} + (-1)^n\right\} cos\left(\frac{n}{2}\right)\right\}$$

$$+ \sum_{n=1}^{N} \frac{(K_{II})_n}{2\mu} \frac{r^{\frac{n}{2}}}{\sqrt{2\pi}} \left\{\kappa\, sin\left(\frac{n}{2}\theta\right) - \frac{n}{2} sin\left(\frac{n}{2} - 2\right)\theta - \left\{\frac{n}{2} + (-1)^n\right\} sin\left(\frac{n}{2}\theta\right)\right\} + \quad (1)$$

$$Pr\, cos(\theta) + Qr\, sin(\theta) + u_{0,x}$$

$$u_y = \sum_{n=1}^{N} \frac{(K_I)_n}{2\mu} \frac{r^{\frac{n}{2}}}{\sqrt{2\pi}} \left\{\kappa\, sin\left(\frac{n}{2}\theta\right) + \frac{n}{2} sin\left(\frac{n}{2} - 2\right)\theta - \left\{\frac{n}{2} + (-1)^n\right\} sin\left(\frac{n}{2}\right)\right\}$$

$$+ \sum_{n=1}^{N} \frac{(K_{II})_n}{2\mu} \frac{r^{\frac{n}{2}}}{\sqrt{2\pi}} \left\{-\kappa\, cos\left(\frac{n}{2}\theta\right) - \frac{n}{2} cos\left(\frac{n}{2} - 2\right)\theta + \left\{\frac{n}{2} - (-1)^n\right\} cos\left(\frac{n}{2}\theta\right)\right\} \quad (2)$$

$$+Pr\, cos(\theta) + Qr\, sin(\theta) + u_{0,y}$$

In the above-mentioned equations, (r, θ) are the crack-tip in polar coordinates, κ is $\frac{3-\mu}{1+\nu}$ for plane stress where μ is the shear modulus and ν is the Poisson's ratio. The coefficients $(K_I)_n$ and $(K_{II})_n$ of the leading terms (when $n = 1$) are the mode-I and mode-II dynamic stress intensity factors, respectively. To evaluate the displacement components after the crack started propagating, the following equations were used [97].

$$u_x = \sum_{n=1}^{N} \frac{(K_I)_n B_I(C)}{2\mu} \sqrt{\left(\frac{2}{\pi}\right)} (n+1) \left\{r_1^{\frac{n}{2}} cos\left(\frac{n}{2}\theta_1\right) - h(n) r_2^{\frac{n}{2}} cos\left(\frac{n}{2}\theta_2\right)\right\} +$$

$$\sum_{n=1}^{N} \frac{(K_{II})_n B_{II}(C)}{2\mu} \sqrt{\left(\frac{2}{\pi}\right)} (n+1) \left\{r_1^{\frac{n}{2}} sin\left(\frac{n}{2}\theta_1\right) - h(\overline{n}) r_2^{\frac{n}{2}} sin\left(\frac{n}{2}\theta_2\right)\right\} + \quad (3)$$

$$Pr\, cos(\theta) + Qr\, sin(\theta) + u_{0,x}$$

$$u_y = \sum_{n=1}^{N} \frac{(K_I)_n B_I(C)}{2\mu} \sqrt{\left(\frac{2}{\pi}\right)} (n+1) \left\{\beta_1 r_1^{\frac{n}{2}} sin\left(\frac{n}{2}\theta_1\right) + \frac{h(n)}{\beta_2} r_2^{\frac{n}{2}} sin\left(\frac{n}{2}\theta_2\right)\right\}$$

$$+ \sum_{n=1}^{N} \frac{(K_{II})_n B_{II}(C)}{2\mu} \sqrt{\left(\frac{2}{\pi}\right)} (n+1) \left\{\beta_1 r_1^{\frac{n}{2}} cos\left(\frac{n}{2}\theta_1\right) + \frac{h(\overline{n})}{\beta_2} r_2^{\frac{n}{2}} cos\left(\frac{n}{2}\theta_2\right)\right\} + \quad (4)$$

$$Pr\, cos(\theta) + Qr\, sin(\theta) + u_{0,y}$$

where,

$$r_m = \sqrt{(X^2 + \beta_m^2 Y^2)}, \theta_m = tan^{-1}\left(\frac{\beta_m Y}{X}\right), m = 1,2$$

$$\beta_1 = \sqrt{1 - \left(\frac{c}{C_L}\right)^2}, \beta_2 = \sqrt{1 - \left(\frac{c}{C_S}\right)^2} \quad (5)$$

$$B_I(C) = \left(\frac{1-\beta_2^2}{D}\right), B_{II}(C) = \left(\frac{2\beta_2}{D}\right), D = 4\beta_1\beta_2 - \left(1+\beta_2^2\right)^2$$

$$h(n) = \begin{cases} \dfrac{2\beta_1\beta_2}{1+\beta_2^2} \\ \dfrac{1+\beta_2^2}{2} \end{cases}; \quad h(\overline{n}) = h(n+1)$$

Here (x, y) and (r, θ) are the cartesian and polar coordinates respectively, c represents the instantaneous crack speed, C_L is the longitudinal wave speed and C_S is the shear wave speed for the composite material. Using these displacement components, stress intensity factor, a fracture parameter was computed within a time regime of -30 μs to 30 μs. The negative sign here does not represent the global time, rather it is a sign convention used by the authors to represent the time instants before the crack initiates. In this context, nine-time instants are considered before the initiation of crack (referred to as the pre-crack initiation regime) and nine are considered after the initiation of crack (referred to as the post-crack initiation regime). When the time instant approaches to zero, the crack initiates. Also, different pulse shaper conditions were used during the experiment to achieve different strain rates. Slopes of stress intensity factor histories in the linearly increasing region upto the crack initiation depends on the loading rate [98] and the measured slopes were ~ 10^7 times higher compared to the usual rates obtained in the quasi-static condition. The strain rates were measured on the long bar using the strain gauge as shown in Figure 3 Details of different pulse shaper conditions are given in Table 2.

Table 2 Pulse shaper conditions

Type	Thickness (mm)	Strain rate (s^{-1})
Polycarbonate washer + Aluminium 100 disc	1.6	3.7
Aluminium 100 disc	0.3	10.7
No pulse shaper	-	42

This experimental determination of dynamic fracture toughness was performed by Kushvaha et al. [43] and the data obtained from their study have been used for developing the predictive model in the current work. The dynamic fracture toughness is largely affected by the material properties but studying the influence of each parameter using such complex and laborious setup is extremely cumbersome. This forms the basis of the problem and the methodology of the proposed solution is given in the next section.

3.2 Methodology

3.2.1 Predictive model-I

In the present work, artificial neural network is used as a surrogate model for predicting the dynamic fracture toughness of glass-filled epoxy composites, wherein a feed-forward multilayer perceptron (MLP) with a back-propagation learning algorithm is implemented. Back-propagation involves the fine tuning of network weights based on the calculated error in each iteration and hence helps in improving the prediction capability of the model. ANN is a non-parametric mathematical model which is comprised of three main layers (input, hidden and output) and many interconnected processing units, commonly known as neurons. The neurons of one layer are connected to the neurons of the next layer and are responsible for summing up the incoming information along with the synaptic weights. The propagation of information between the neurons of different layers is determined by an activation function. These functions filter out the information of every neuron based on its relevance for the model's prediction and help in normalizing each neuron's output within a specific range.

In the current study, aspect ratio (AR), dynamic elastic modulus (E_d), volume fraction (V_f) and time (t) are used as the input parameters and the dependent variable i.e., stress intensity factor is the output parameter. To improve the network training, 'standardized' technique is used to rescale the covariate space. The entire available data is partitioned in training and testing datasets following a partition ratio of 70:30. The used ANN model follows a custom architecture wherein two hidden layers are used (refer to Figure 4).

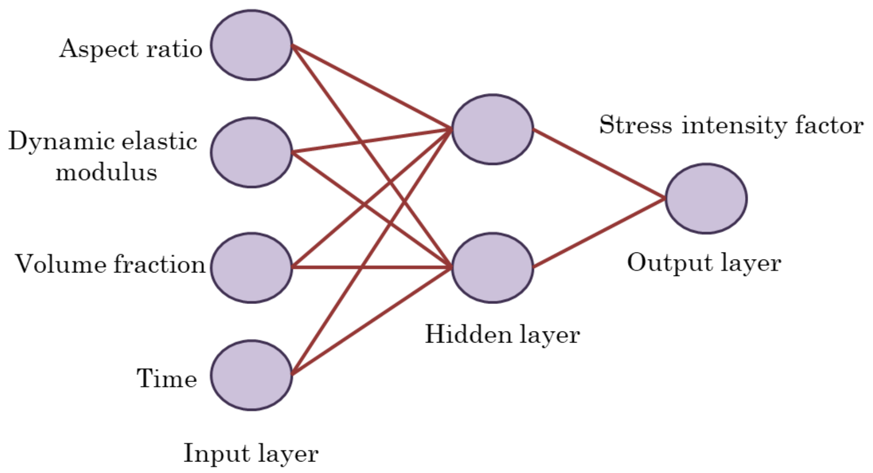

Figure 4 Network architecture used for the prediction of SIF

Sigmoid and hyperbolic tangent are used as the activation functions for the hidden and the output layer respectively. Considering the computational efficiency, gradient descent is used as the optimization algorithm [99] with hyperparameters like initial learning rate = 0.4, momentum = 0.9 and batch as the training type. Batch is considered to be the most suitable training type for smaller datasets due to it's ability to minimize the total error by choosing the synaptic weights appropriately [99]. Learning rate and momentum are two very important configurations of the ANN model. Learning rate determines the pace and degree to which the model can be changed in response to the error calculated from the updation of synaptic weights at each time, while momentum controls the instabilities of the network caused by a very high/low learning rate.

The data in corresponding to aspect ratio 1 (spherical fillers) and 80 (rod shaped fillers) are fed into the above-mentioned neural network. The performance accuracy is statistically evaluated by calculating Mean Absolute Percentage Error (MAPE) and the coefficient of determination (R^2) using the following equations:

$$MAPE = \frac{100}{n}\sum_{i=1}^{n}\frac{|T_i - P_i|}{T_i} \quad (6)$$

$$R^2 = 1 - \frac{\sum_{i=1}^{n}(P_i - T_i)^2}{\sum_{i=1}^{n}(T_i - T_m)^2} \quad (7)$$

where n is the number of data points, T_i is the true value, P_i is the predicted value and T_m is the mean of the true values. After obtaining a satisfactory network performance with the selected architecture, SIF is predicted for the flake shaped glass fillers corresponding to aspect ratio 6. Further, to get more confidence, crack initiation toughness (SIF at t = 0) was predicted for intermediate values of *AR* i.e. 3.5 and 43. The results corresponding to these aspect ratio were given in [43] through an empirical relation,

$$K_1 = C_1 * \log(AR) + C_2 \quad (8)$$

where, K_1 is the crack initiation toughness, C_1 and C_2 are constants (for 5% V_f; C_1 = 0.49 MPa√m and C_2 = 1.69 MPa√m; for 10% V_f; C_1 = 0.59 MPa√m and C_2 = 1.97 MPa√m and for 15% V_f; C_1 = 0.58 MPa√m and C_2 = 2.37 MPa√m).

Additionally, the normalized importance is evaluated to express the importance of each parameter relative to the most important parameter based on the synaptic weights assigned to each predictor in the neural network. Also, a fractographic study using a Scanning Electron Microscope (SEM) is conducted to examine the undergoing failure mechanisms that contributed for improving the dynamic fracture toughness of the resulting composites.

3.2.2 Predictive model-II

Another ANN model is developed to predict the dynamic fracture toughness of glass-filled epoxy composites at varying loading rates. For this study, the experimental data available corresponding to three different loading rates as mentioned in section 3.1 are used. Five parameters are fed to the input layer as predictors. Those input parameters include loading rate (*LR*), shear wave speed (C_s), longitudinal wave speed (C_l), volume fraction (V_f) of the glass fillers and time (*t*). The volume fraction considered here is 0% and 10% for neat epoxy and rod shaped glass fillers respectively. A feed forward back propagation architecture with one hidden layer is used (refer to Figure 5). Hyperbolic tangent and identity are used as activation functions for the hidden and output layer respectively. Again the training type is selected as batch and gradient descent is utilized as the optimization algorithm to estimate the synaptic weights as it is computationally efficient and produces stable errors with stable solution convergence. 70% of the available data chosen randomly, is used as the training set and remaining 30% is for the validation purpose.

Data corresponding to loading rate = 3.7 s^{-1} and 10.7 s^{-1} are utilized to train the model and the validation was done using the data corresponding to loading rate = 42 s^{-1} by predicting the SIF values corresponding to this loading rate. Similar to the first predictive model as mentioned in the previous section, MAPE and R^2 are used as the accuracy metrics to check the reliability of the given model. Further, a fractographic analysis is also performed to understand the underlying toughening mechanisms.

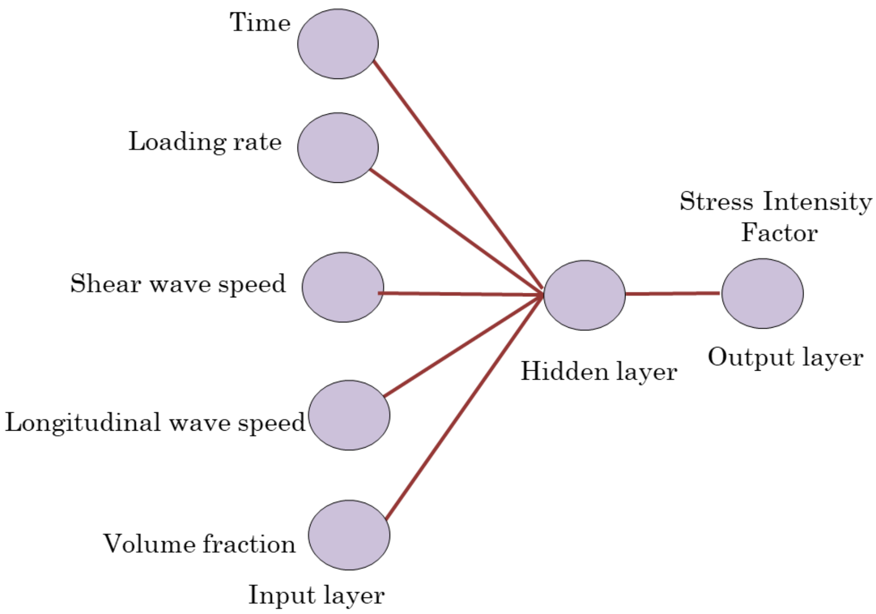

Figure 5 ANN architechture

3.3 Results and Discussions

3.3.1 Predictive model-I

The proposed model predicts the SIF histories at different aspect ratios of glass-fillers. Using the experimental values of SIF corresponding to *AR* = 1 and 80, SIF values are predicted for *AR* = 6. Those predicted values are compared with the experimental ones and are found to have a close fit. Figure 6 shows the closeness of the experimental and predicted values (goodness of the fit) from the proposed model and the coefficient of determination is 0.9963.

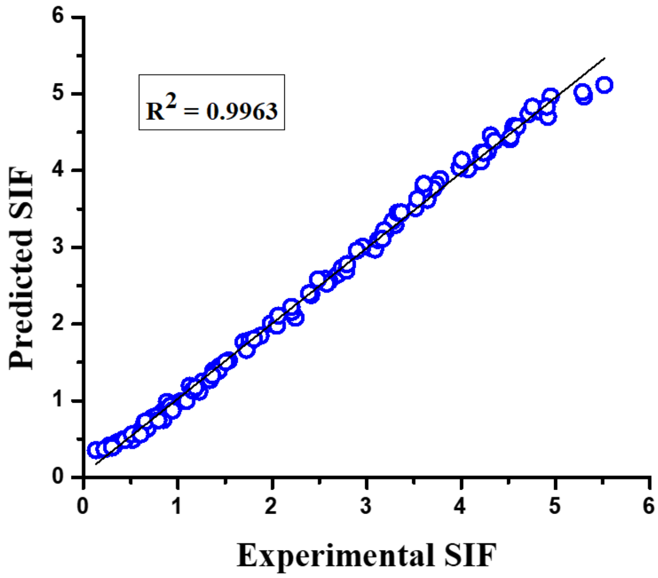

Figure 6 Goodness of fit

The mean absolute percentage error in the predicted values is 9.01% and the prediction accuracy is 90.99%. Comparison of the predicted and experimental values of SIF can be seen in the following figures. Predicted values are found to be in good agreement with the experimental ones. Figure 7 and Figure 8 show the increment in SIF with time before and after the crack initiates. Maximum value of SIF is observed in case of rod shaped fillers with highest aspect ratio i.e. 80. Increase in *AR* results in improved energy release rate and more active participation of fillers in crack bridging phenomena, hence the fracture toughness increases.

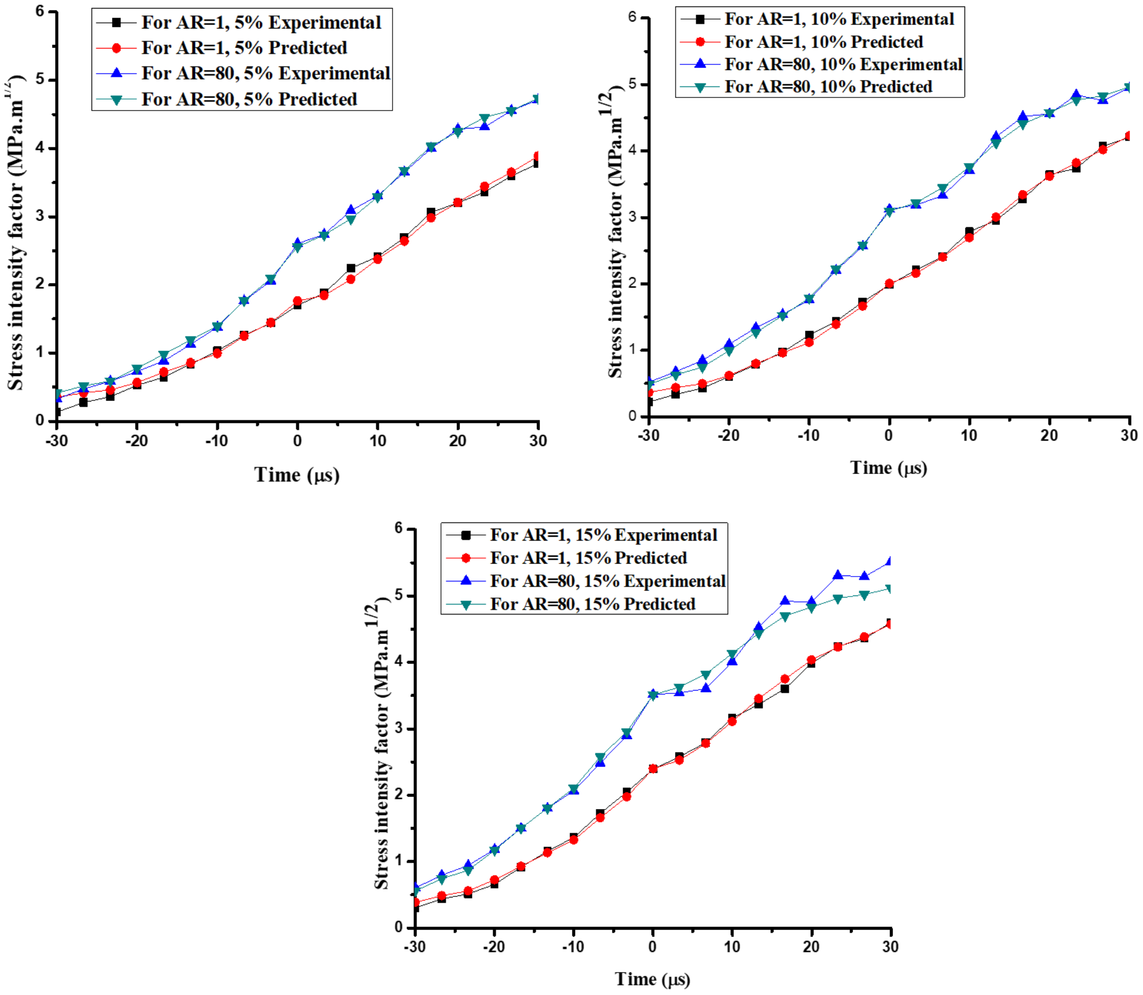

Figure 7 Comparison of experimental and predicted values of SIF for *AR* = 1, 80

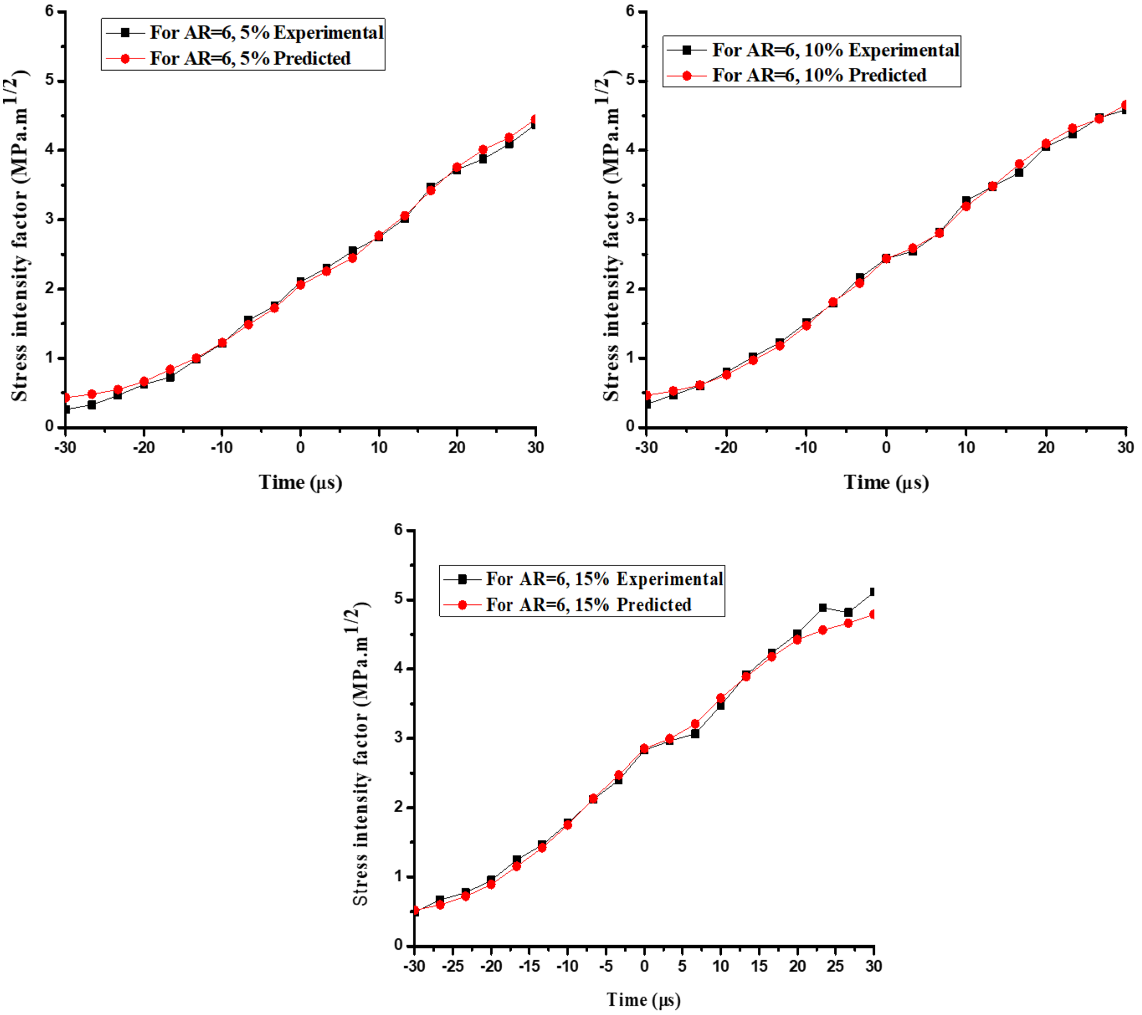

Figure 8 Comparison of experimental and predicted values of SIF for *AR* = 6

Further, the crack initiation toughness (SIF at t = 0 s) of the experimental and predicted values are also found to be in close agreement with each other as shown in Figure 8. It is evident from the figure that crack initiation toughness increases with the increase in the aspect ratio and hence the fillers with *AR* = 80 showed the maximum toughness (3.516 MPa.$m^{1/2}$). This can be attributed to the fact that increase in *AR* increases the energy density (energy stored in the composite system per unit volume) which in turn improves the overall strength [100,101]. As the results are available for only three different kinds of filler shape (aspect ratio), it is desirable to know the nature of SIF histories for the different values of *AR*. Therefore, to determine the SIF histories corresponding to different aspect ratio, intermediate values (3.5 and 43) are chosen and the predicted values are compared with the results obtained corresponding to the empirical equation as mentioned in the methodology section (refer to Figure 9).

Results from both are found to be in close agreement with each other, indicating the reliability and effectiveness of the developed ANN model in the present work. Figure 10 shows the normalized importance based on the calculated synaptic weights. Since it is a dynamic study, time is inevitably the most influential parameter. After time, the aspect ratio is observed to have the most dominant effect on forming the neural network for the prediction of SIF histories.

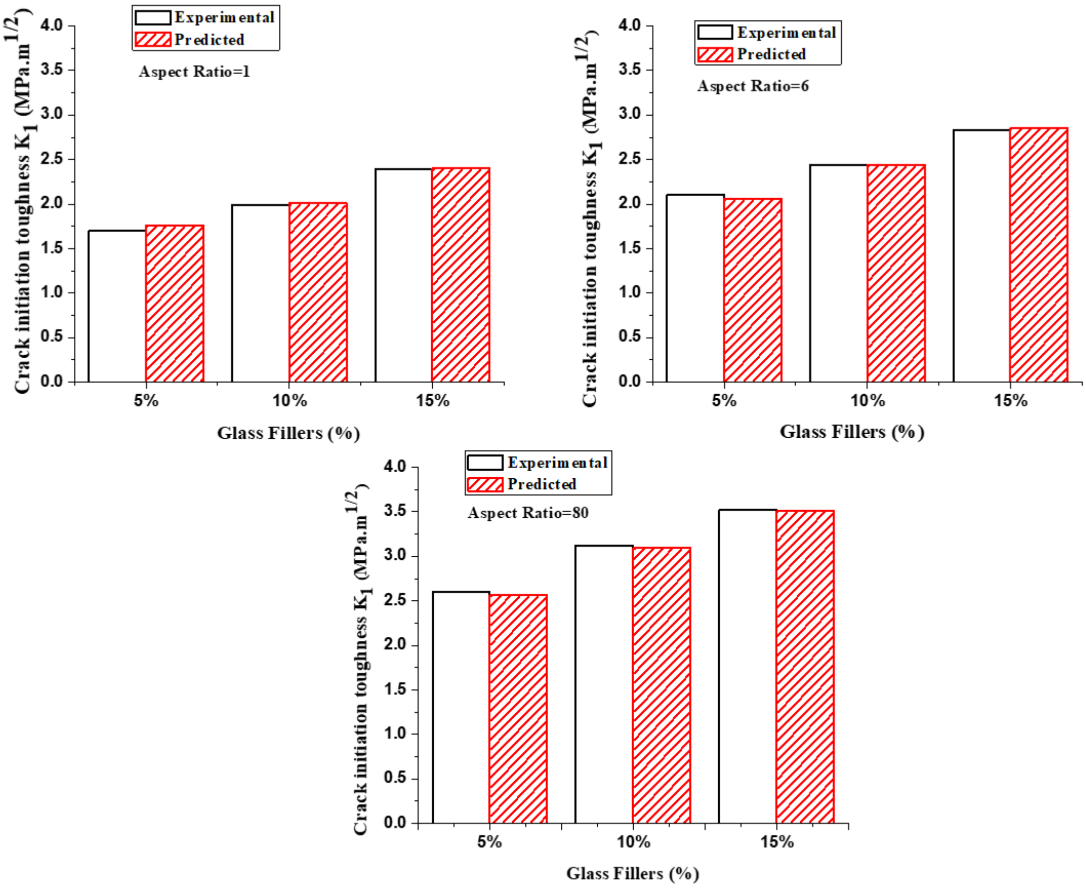

Figure 9 Comparison of predicted and experimental and predicted values of crack initiation toughness

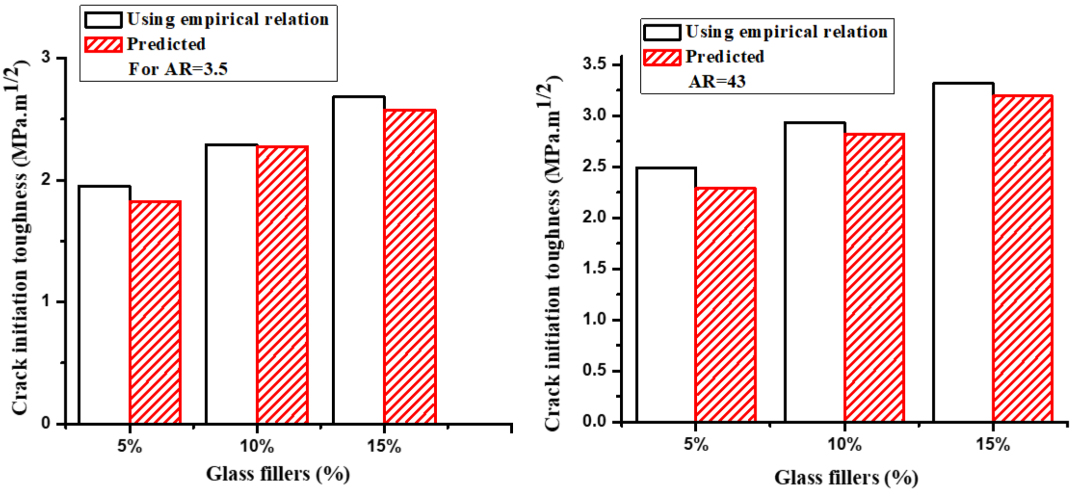

Figure 10 Comparison of predicted and experimental and predicted values of crack initiation toughness at AR = 3.5 and 43

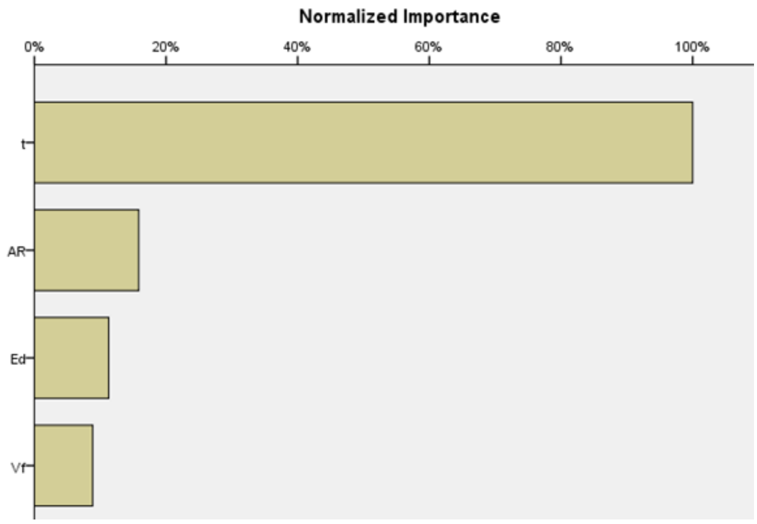

Figure 11 Independent variable importance

It is evident from the plots that SIF increases with increase in the aspect ratio and to understand the underlying toughening mechanisms, a fractographic study is done. The SEM images shown in Figure 12 - Figure 14, indicate that the specimens have failed in four different failure modes namely; matrix cracking, filler-matrix interface separation, filler breakage and the filler pull-out. The dominant modes that are observed from the fractographs of spherical fillers (Figure 12) are matrix cracking and matrix-filler interface separation. Some of these particulate fillers are observed to be pulled out but no filler breakage is found. Owing to the low aspect ratio (AR = 1) in this case, bridging of the crack is assumed to be inactive. The circumvention of crack by the spherical filler is observed which resulted in momentary crack arrest followed by its reinitiation. A lower value of crack initiation toughness is found in this case because the spherical shape of the fillers did not actively participate to arrest the crack growth.

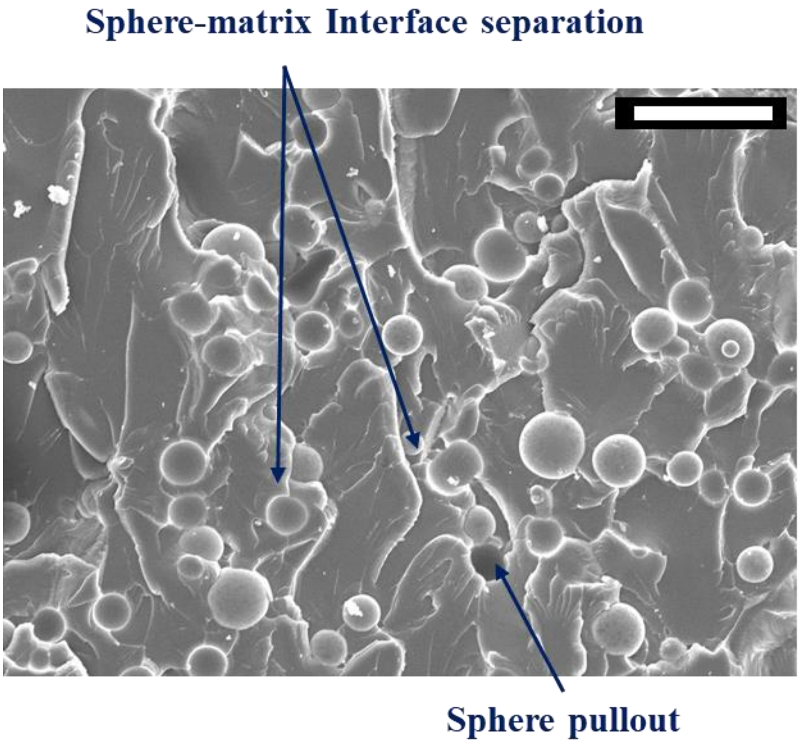

Figure 12 Fractograph of the fractured composite with spherical fillers in Vf = 10% (scale bar = 200 μm)

The dominant failure modes observed in the case of flake shaped fillers are more or less same as that of spherical ones. However, the additional failure mode in this case is the filler breakage (Figure 13) which contributes to increased energy dissipation and relatively higher fracture toughness.

Among the three kinds of filler shapes, the rod shaped fillers exhibited the highest fracture toughness by undergoing additional failure modes, filler breakage and filler pull-out. This enhancement in toughness can be attributed to the increased energy dissipation by the rod shaped fillers because of several identified filler breakages (see Figure 14). The rod- shaped glass filler has an average length of 800 μm which makes it quite likely for the filler to bridge the crack and provide enough resistance for the crack propagation until the filler particle either fractures or gets pulled out. Relatively high energy dissipation because of the filler breakages is due to the fact that the tensile strength of the used glass particles is 3 GPa in comparison to the neat epoxy which is 70 MPa. Therefore, even a couple of fiber breakages can result in a fairly high fracture toughness of the composite.

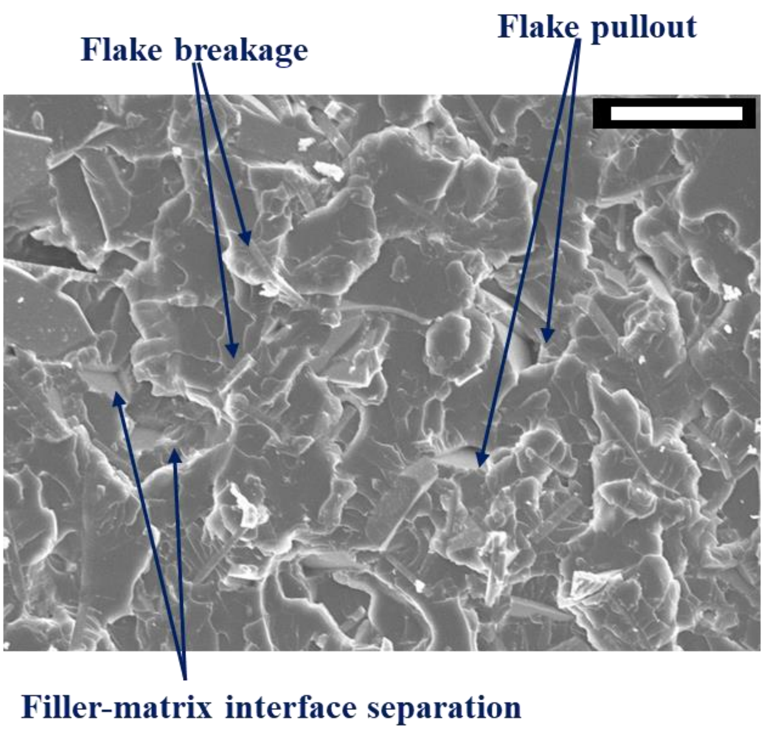

Figure 13 Fractograph of the fractured composite with flake-shaped fillers in Vf = 10% (scale bar = 200 μm)

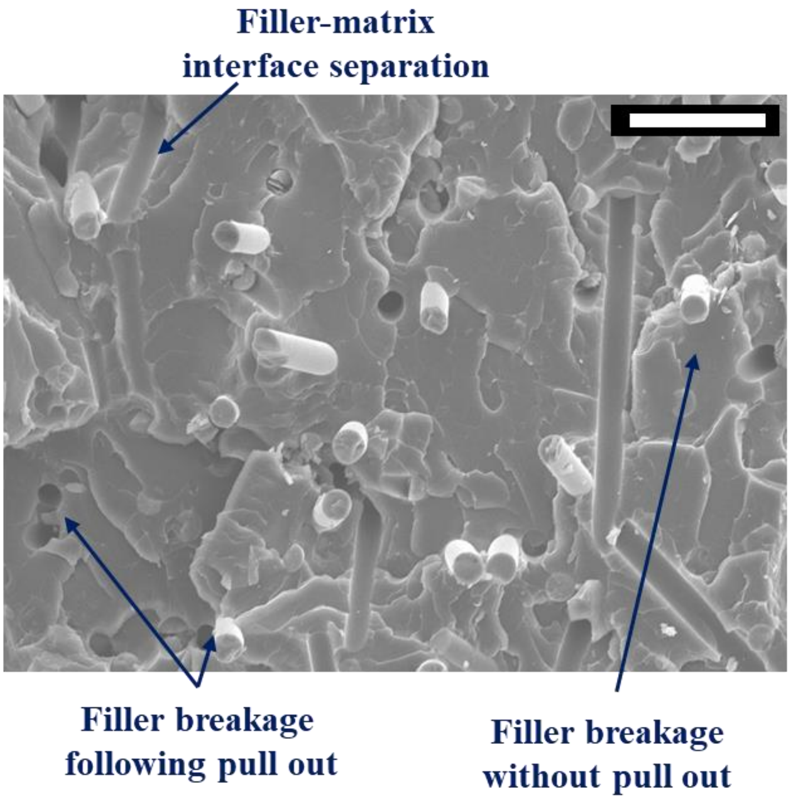

Figure 14 Fractograph of the fractured composite with rod-shaped fillers in Vf = 10% (scale bar = 200 μm)

These results clearly indicate that the filler shape (aspect ratio) has a significant influence on the crack initiation toughness of the glass-filled epoxy composites. Higher aspect ratio promotes percolation at low volume fraction and forms an interconnected network that results in extremely high specific surface area, stiffness, strength and fracture toughness [102].

3.3.2 Predictive model-II

As results in section *3.3.1* have shown that the epoxy reinforced with rod-shaped fillers exhibited highest fracture toughness, the effect of varying loading rate on the dynamic fracture toughness is studied with rod-shaped fillers and the comparison is shown between the neat epoxy and epoxy reinforced with 10% V_f of the fillers.

Data corresponding to loading rate, 3.7 s^{-1} and 10.7 s^{-1} are used to train the neural network and predicted results are then compared with the experimental ones. Coefficient of determination and mean absolute percentage error is found to be 0.97 and 14 % respectively. Goodness of fit between the predicted and the experimental SIF histories can be seen in Figure 15. SIF histories are predicted within a time frame of -30 µs to 30 µs. Stress intensity factor is found to increase with increase in time and loading rate. The effect of loading rate is not very significant until the crack initiates, while in the post crack regime, noticeable increase in SIF can be observed. In addition to this, it is observed that reinforcing the epoxy matrix with rod-shaped silica fillers improves the fracture toughness of the resulting composite. The results obtained from the proposed ANN model are in good agreement with the experimental values of stress intensity factor and the same can be seen in Figure 16 and Figure 17.

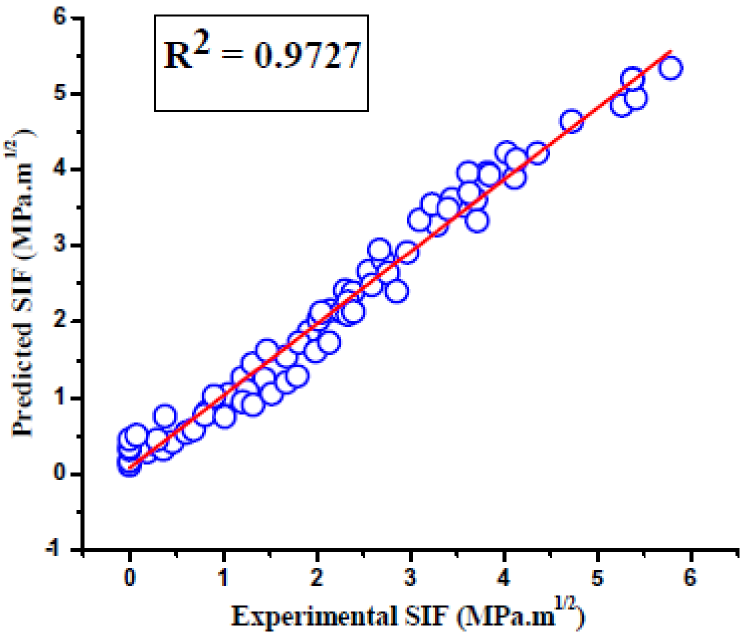

Figure 15 Goodness of fit between the predicted and experimental values

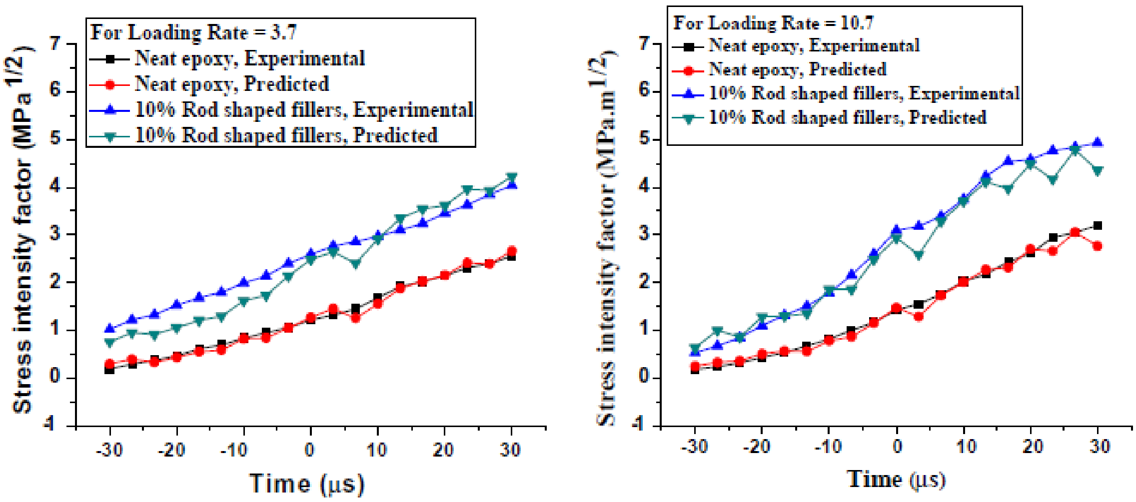

Figure 16 Comparison of the predicted and experimental values of SIF for LR = $3.7\ s^{-1}$ and $10.7\ s^{-1}$

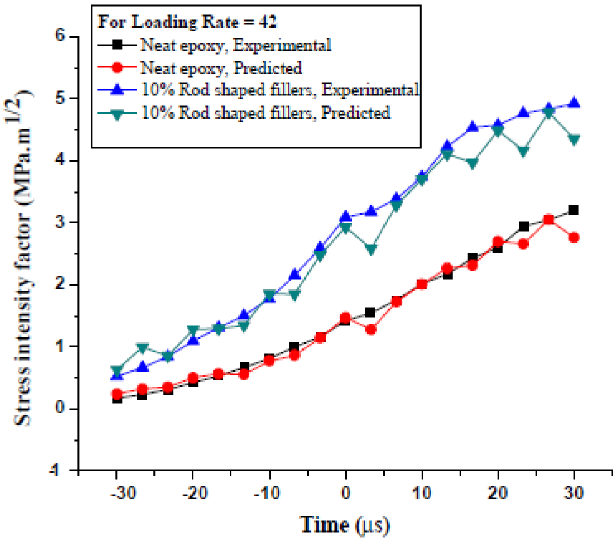

Figure 17 Comparison of predicted and experimental values of SIF for LR = 42 s^{-1}

Figure 18 shows the importance of each input parameter relative to the parameter having the highest importance in determining the neural network for the prediction of stress intensity factor. As it is a dynamic study, time is certainly the most significant parameter among all. Moreover, the loading rate is also a time dependent parameter which justifies it having the highest normalized importance. Loading rate is the second most important parameter as varying the rate of loading changes the material response and the same has been supported experimentally and also by the proposed neural network model. As mentioned earlier in the section 3.1 that the stress wave propagation leads to the event of fracture in the specimen, shear wave speed and the longitudinal wave speed are found to be the next important parameters in the analysis. Shear stress waves propagate radially through the specimen leading to the cracking of the matrix and the fractographs also suggest that matrix cracking is the most dominant mode of failure. Therefore, shear wave speed is one of the important parameters followed by longitudinal wave speed and the volume fraction.

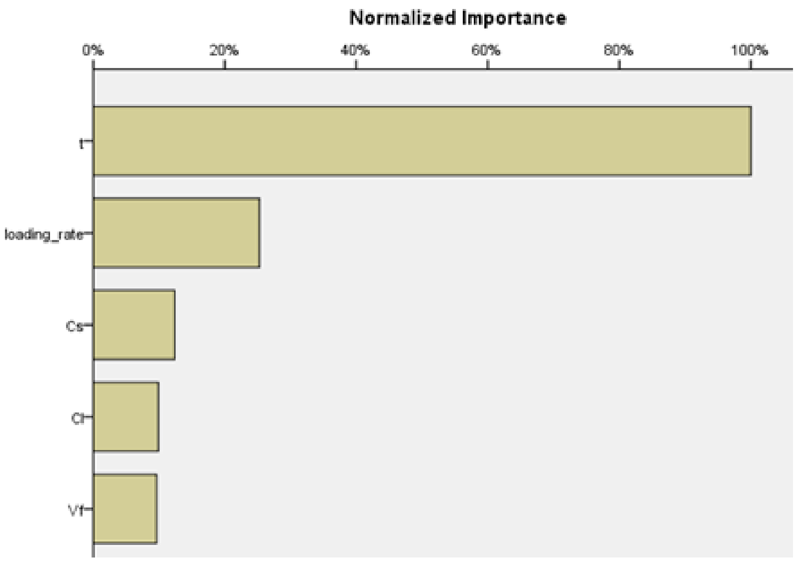

Figure 18 Order of parameter importance

Results indicate that the glass filled polymer composites exhibit more crack initiation toughness compared to neat epoxy composites due to the tendency of glass fillers to arrest the crack growth. Also, the crack initiation toughness of these composites increases with the increase in the loading rate (refer to Figure 19) and this can be attributed to the fact that at higher strain rate the material undergoes a combination of different failure modes resulting in higher energy dissipation. This can be further explained with the help of fractographs shown in Figure 20 where the fractographs of the two most contrasting conditions (no pulse shaper and polycarbonate washer + aluminium disc) are given. Figure 20 (a) shows the surface morphology of the material when pulse shaper is not used during the event of fracture. In this case, matrix cracking, filler-matrix interface separation and filler pull-out are observed as the undergoing failure modes and each of these modes contribute to the overall energy dissipation. At higher loading rate, the fillers tend to behave stiffer resulting in breakage of fillers as the crack continues to grow. This results in higher energy dissipation because the reported tensile strength of fillers is 3 GPa (while for neat epoxy, it is ~70 MPa) [43] which means that even a few filler breakages can result into huge energy dissipation and hence an overall increase in the crack initiation toughness is observed. Figure 20 (b) shows the fractograph of the material when polycarbonate + aluminium disc pulse shaper is used. Even in this case, the material undergoes the above mentioned failure modes but due to lower loading rate, fillers get pulled out rather than breaking. Hence the energy dissaipation is comparatively less which ultimately results in relatively lower crack initiation toughness.

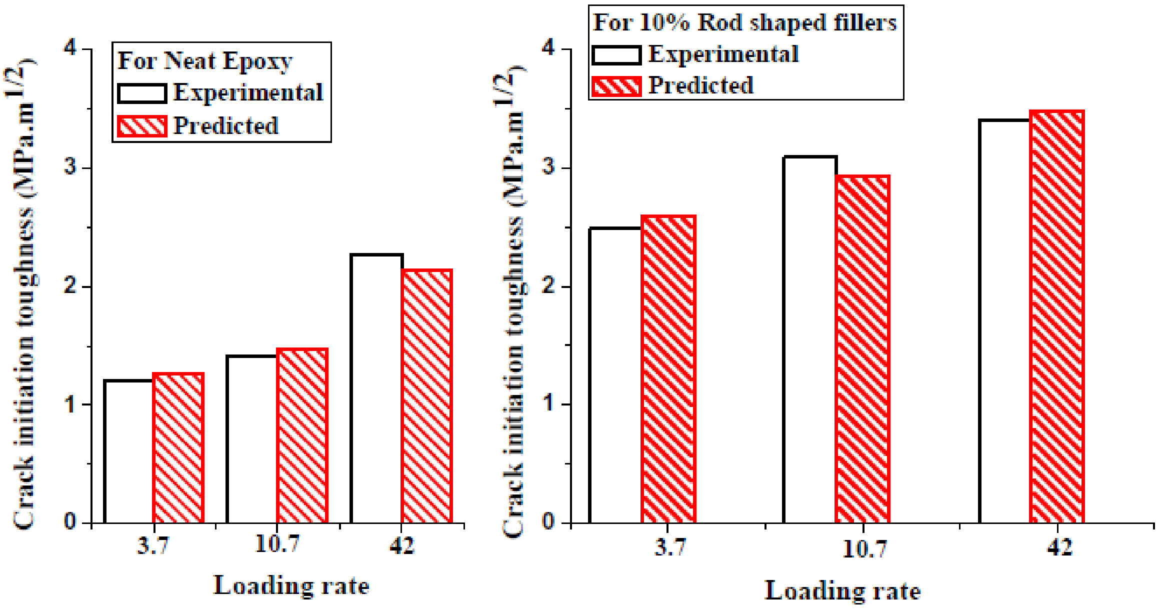

Figure 19 Crack initiation toughness at varying loading rate

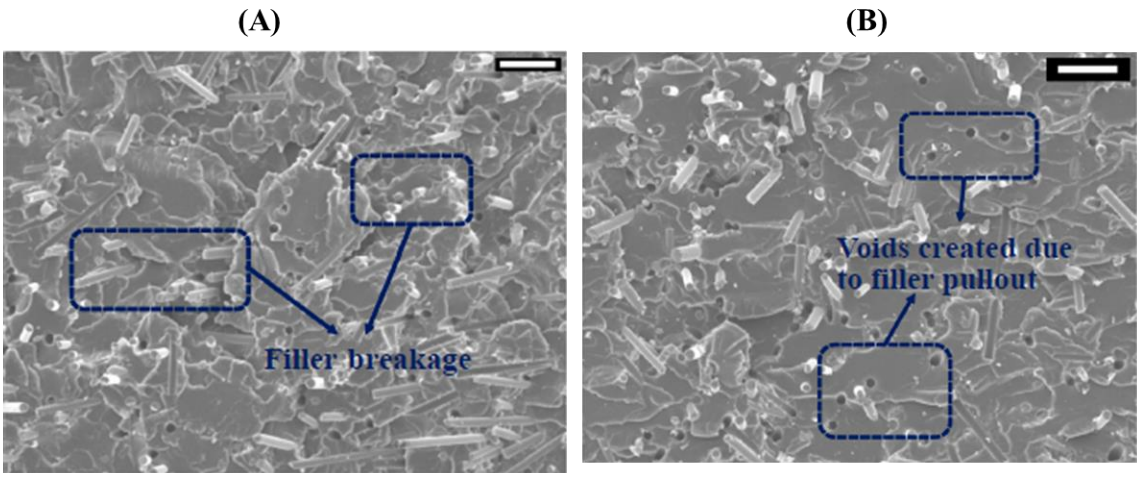

Figure 20 Fractographs of glass filled epoxy composites **(A)** for no pulse shaper and **(B)** polycarbonate + aluminium disc pulse shaper case (scale bar = 100 µm)

Chapter 4

Uncertainty quantification of the dynamic fracture toughness

Outcomes based on experimental data essentially bring us to the realization that quantification of uncertainty is of utmost importance for developing a reliable and practically relevant inclusive analysis and design framework for the dynamic fracture of particulate composites. With limited literature available on the determination of fracture toughness considering inertial effects, this chapter demonstrates a computationally efficient approach for uncertainty quantification and sensitivity analysis of dynamic fracture toughness of particulate polymer composites based on surrogate modeling.

4.1 Background

A realistic analysis and design framework for particulate composites should account for the possible uncertainties due to the inherent inhomogeneity and multiphase nature of the PPCs. Moreover, the unavoidable variation in process parameters due to the varying physical properties of matrix and reinforcement, degree of polymerization, environmental conditions and filler dispersion can significantly affect the ultimate response of PPCs. To ensure the accurate assessment of the ultimate composite performance and to avoid the deviation from the expected material behaviour, uncertainty quantification is critically important [103].

The uncertainties can be categorized as model uncertainties and parameter uncertainties. The model uncertainties arise from the oversimplification of the physics involved while the uncertainty in the parameters arises from stochasticity in the inputs [104]. The uncertainties in the inputs (often correlating directly to the manufacturing uncertainties) have more influence and their propagation is complicated due to the ineffable relationships between the parameters. Expressing complex stochastic input-output relationships requires statistical approaches where the results can be computed with a variability bound in the inputs to provide the confidence interval of the potential outputs. Several statistical approaches such as Monte Carlo simulation, perturbation method, surrogate-based modeling etc. have been explored in this context in numerous engineering problems [105–110]. One of the prevalent methods is the Monte Carlo (MC) technique for the quantification and propagation of uncertainties due to its simplicity and high statistical accuracy up to a large extent of input variability [111–113]. The MC simulation method is a sampling-based approach that generates thousands of samples corresponding to the random input variables as per their probability distribution and subsequently, the probabilistic distribution of the output quantity of interest is characterized. However, the downside of the standard Monte Carlo method is its slow convergence and a large number of realizations ($\sim 10^4$) are required to attain the desired accuracy. To mitigate the computationally expensive nature of MCS, the possible avenues could be parallelization of the Monte Carlo simulations [114] or utilization of surrogate modeling approaches [115,116]. Even though parallelization may be able to reduce the time for Monte Carlo Simulations, it still requires high computational effort. On the other hand a surrogate model can effectively replace the expensive simulation models or physical experiments based on a limited optimum sample evaluation. Thus in case of experimental stochastic characterization, based on a few experimental tests a computational mapping can be established between the stocahstic input parameters and the output quantity of interest using surrogate modeling. Subsequently, the surrogate model can be exploited for predicting the output parameter corresponding to any random combination of the input parameters within the design domain and the Monte Carlo simulation can be performed efficiently.

In this chapter, an ANN based uncertainty quantification approach is presented to quantify the stochastic variability in the dynamic fracture toughness of glass-filled epoxy composites due to the inevitable random stochasticity in the geometrical and material properties (such as aspect ratio, dynamic elastic modulus and volume fraction). The gap between the necessity of large-scale data generation for Monte Carlo simulation and the limitation of carrying out multiple experimentations is proposed to be addressed by adopting ANN based surrogate modeling approach here.

4.2 Methodology

4.2.1 Surrogate modeling

In the current study, the experimental dataset is taken from Kushvaha et al. [43] for developing ANN model to predict the dynamic fracture toughness. Aspect ratio (AR), dynamic elastic modulus (E_d), volume fraction (V_f) and time (t) are used as the input parameters and the stress intensity factor is the output parameter. To improve the network training, 'standardized' technique is used to rescale the covariate space. The entire available data is partitioned in training and testing datasets following a partition ratio of 70:30. The used ANN model follows the architecture of one hidden layer with two neurons. Hyperbolic tangent and identity are used as the activation functions for the hidden and the output layer respectively.

Considering the computational efficiency, gradient descent is used as the optimization algorithm [99] with hyperparameters like initial learning rate = 0.4, momentum = 0.9 and batch as the training type. The data corresponding to aspect ratio 1 (spherical fillers) and 80 (rod shaped fillers) are fed into the above-mentioned neural network and the pridiction accuracy is cgeched using MAPE and R^2 as accuracy metrics. After obtaining a satisfactory network performance with the selected architecture, SIF is predicted for the flake shaped glass fillers corresponding to aspect ratio 6.

4.2.2 Surrogate based stochastic approach

The stochastic response of dynamic fracture toughness of glass-filled epoxy composites is investigated under the inherent uncertainty in the input parameters (aspect ratio, dynamic elastic modulus and volume fraction of fillers). Since fracture in this study is a dynamic event, stochasticity in the input parameters is introduced corresponding to each time instant. The considered cases of uncertainty (stochastic variation) here are as follows:

i. Uncertainty in aspect ratio only: $g\left\{AR\{\overline{SIF}\}\right\} = \{AR_1, AR_2, AR_3, \ldots, AR_n\}$

ii. Uncertainty in aspect ratio and dynamic elastic modulus: $g\{E_d\{\overline{SIF}\}, AR\{\overline{SIF}\}\} = \{\Phi_1\{AR_1, AR_2, AR_3, \ldots, AR_n\}, \Phi_2\{E_{d1}, E_{d2}, E_{d3}, \ldots, E_{dn}\}\}$

iii. Uncertainty in aspect ratio and volume fraction: $g\left\{V_f\{\overline{SIF}\}, AR\{\overline{SIF}\}\right\} = \left\{\Phi_1\{AR_1, AR_2, AR_3, \ldots, AR_n\}, \Phi_2\{V_{f1}, V_{f2}, V_{f3}, \ldots, V_{fn}\}\right\}$

iv. Combined uncertainty in aspect ratio, dynamic elastic modulus and volume fraction:

$$g\left\{V_f\{\overline{SIF}\}, AR\{\overline{SIF}\}, E_d\{\overline{SIF}\}\right\} = \left\{\Phi_1\{AR_1, AR_2, AR_3, \ldots, AR_n\}, \Phi_2\{V_{f1}, V_{f2}, V_{f3}, \ldots, V_{fn}\},\right.$$
$$\left.\Phi_3\{E_{d1}, E_{d2}, E_{d3}, \ldots, E_{dn}\}\right\}$$

Here the symbol $\overline{SIF}$ indicates the parametric stochasticity, while *n* represents the number of data points.

To account for these cases of uncertainty, Monte Carlo simulation (MCS) method is integrated with the ANN model for generating a large-scale dataset based on limited experimental results. Although the PPCs are macroscopically isotropic, the inhomogeneities in the composite are responsible for the complex mechanical behavior governed by coupled parameters. The development of satisfactory computational models accounting for uncertainties in such coupled parameters using MCS is very expensive in terms of time and cost. Obtaining solutions using the conventional numerical approaches requires thousands of simulations. Thus we exploit experimental data that captures the stochastic variations realistically [43]. A flowchart for the proposed ANN assisted MCS methodology is given in Figure 21.

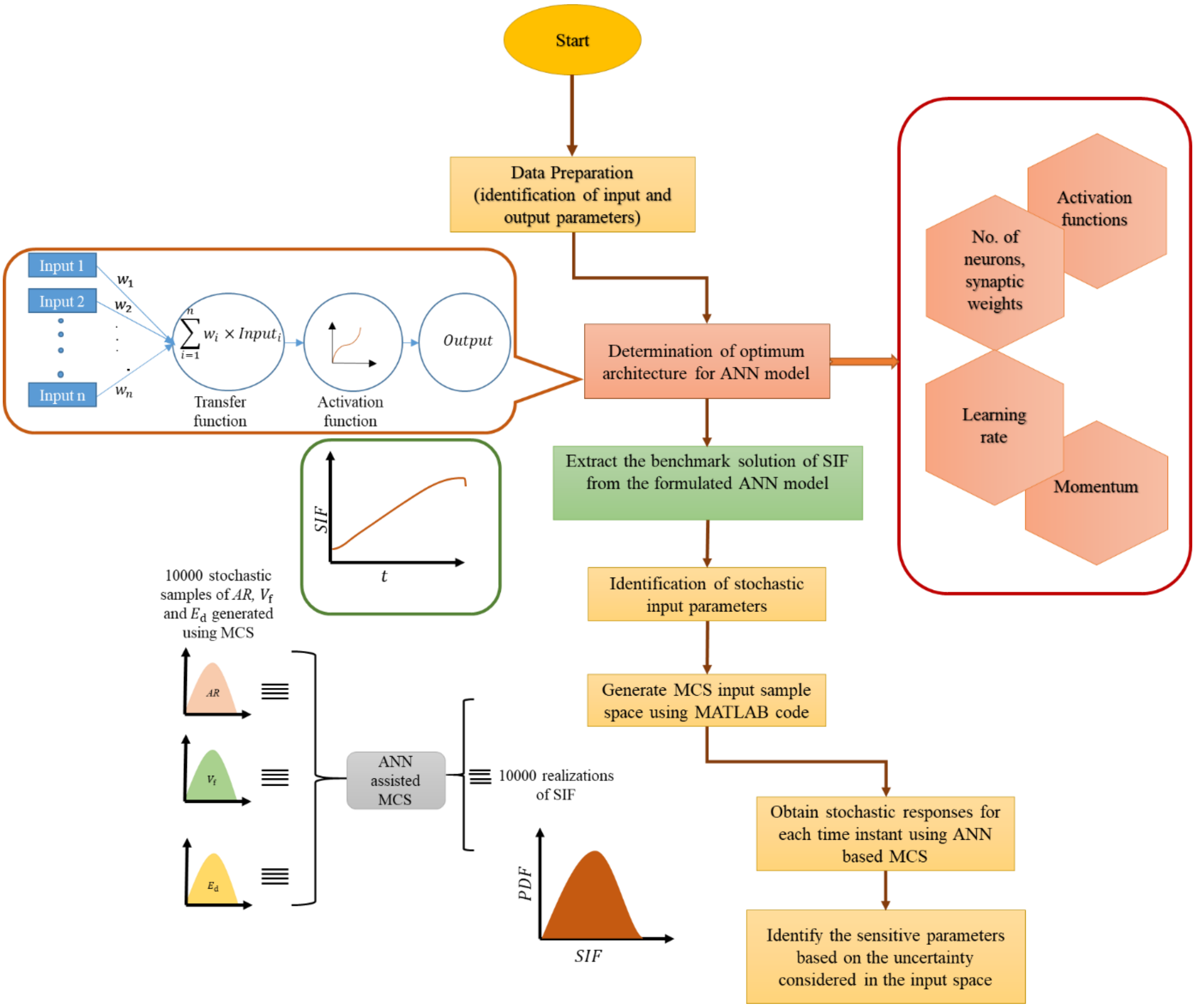

Figure 21 Flowchart for ANN assisted MCS methodology

A sample space of 10000 × 3 is generated for each time instant using a pseudo-random distribution within the design space [117]. Based on the range of available data and physical intuition from experimental observation, a certain stochastic band is selected for the aspect ratio, volume fraction and dynamic elastic modulus. The Degree of Stochasticity (DOS) for the considered band is 30%, 20% and 10% for aspect ratio, volume fraction and dynamic elastic modulus respectively. DOS in aspect ratio is a direct result of the fact that it is very difficult at the manufacturer's end to have a high degree of precision when it comes to the filler size distribution. Also, there are significant chances of variability while coming down to a specific filler shape. Usually the buyer gets a technical sheet from the manufacturer, stating the average size of the filler without any tolerance band [118]. The considered DOS in volume fraction and elastic modulus comes mainly from the inevitable measurement error. Even though we have considered the above-mentioned DOSs in the present analysis, following the proposed ANN based stochastic methodology other DOSs can also be considered if necessary. Using this degree of stochasticity, an input space is created and fed into the developed ANN model corresponding to which stochastic responses of SIF are obtained. These stochastic responses resulting from the forward propagation of uncertainties are then statistically characterized by computing their probability density function (PDF) at each time instant. The computed probability density function reflects the statistical moments along with the likelihood of stress intensity factor at a given time instant.

4.2.3 Sensitivity analysis

To examine the model robustness and evaluate the effect of individual or joint contribution of the parametric uncertainties on the model response, a global sensitivity analysis is performed further. Among several available variance-based methods, the variance decomposition-based Sobol sensitivity analysis is known to quantify the contributions of each input parameter and their interactions to the overall model output variance accurately. The output variance is decomposed into summands of variances using the combinations of input parameters in increasing dimensionality. A model of the form, $y = f(X_1, X_2, X_3, \dots, X_n)$ can be decomposed into terms of increasing dimensionality as follows [119] :

$$f(X_1, X_2, X_3, \dots, X_n) = f_0 + \sum_{i=1}^{n} f_i(X_i) + \sum_{1\le i<j\le n} f_{ij}(X_i, X_j) + \dots + f_{1,\dots n}(X_1, \dots, X_n) \quad (9)$$

where, y is model output, $f_0 = \int_\Omega f(X)\, dX, X_i$ represents Input parameters, n is the number of input parameters. Similarly, the variance of the output can be decomposed as:

$$Var\,[f(X)] = \sum_{i=1}^{n} Var[f_i(X_i)] + \sum_{1\le i<j\le n} Var[f_{ij}(X_i, X_j)] + \dots + Var[f_{1,\dots n}(X_1, \dots, X_n)] \quad (10)$$

The decomposed variances can also be represented as:

$$\begin{gathered} Var[f_i(X_i)] = Var[E(Y|X_i)], \\ Var[f_{ij}(X_{ij})] = Var[E(Y|X_i, X_j)] - Var[E(Y|X_i)] - Var[E(Y|X_j)], \\ Var[f_{1,\dots n}(X_1, \dots X_n)] = Var[y] - \sum_{i=1}^{n} V[f_i(X_i)] - \\ \sum_{1\le i<j\le n} Var[f_{ij}(X_i, X_j)] - \dots - \sum_{1\le i<j\le n-1} Var[f_{1,\dots n-1}(X_1, \dots, X_{n-1})] \end{gathered} \quad (11)$$

Normalizing the equation with unconditional variance of output, $Var[y]$ we get,

$$1 = \sum_{i=1}^{n} S_i + \sum_{1 \le i < j \le n} S_{ij} + \cdots + S_{1,\ldots n} \tag{12}$$

This decomposition results in normalized indices more commonly known as Sobol sensitivity indices. Measure associated with the first term of equation (12) is known as the first order sensitivity index (S_i) and accounts for the effect of X_i on the output of the model. The subsequent terms give a measure of higher order indices that interpret the parametric interactions and the effect of a single input parameter along with all its possible interactions, leading to total effect sensitivity index (S_{Ti}). The expressions for these two indices are given as:

$$S_i = \frac{V_{X_i}(E_{\boldsymbol{X}_{\sim i}}(Y|X_i))}{V(Y)} \tag{13}$$

$$S_{Ti} = \frac{E_{\boldsymbol{X}_{\sim i}}(V_{X_i}(Y|\boldsymbol{X}_{\sim i}))}{V(Y)} \tag{14}$$

where X_i is the i-th parameter and $\boldsymbol{X}_{\sim i}$ denotes the matrix of all factors but X_i. In the present study, the same has been implemented using a python library [120].

4.3 Results and discussions

4.3.1 Results of the surrogate model

The proposed architecture of ANN model is used to predict the SIF histories corresponding to different aspect ratios and volume fractions of glass fillers. A study highlighing the optimal balance of bias and variance corresponding to the different sizes of training dataset is performed and the results for the same are shown in Figure 22. Based on this study, the experimental data corresponding to aspect ratio 1 and 80 are used to train the network and the experimental and predicted SIF values are compared as shown in Figure 23. The used ANN model is found to have a good prediction accuracy as the mean absolute percentage error and the coefficient of determination are found to be 3.8% and 0.99 respectively. Later the SIF histories for aspect ratio 6 are predicted using this trained neural network and the results for the same are shown in Figure 24.

The results shown in Figure 23 and Figure 24 demonstrate the ability of the proposed ANN model to efficiently handle the complex relationship of the input parameters and predict the SIF response of the composite accurately for unforeseen scenarios. Such ANN model can also provide a clear representation of output space in terms of the interactive plots of different input parameters. Figure 25 is one such representation where the distribution of SIF at three different time instants is given over the entire domain of aspect ratio and volume fraction (note that only based on experimental characterization it will be practically impossible to investigate such detailed interactive effects due to the expense and time involved with such endeavor). It is observed that with an increase in the volume fraction and aspect ratio of glass fillers, the SIF increases with time, which in turn increases the resistance of the composite material to crack growth. It is evident that irrespective of the aspect ratio, an increase in the volume fraction of the fillers increases the crack initiation toughness (SIF corresponding to t = 0). However, the resistance to crack growth is more dominant for rod shaped fillers (AR = 80) with a higher volume fraction. The reason for the rod shaped fillers to have the maximum fracture toughness is the highest dissipation of energy in this case owing to the underlying failure mechanisms (as mentioned in chapter 3).

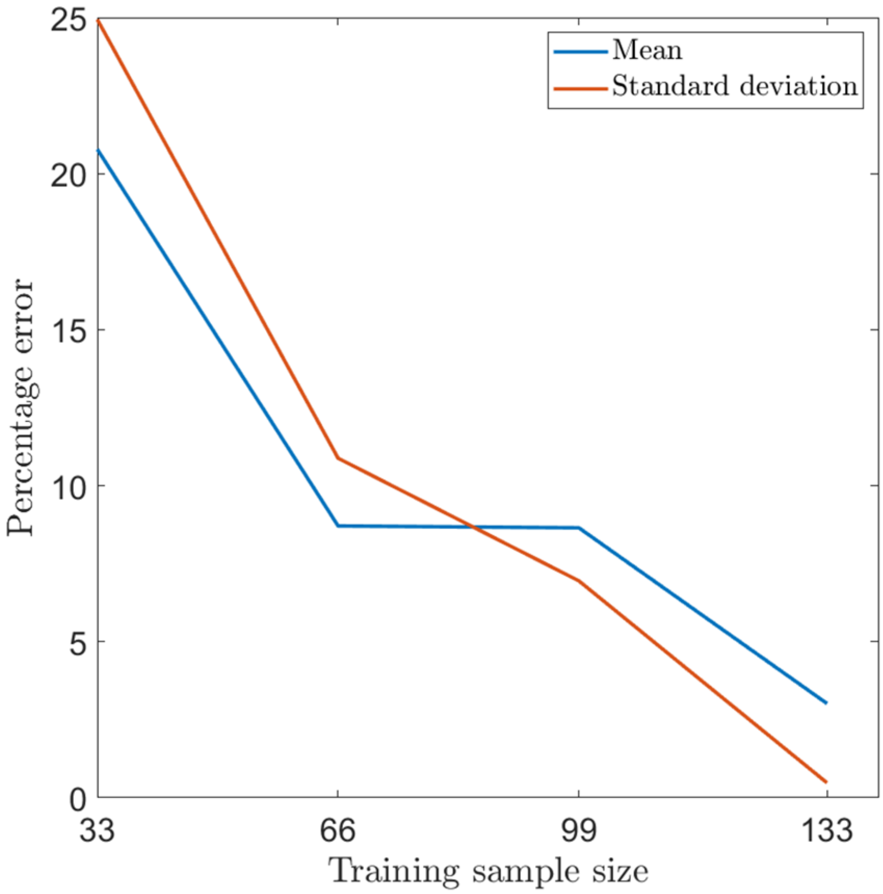

Figure 22 Effect of the size of training dataset on the predicted values in terms of percentage error in the predictions of mean and standard deviation of remaining samples

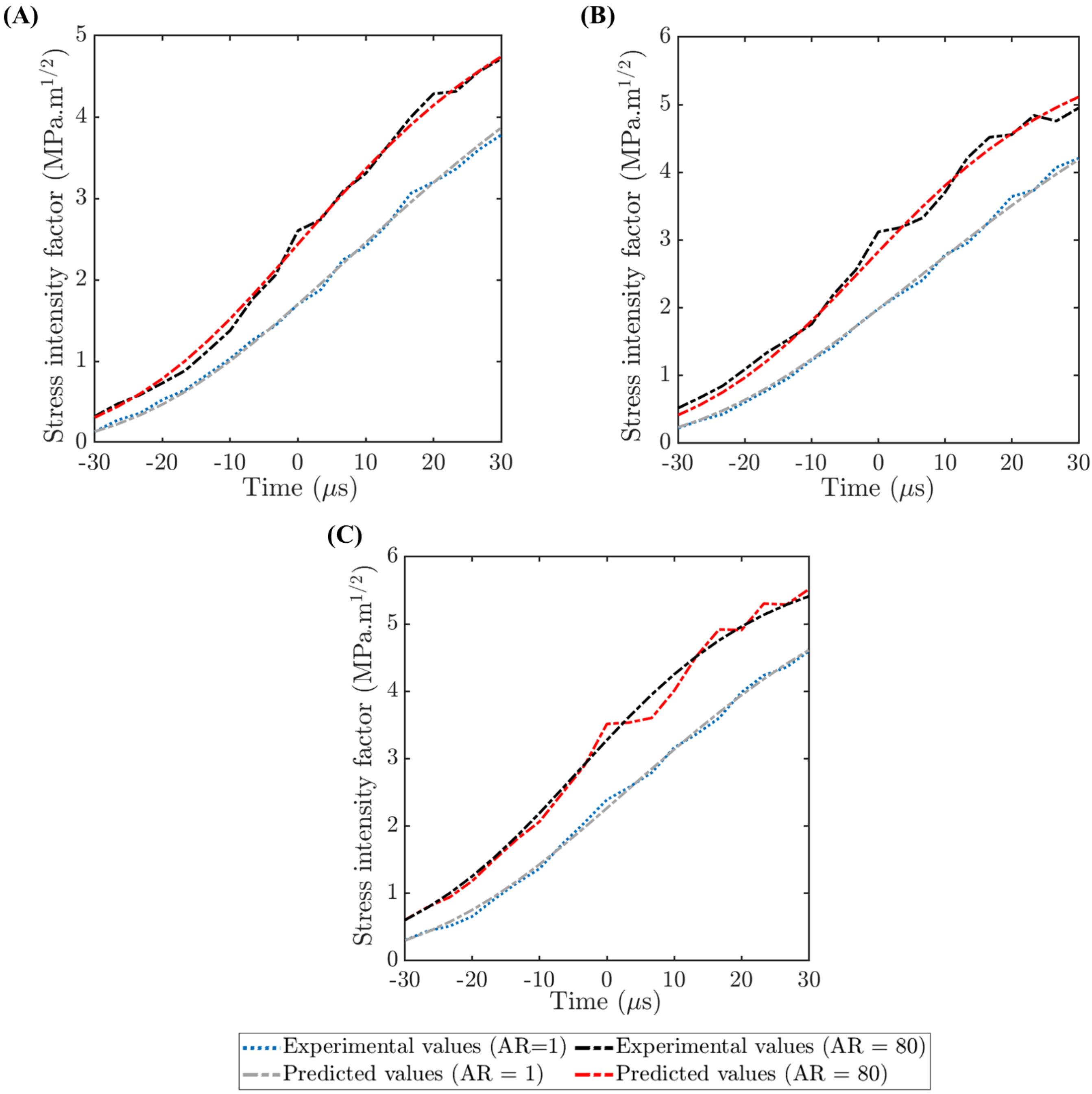

Figure 23 Comparison of experimental and predicted values of stress intensity factor **(A)** for 5% Vf , **(B)** for 10% Vf and **(C)** for 15% Vf when the ANN model is trained with the data corresponding to aspect ratio 1 and 80

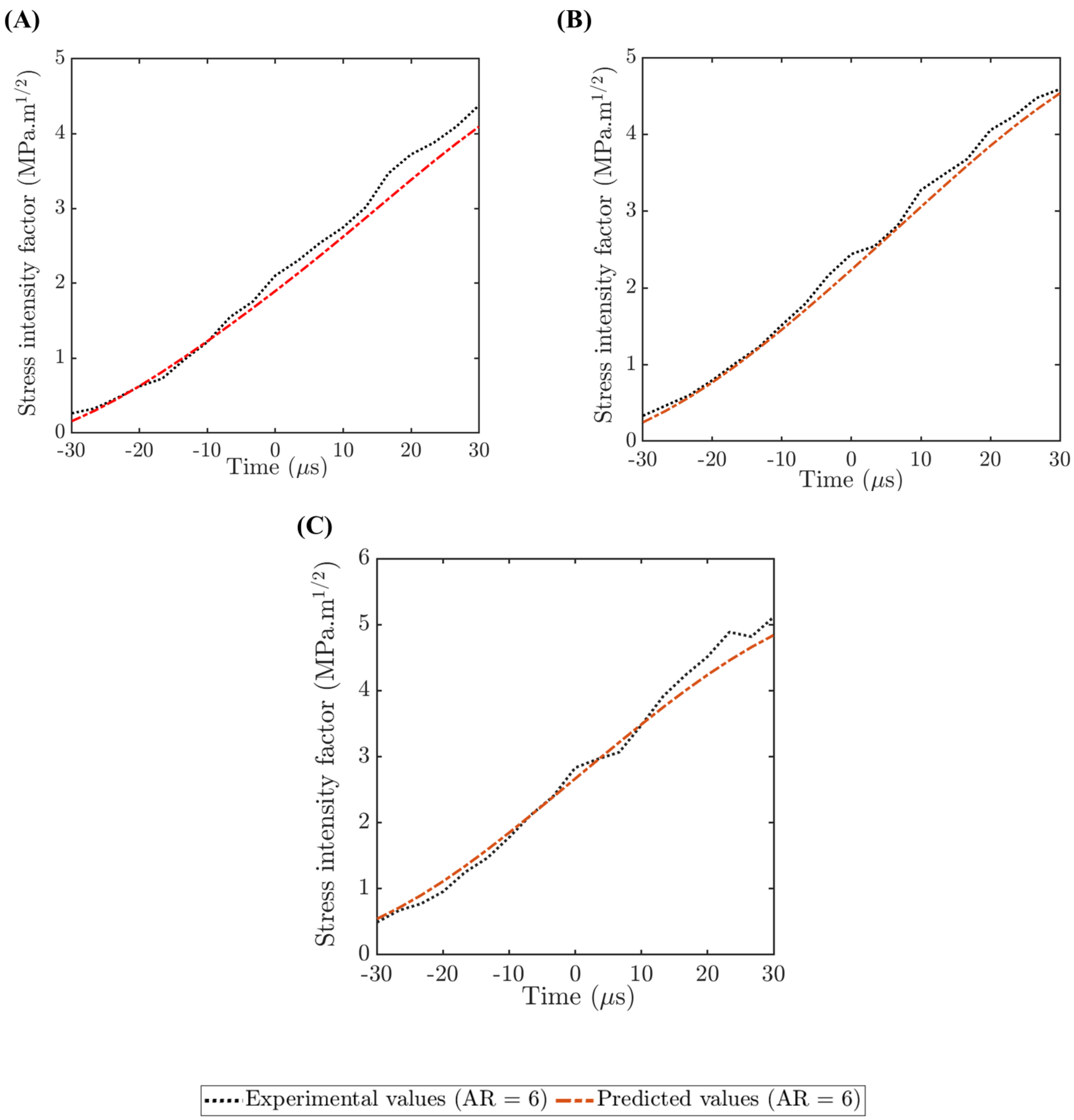

Figure 24 Comparison of experimental and predicted values of stress intensity factor using the dataset corresponding to aspect ratio 6 for **(A)** 5% V_f, **(B)** 10% V_f and **(C)** 15% V_f

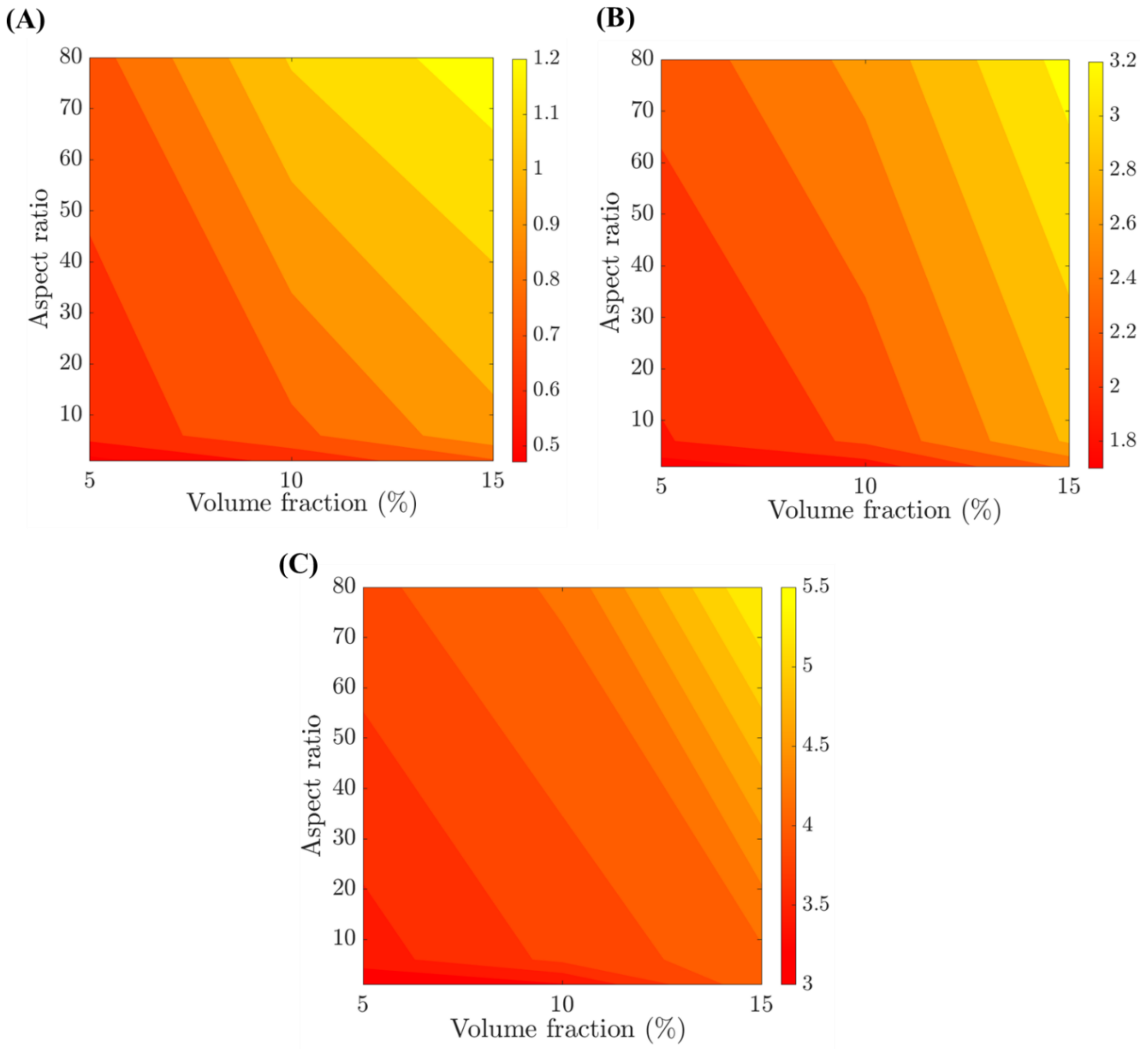

Figure 25 ANN based predictions of SIF in three different time regimes over the complete domain of aspect ratio and volume fraction **(A)** within the pre-crack initiation regime (at t = -19.98 μs), **(B)** when the crack initiates (at t = 0 μs) and **(C)** within the post-crack initiation regime (at t = 19.98 μs)

4.3.2 Uncertainty quantification

Having the ANN based predictive framework validated in the preceding subsection, here we exploit the ANN model further for quantifying the effect of stochasticity in material and geometric attributes at different time instants. The uncertainty quantification of dynamic fracture toughness of glass-filled epoxy composites (leading to complete probabilistic characterization) is carried out considering the stochastic effects in aspect ratio, dynamic elastic modulus and volume fraction. The main idea of uncertainty analysis is to describe the complete set of possible outcomes corresponding to the random/uncertain input space with the associated probability distributions. The probability of having stochastic output values within a certain range is characterized by a probability distribution. Following this probabilistic approach, here the uncertainty in the response of SIF history is described in terms of probability density function and stochastic bounds. The PDF response of SIF after introducing the aforementioned degree of stochasticity in the input parameters as per the cases specified in section *4.2.2*, for rod, flake and spherical shaped fillers is shown in Figure 26 - Figure 28 respectively. In these figures, probabilistic values of SIF are normalized with respect to the corresponding deterministic SIF values, as presented in Figure 23 and Figure 24. These figures are the illustrations of the probabilistic analysis conducted using the ANN model to predict the SIF history corresponding to seven time instants. Probabilistic characterization of the stochastic response of stress intensity factor corresponding to the cases where input stochasticity is considered as the coupled effect of all factors, is presented for only 10% volume fraction of glass fillers for the sake of brevity.

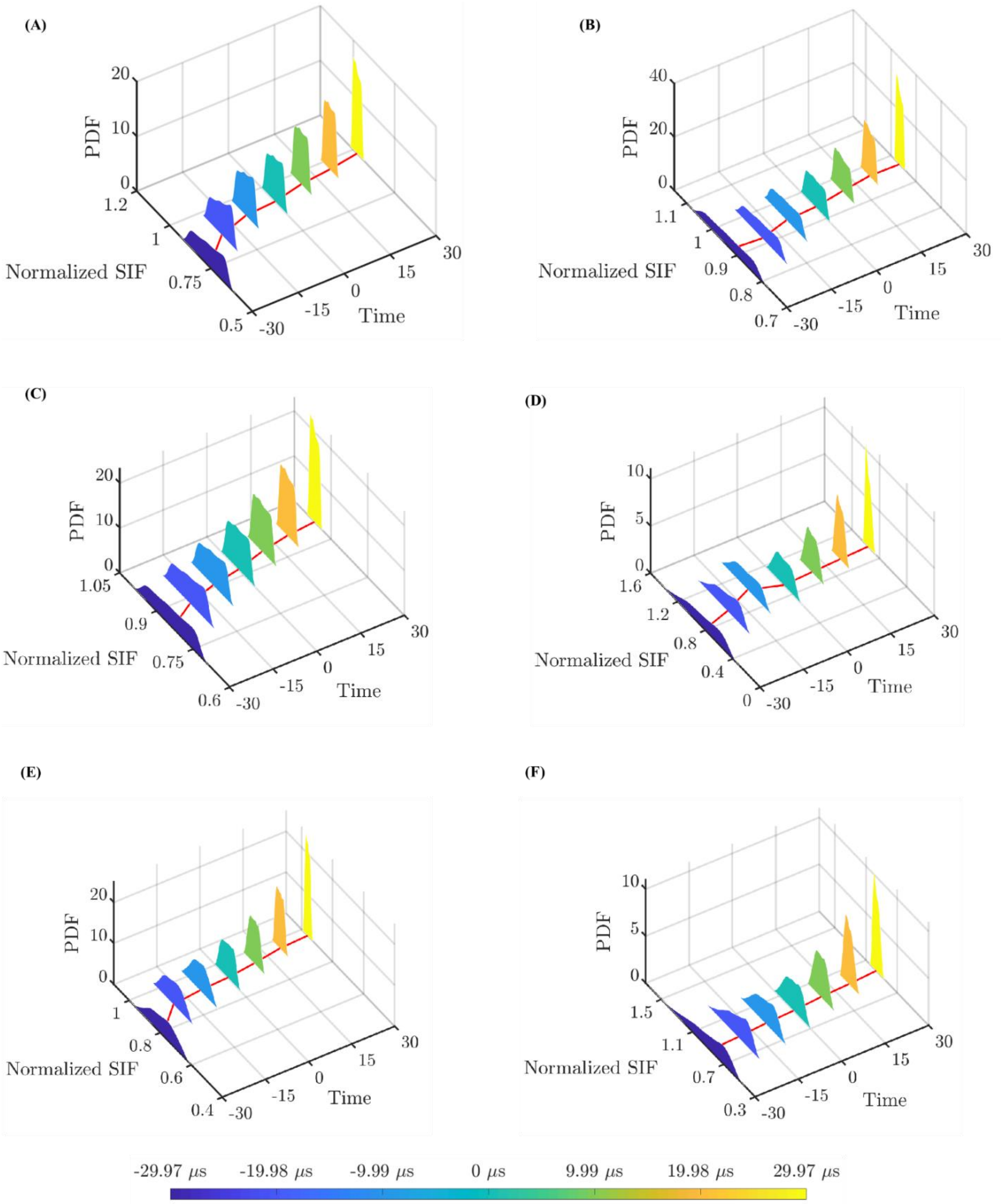

Figure 26 PDF plots of rod-shaped fillers accounting for the stochastic response of SIF for variation in only aspect ratio **(A)** at 5% V_{f},, **(B)** at 15% $V_{f,}$ and PDF responses of normalized SIF history for 10% V_f of fillers when a stochastic variation is introduced **(C)** only in the aspect ratio, **(D)** simultaneously in aspect ratio and dynamic elastic modulus, **(E)** simultaneously in aspect ratio and volume fraction and (F) simultaneously in aspect ratio, dynamic elastic modulus and volume fraction. Thus we show the results for the individual stocahsticity in aspect ratio for 5%, 10% and 15% V_f, while different compound effects of stocasticity are shown considering 10% V_f . The corresponding deterministic results are shown in Figure 23

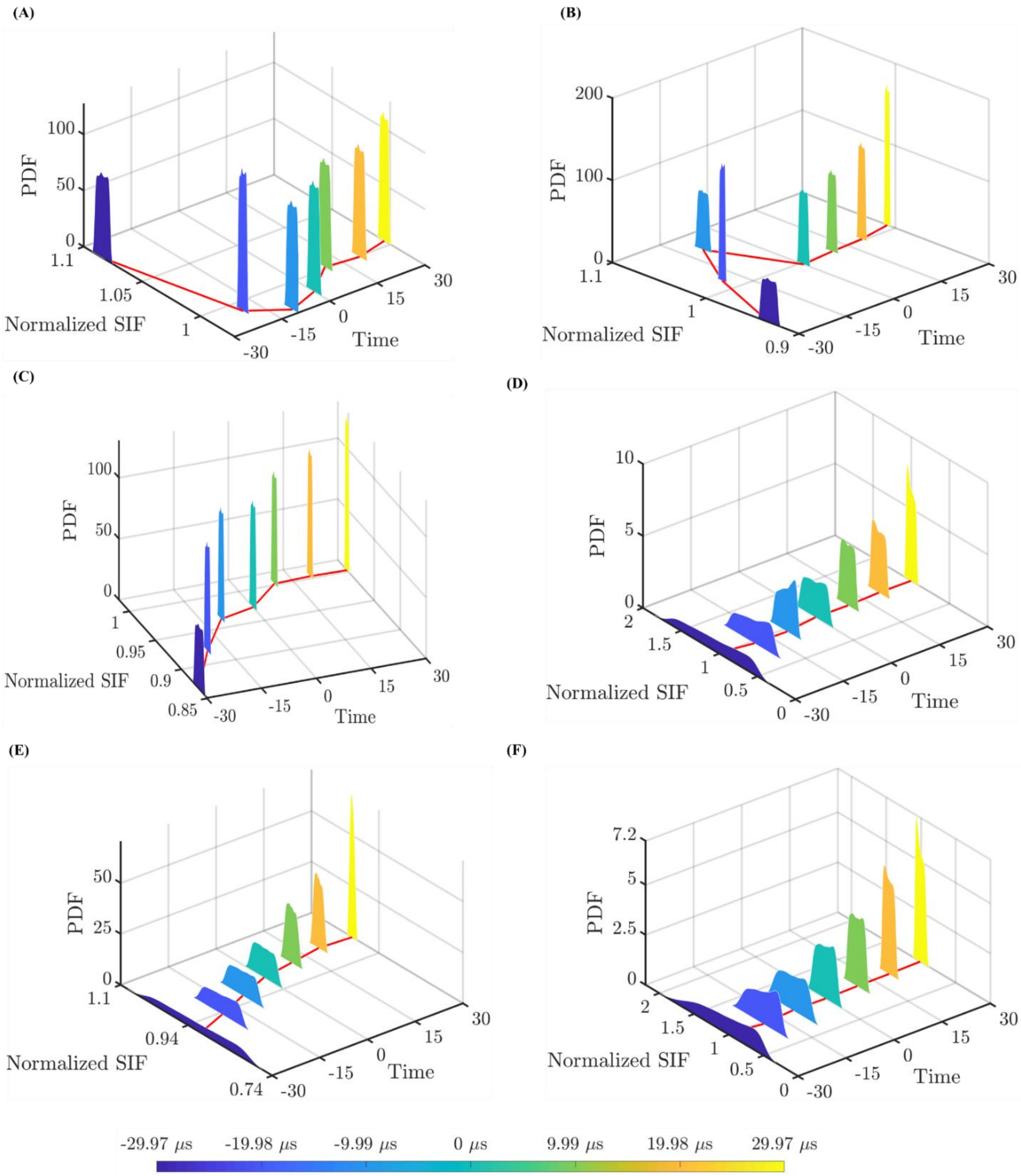

Figure 27 PDF plots of flake-shaped fillers accounting for the stochastic response of SIF for variation in only aspect ratio **(A)** at 5% V_{f},, **(B)** at 15% $V_{f,}$ and PDF responses of normalized SIF history for 10% V_f of fillers when a stochastic variation is introduced **(C)** only in the aspect ratio, **(D)** simultaneously in aspect ratio and dynamic elastic modulus, **(E)** simultaneously in aspect ratio and volume fraction and **(F)** simultaneously in aspect ratio, dynamic elastic modulus and volume fraction. Thus we show the results for the individual stocahsticity in aspect ratio for 5%, 10% and 15% V_f, while different compound effects of stocasticity are shown considering 10% V_f . The corresponding deterministic results are shown in Figure 24

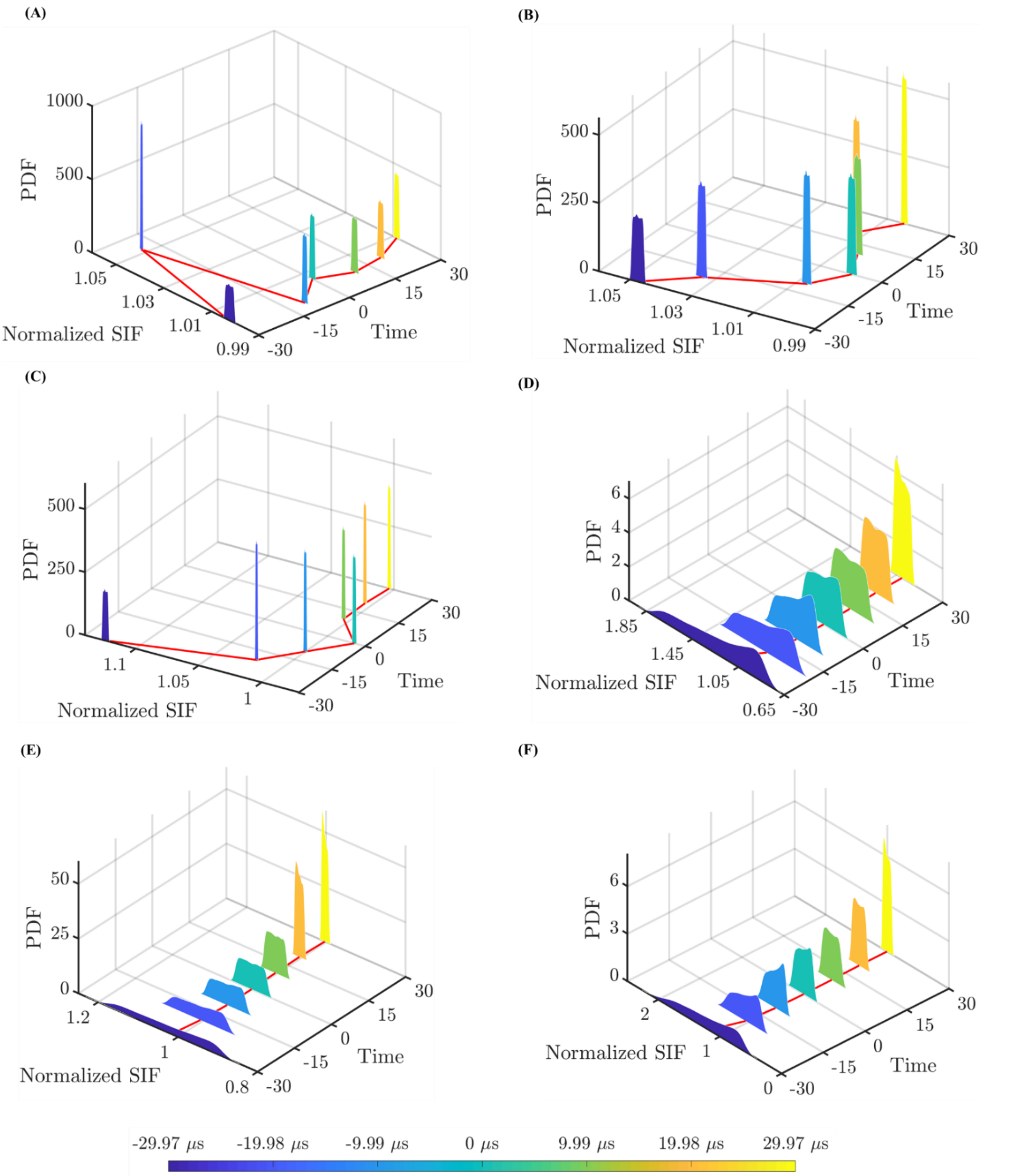

Figure 28 PDF plots of spherical-shaped fillers accounting for the stochastic response of SIF for variation in only aspect ratio **(A)** at 5% $V_{f,}$, **(B)** at 15% $V_{f,}$ and PDF responses of normalized SIF history for 10% V_f of fillers when a stochastic variation is introduced **(C)** only in the aspect ratio, **(D)** simultaneously in aspect ratio and dynamic elastic modulus, **(E)** simultaneously in aspect ratio and volume fraction and **(F)** simultaneously in aspect ratio, dynamic elastic modulus and volume fraction. Thus we show the results for the individual stocahsticity in aspect ratio for 5%, 10% and 15% V_f, while different compound effects of stocasticity are shown considering 10% V_f. The corresponding deterministic results are shown in Figure 23

As a reference to the individual or combined input variation, a solid line is drawn at the mean level in all the PDF plots indicating the variability in the crack propagation. Skewness in the shape of PDF plots indicates the increase in the non-linear relationship between the input and output space due to the introduced uncertainty. The 3D plots of the PDF clearly indicate that as the time progresses, the effect of introduced stochasticity in the input space has a less pronounced effect on the SIF response. The input parameters are primarily responsible for the interfacial bond strength that contributes in the energy dissipation properties of the composite, which in turn helps in resisting the crack initiation. However, once the SIF reaches its critical value, a crack is initiated and as the crack progresses the effect of stochasticity in the input space is less influential for the fillers with lower aspect ratio (spheres and flakes) while sizeable influence can be observed for the rod shaped fillers. To account for the propagation of introduced stochasticity, uncertainty bounds for different filler shapes corresponding to different stochastic cases are presented further in 29 – Figure 31, as discussed in the following paragraphs.

The load transfer from the polymeric matrix to the filler reinforcement is the basic mechanism for the working of a polymer composite material. This load transfer mechanism is governed by the interfacial strength of the composite. Filler reinforcements embedded in the polymeric matrix cause perturbations at the interface between the matrix and the reinforcement. The extent of these perturbations depends on the geometry and the volume fraction of the fillers. Hence the overall composite behavior in terms of strength, stiffness and toughness strongly depends on the state of the polymer-filler interface. The stochastic variability bounds in the composite fracture toughness due to the effect of considered stochasticity in the input parameters are shown in 29 – Figure 31.

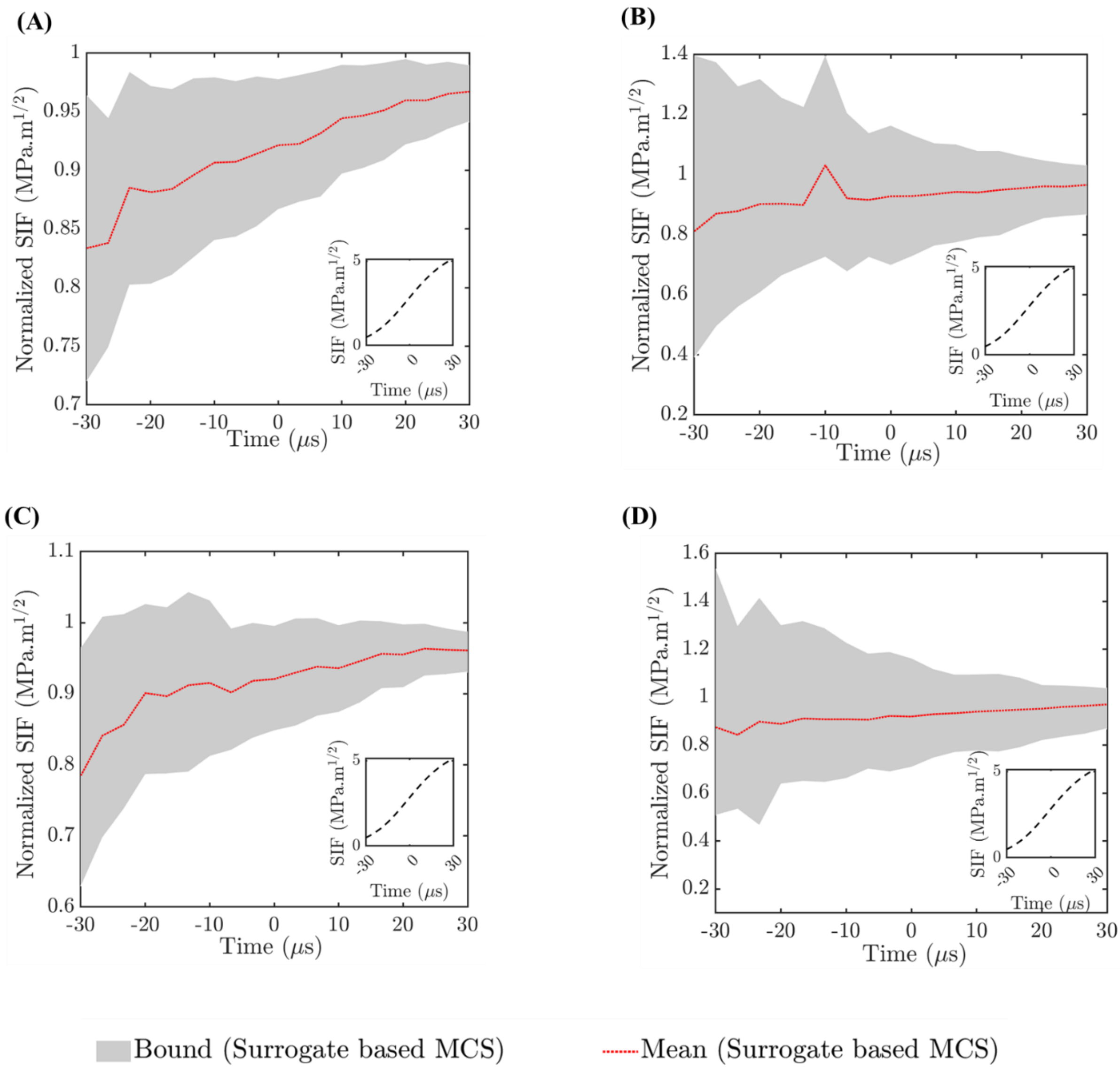

Figure 29 Response bands for SIF history of rod-shaped fillers after introducing stochasticity **(A)** only in the aspect ratio (DOS = 0.3), **(B)** simultaneously in aspect ratio (DOS = 0.3) and dynamic elastic modulus (DOS = 0.1), **(C)** simultaneously in aspect ratio (DOS = 0.3) and volume fraction (DOS = 0.2) and **(D)** simultaneously in aspect ratio (DOS = 0.3), dynamic elastic modulus (DOS = 0.1) and volume fraction (DOS = 0.2). The corresponding deterministic results are shown in the insets.

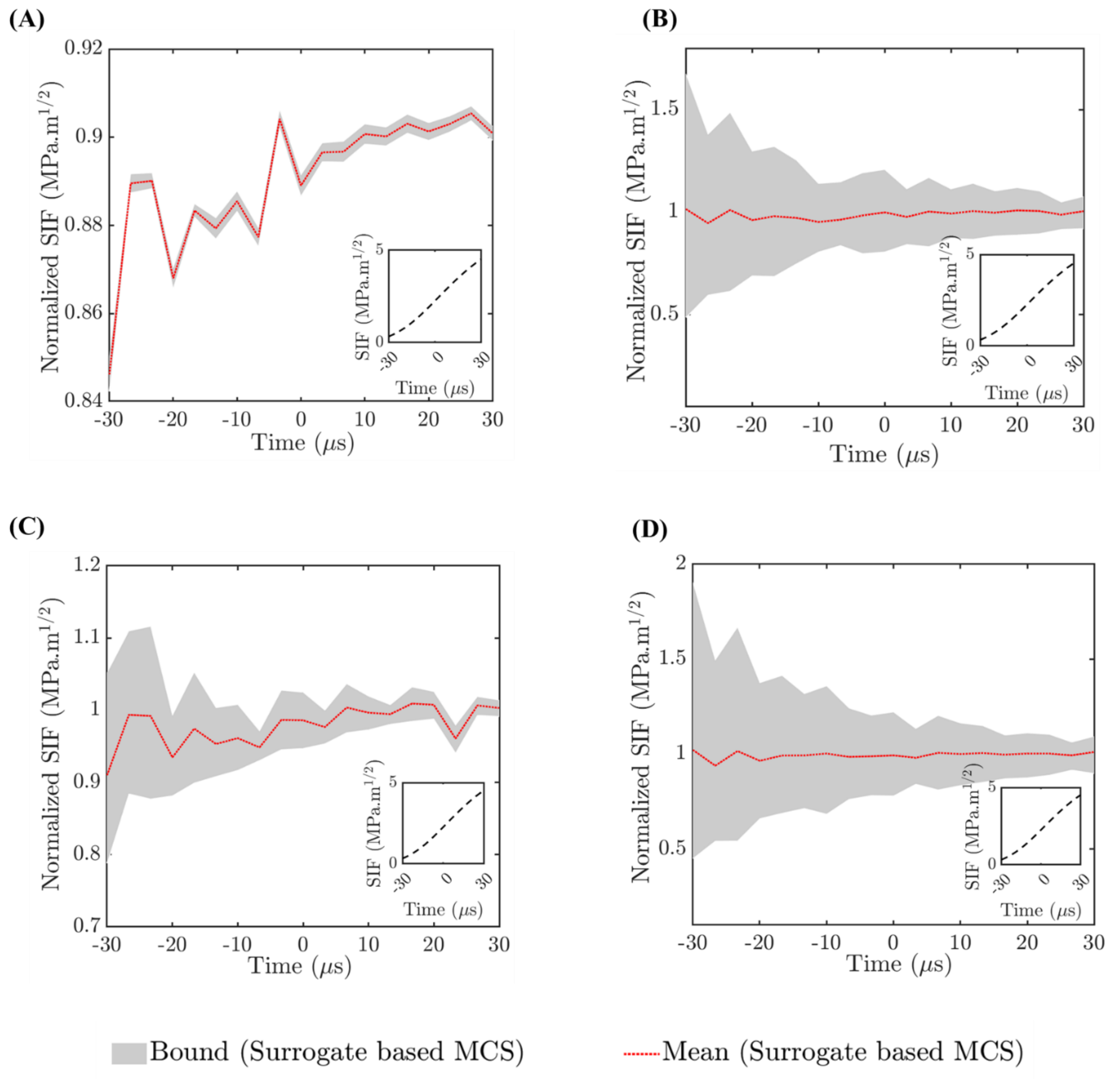

Figure 30 Response bands for SIF history of flake-shaped fillers after introducing stochasticity **(A)** only in the aspect ratio (DOS = 0.3), **(B)** simultaneously in aspect ratio (DOS = 0.3) and dynamic elastic modulus (DOS = 0.1), **(C)** simultaneously in aspect ratio (DOS = 0.3) and volume fraction (DOS = 0.2) and **(D)** simultaneously in aspect ratio (DOS = 0.3), dynamic elastic modulus (DOS = 0.1) and volume fraction (DOS = 0.2). The corresponding deterministic results are shown in the insets.

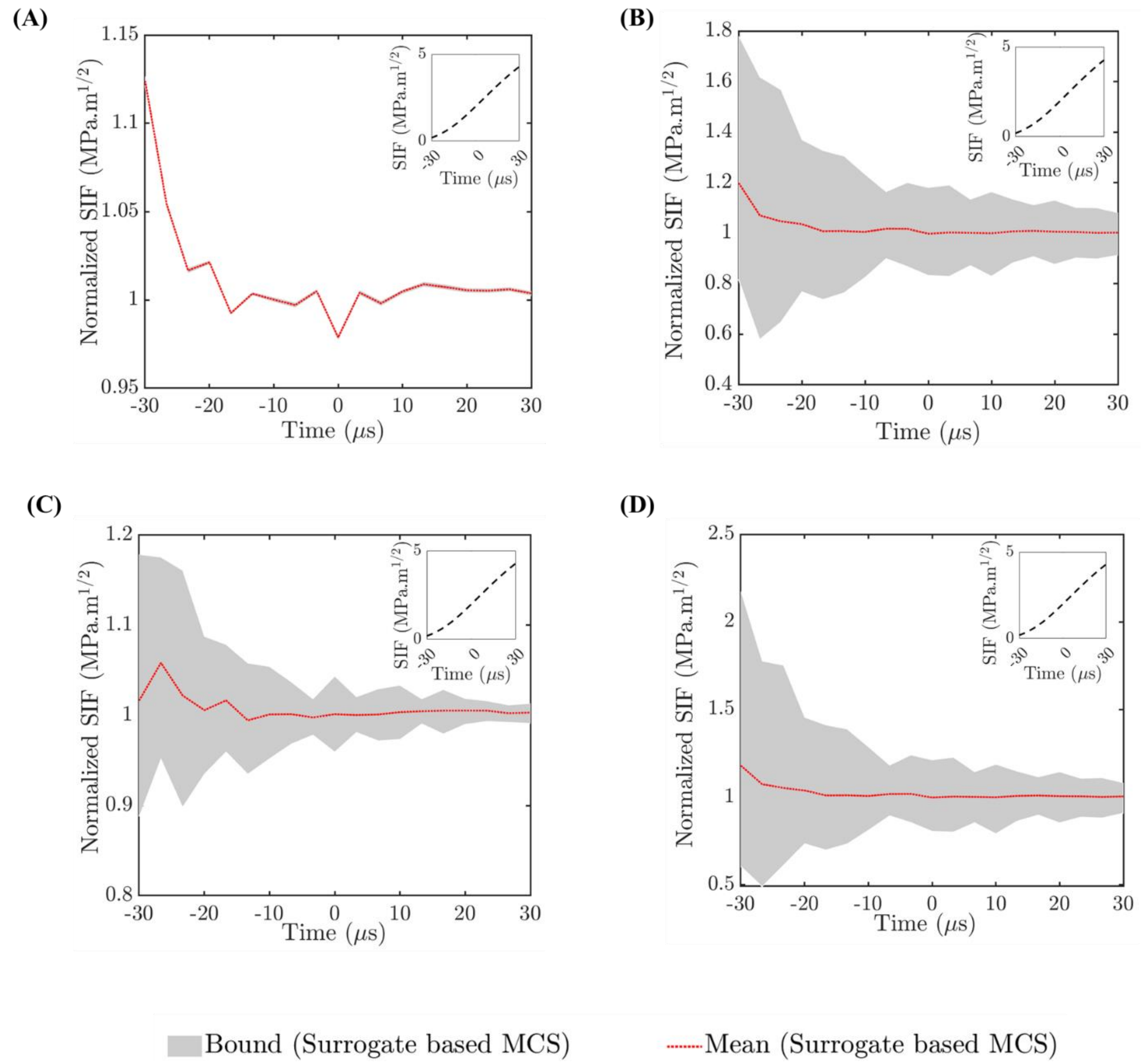

Figure 31 Response bands for SIF history of spherical-shaped fillers after introducing stochasticity **(A)** only in the aspect ratio (DOS = 0.3), **(B)** simultaneously in aspect ratio (DOS = 0.3) and dynamic elastic modulus (DOS = 0.1), **(C)** simultaneously in aspect ratio (DOS = 0.3) and volume fraction (DOS = 0.2) and **(D)** simultaneously in aspect ratio (DOS = 0.3), dynamic elastic modulus (DOS = 0.1) and volume fraction (DOS = 0.2). The corresponding deterministic results are shown in the insets.

Additionally, such a framework of uncertainty quantification facilitates ready assessment of the confidence in the experimental predictions for further industrial adoption. Considering the first stochastic case (only *AR*), among the three filler types, rod-shaped glass fillers are found to exhibit maximum variation in the SIF response. The geometrical aspect of the fillers is directly related to the interfacial strength and hence has a direct impact on the failure mechanisms. Considering the larger aspect ratio of rod shaped fillers, any variability in the size will lead to a significantly varying SIF response while for the other two filler types, the variability in the SIF response is relatively less owing to the inherited shape and lower aspect ratio. When stochasticity is introduced simultaneously in two parameters (AR and E_d ; AR and V_f), as shown in Figures 4.9 (B), (C) – 4.11 (B), (C), an increase in the variability bound is found. Also, it is evident from the above figures that combined uncertainty in the input parameters (Figures 4.9 (D) – 4.11 (D)) results in higher variability (wider bound) in the stochastic SIF history compared to the other cases.

The deviation in the stochastic SIF responses from the deterministic SIF values for all the filler types at three different time instants is shown in Figure 32. The rod shaped fillers show maximum deviation from the deterministic SIF values in all the three time regimes. In case of spherical shaped glass fillers, once the crack initiates, the deviation caused by introducing uncertainty simultaneously in the aspect ratio and dynamic elastic modulus has shown a less prominent effect on the SIF when compared with the deterministic values. Also, in the pre-crack initiation regime, in case of spherical fillers, the combined uncertainty in the aspect ratio and volume fraction, results in a comparatively lesser deviation in SIF while in the post-crack initiation regime, this deviation is in almost the similar range with flake shaped fillers. Although the dynamic elastic modulus is one of the key parameters in describing the fracture toughness, not much variation is seen in this factor for the different shapes of fillers. However, the filler shape is observed to have more control over the kind of crack interaction that takes place and consequently affects the ultimate fracture toughness of the composite. The sensitivity of different such critical input parameters is further quantified in the next subsection.

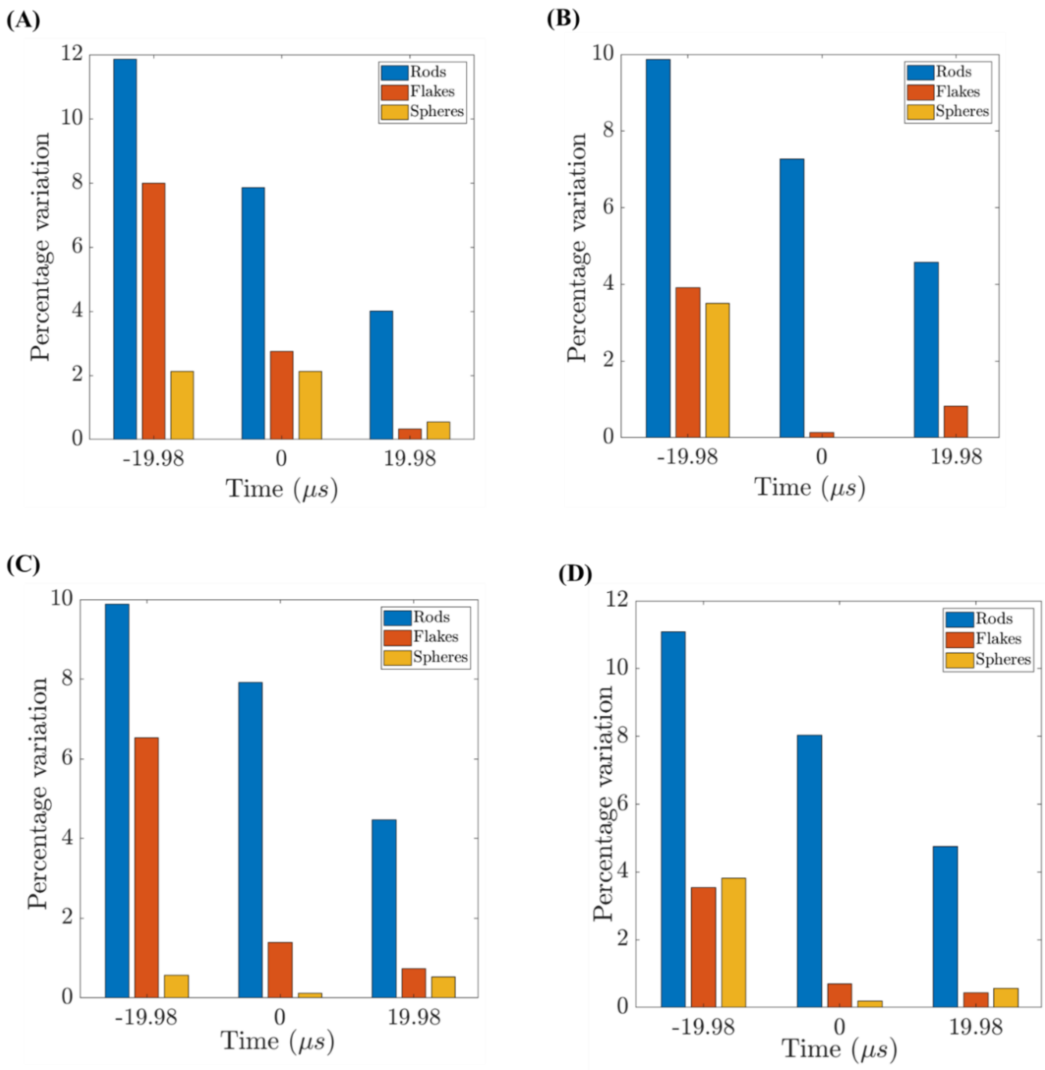

Figure 32 Deviation of mean stochastic SIF responses from the deterministic values when there is uncertainty **(A)** only in the aspect ratio (DOS = 0.3), **(B)** simultaneously in aspect ratio (DOS = 0.3) and dynamic elastic modulus (DOS = 0.1), **(C)** simultaneously in aspect ratio (DOS = 0.3) and volume fraction (DOS = 0.2) and **(D)** simultaneously in aspect ratio (DOS = 0.3), dynamic elastic modulus (DOS = 0.1) and volume fraction (DOS = 0.2)

4.3.3 Sensitivity analysis

In order to quantitatively characterize the importance of each input parameter along with the consideration of parametric interactions, a global sensitivity analysis as discussed in section *4.2.3*, is performed. This facilitates the identification of the input parameter with the most crucial effect on the crack initiation toughness. The sensitivity analysis is carried out on the rod shaped fillers here as these fillers have shown the most pronounced effect of uncertainty. Therefore, to account for the probabilistic distribution of the input space and the parametric interactions, Sobol's first order and total effect indices are calculated. Parametric interactions are a result of the non-additive effect of nonlinear components for the prediction of crack initiation toughness. Keeping in view the inherent uncertainties and the resulting random input fields, Sobol's sensitivity indices act as performance measures of the random output variable for achieving adequate control and reliable manufacturing process. Based on the output variance decomposition, the statistically most important parameter is discovered and the results are shown in Figure 33.

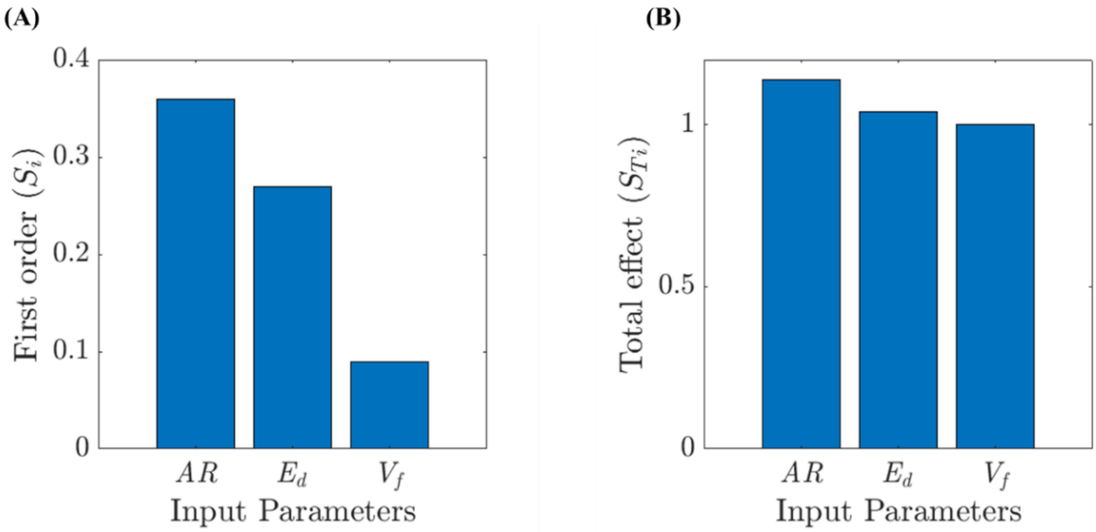

Figure 33 Global sensitivity analysis for crack initiation toughness **(A)** Sobol's first order sensitivity index **(B)** Sobol's total effect sensitivity index

Out of the three critical parameters under consideration, aspect ratio is found to have the highest value of Sobol's first order sensitivity index followed by dynamic elastic modulus and then the volume fraction. The reason for this trend could be attributed to the resulting change in internal stresses and strains within the composite in response to the aspect ratio variations, which in turn affects the overall toughness of the composite. Additionally, the analysis with the consideration of all the possible parametric interactions of any one parameter with the remaining two, indicates the same order of sensitivity indices. In general, the quantitative analyses considering both individual and interaction effects of sensitivity reveal that the aspect ratio of the glass fillers is the most influential parameter, leading to the highest variability impact on the crack initiation toughness of particulate polymer composites.

Chapter 5

Fatigue: A crack initiation and propagation study

One of the most critical attributes for a material to be utilized for engineering applications is its ability to resist crack under different loading conditions. To ensure the long-term serviceability of these materials, studying the behavior of particulate polymer composites under cyclic loading is of prime importance. In this context, this chapter gives a comprehensive information about the behaviour of glass-filled epoxy composites under cyclic loading conditions along with the detailed methodology of fabricating these composites.

5.1 Background

Fatigue life of any material is expressed in two important segments, the number of load-cycles required for the crack initiation and the number of load-cycles required for failure resulting from the crack growth. The primary reason for any material to fail is related to the crack initiation. In an effort to address fatigue, it is necessary to understand the undergoing mechanisms that promote crack initiation.

Most of the existing work focuses on the investigation of the fatigue response of composite materials in terms of crack propagation where a pre-existing notch is introduced in the sample. Thus, leaving a wide gap in understanding the phenomena of crack initiation during cyclic loading conditions without the presence of a sharp notch. Also, since it has been indicated in our previous studies that the dynamic fracture toughness of epoxy composites significantly improves when reinforced with micron-sized glass particles, the fatigue response of the same needs to be investigated in sufficient detail. Therefore, it is a logical progression to investigate the crack initiation behavior and the progressive failure of particulate polymer composites under cyclic loading.

5.2 Methodolgy

5.2.1 Specimen fabrication

The particulate polymer composite used in this study is prepared by reinforcing micron-sized rod-shaped glass particles in an epoxy system. The average longitudinal dimension of the glass paricles is 800 µm and the average diameter is 10 µm with a tensile strength of around 3 GPa. The epoxy system comprised of a medium viscosity Bisphenol-A based resin (Grade-

LY556, from Huntsman) and a low viscosity aradur hardener of grade HY951 from Huntman. The density of the resin and hardener is 1150 Kg/m^3 and 980 Kg/m^3 respectively. The first step is to degass the resin in a vacuum chamber until it seems to be free from the entrapped air. Then the glass particles in different volume fractions; 0% (neat epoxy), 5%, 10% and 15% are added in the degassed epoxy resin. To ensure uniform dispersion of glass particles in the epoxy resin, a magnetic stirrer followed by an ultrasonicator is used. The mixture is again degassed to remove the air bubbles followed by the addition of hardener in the ratio of 10:1 (10 parts of hardener and 1 part of epoxy) by weight. The settlement of the glass particles is avoided by constantly stirring this mixture until it became gel-like. Then this mixture is poured into the molds and sheets having different volume fraction of glass particles (0%, 5%, 10% and 15%) are cast and cured for 48 hours. After this, the sheets are demolded and machined into specimens of desired dimensions for further testing. Figure 34 shows a schematic of all the steps followed for the fabrication of the glass-filled epoxy composite.

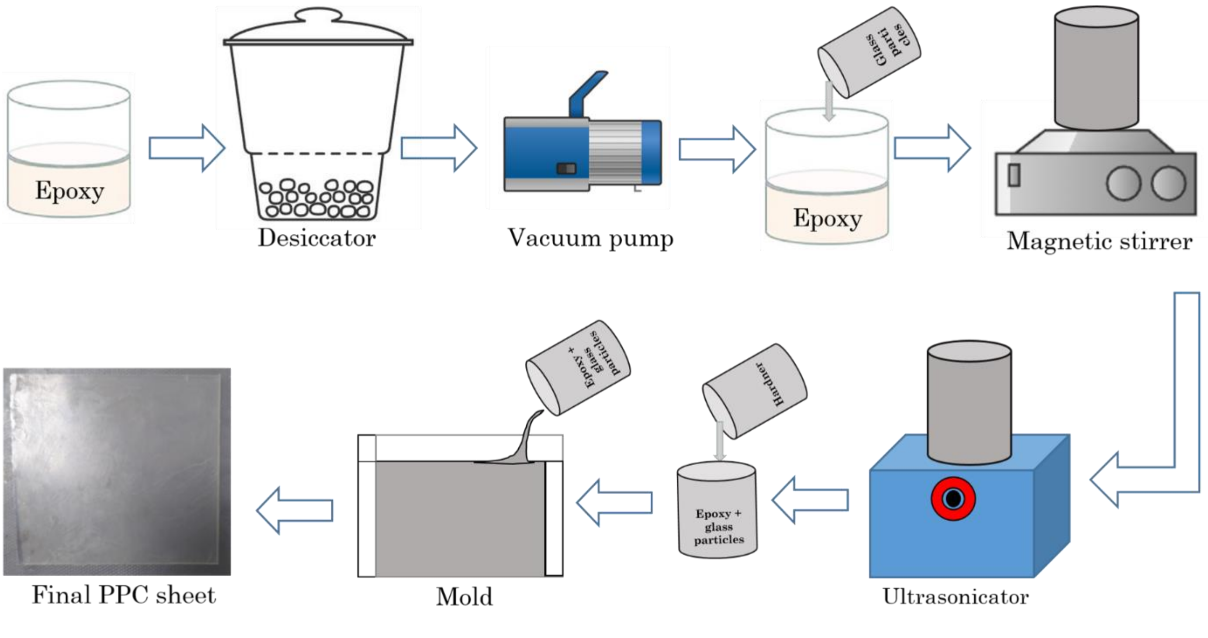

Figure 34 Schematic of the sample preparation

For performing both tensile and fatigue tests, dogbone-shaped specimens are prepared by machining the cured composite sheet. Additionally, a shallow depression is induced in the fatigue specimens within the gauge section that served as the region of interest (RoI) (refer to Figure 35) to observe crack initiation during tension-tension fatigue loading under Scanning Electron Microscope (SEM).

After machining, all the prepared specimens are polished with different grades of SiC grit paper from 100 to 2000 grit size. Afterwards, the specimens are carefully polished on a cotton cloth with 8 μm, 6 μm, 3 μm, 0.25 μm diamond paste to achieve a deformation free smooth surface. Further, the specimens are decorated with silver paste around the RoI to give a conductive path as the composite specimens are non-conductive. Finally, platinum sputtering is done on the surface of specimens to limit the charging of electrons within the RoI completely. Due to the random orientation of fibers in the epoxy matrix, different length and shape of reinforcement fibers are exposed at the surface.

5.2.2 Quasi-static tension test

A uniaxial tensile test is performed on dogbone-shaped specimens of the prepared composite to determine the Ultimate Tensile Strength (UTS), elastic modulus and the strain at failure. This test is performed using a 10 kN tensile/compression module (from Kammrath & Weiss, Germany) at a strain rate of 2.4×10^{-4}/s. Three samples of each volume fraction are tested to ensure repeatability.

5.2.3 In-situ fatigue testing

Since the study focuses on the crack-initiation phenomena, the low cycle fatigue (LCF) test is performed using 10 kN tensile/compression module under a scanning electron microscope. Tests are performed at room temperature in the displacement control mode at an average frequency of 0.25 Hz and the strain ratio (R) is maintained at 0.5. Considering the different failure strain for different specimens with varying volume fraction of the glass fillers, the mean stress in the first cycle is kept same (35 MPa) for every specimen to make a relevant comparison of the fatigue response. To observe the RoI and to capture SEM images of the undergoing deformation, crack initiation and propagation, the fatigue tests are paused after every 25 cycles. The number of cycles to crack initiation and failure are recorded and reported.

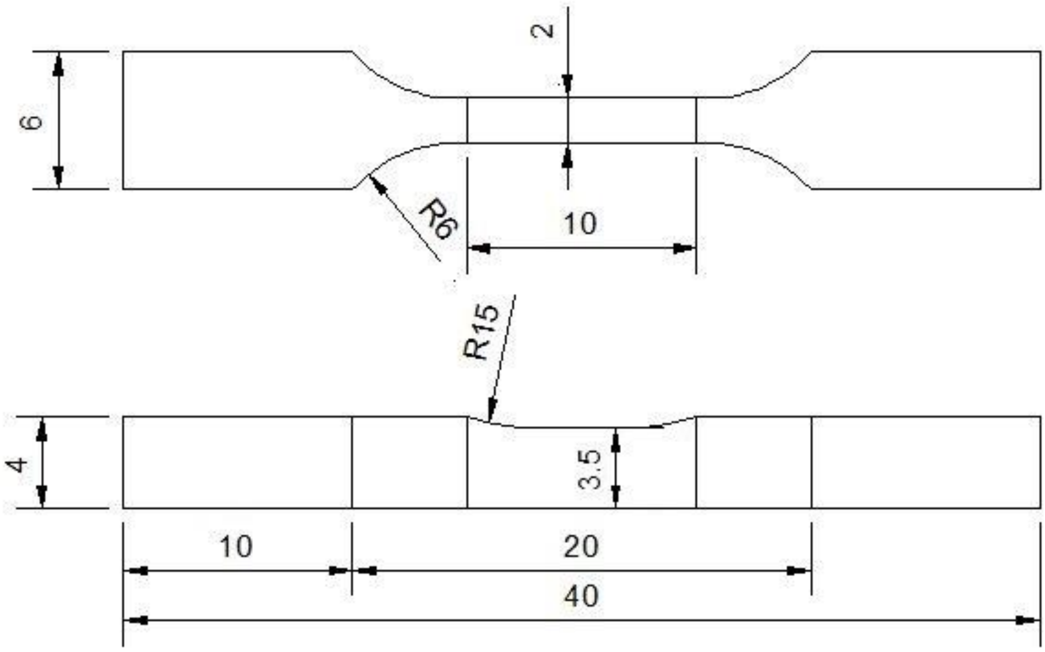

Figure 35 Detailed drawing of the specimen used for the crack initiation study [121]. All the dimensions are in mm

5.3 Results and discussions

5.3.1 Tensile test

The true stress-strain behaviour of different specimens of epoxy reinforced with rod shaped glass fillers with a volume fraction of 0%, 5%, 10% and 15% is shown in Figure 36. Out of all the specimens, neat epoxy specimens are found to have the highest ultimate tensile strength and the failure strain. Although a marginal increase in the UTS of the reinforced epoxy specimens is observed with increasing volume fraction. Also, with increasing volume fraction of the particles in the epoxy matrix, an increase in the elastic modulus is observed. This is attributed to the fact that the presence of glass particles in the epoxy matrix results in stress concentrated regions thus lowering the tensile strength. But at the same time these particles enhance the stiffness of the matrix and act as anchors to resist the stretching of the polymeric chain. This results in lower strains and is also responsible for the higher elastic modulus despite lower tensile strength [122].

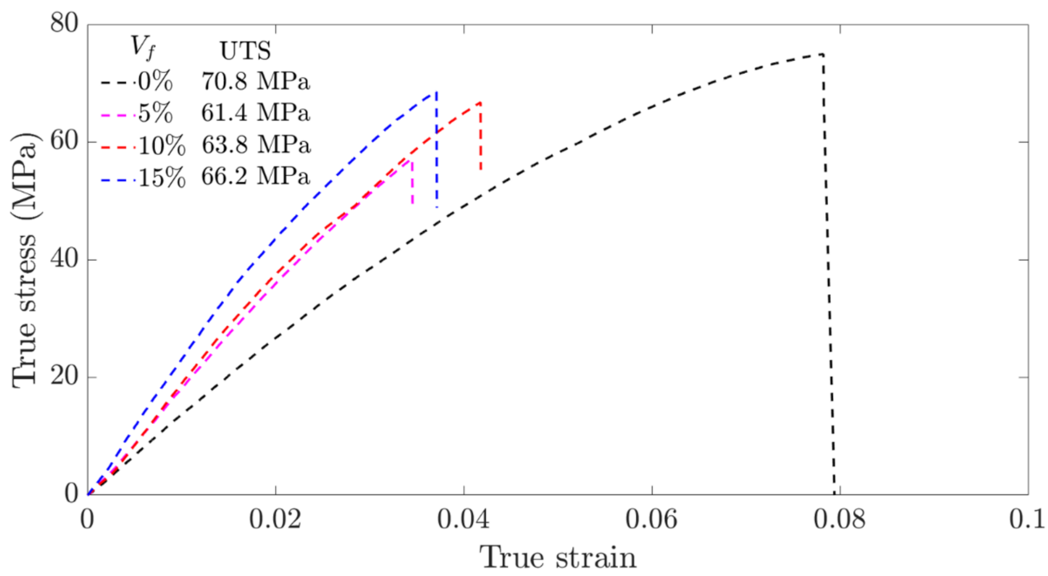

Figure 36 True stress-strain behaviour for different specimens of epoxy reinforced with rod shaped glass fillers with a volume fraction of 0%, 5%, 10% and 15%

5.3.2 Fatigue test

Corresponding to the applied cyclic loading, the total number of cycles to crack initiation and failure are recorded and reported in this section (refer to Table 3). A fractographic analysis is also presented to understand the underlying mechanisms that resulted in the initiation, coalescence and propagation of cracks at different sites and their effects on the total fatigue life. Mean stress variation in all the specimens during the entire LCF testing is shown in Figure 37. As the LCF is done in strain controlled manner, stress response is recorded throughout the fatigue life for every specimen. It is evident from the data shown in Table 3 that the average fatigue life of neat epoxy specimens is least in all the cases.

The samples with 5% V_f and 15% V_f have almost same average fatigue life but the variation in mean stress is different. Softening is observed in all the specimens, however, the 15% V_f specimens are observed to have undergone a substantially more softening compared to the other specimens. In comparison with 0% V_f , 5% V_f counterparts exhibited more softening and fatigue life. For 0% V_f and 10% V_f specimens, variation of mean stress is almost the same, but 10% V_f specimens exhibited longer fatigue life than any other specimen. Further, the number of fatigue cycles for crack initiation in all the specimens reinforced with glass fibres is same irrespective of their total fatigue life. This indicates that the variation in mean stress and total fatigue life is dependent on different volume fraction and crack propagation mechanisms. Therefore in the present study, it is found that the variation in the total failure during fatigue loading is dependent on different crack initiation sites, their distribution due to the different volume fractions, corresponding crack coalescence and propagation phase.

Table 3 Number of load cycles to crack initiation and failure

Filler volume fraction	No. of load cycles	
V_f	For crack initiation	For fracture
0%	-	190 ± 10%
5%	200 ± 14%	315 ± 14%
10%	200 ± 14%	1170 ± 16%
15%	200 ± 14%	291 ± 20%

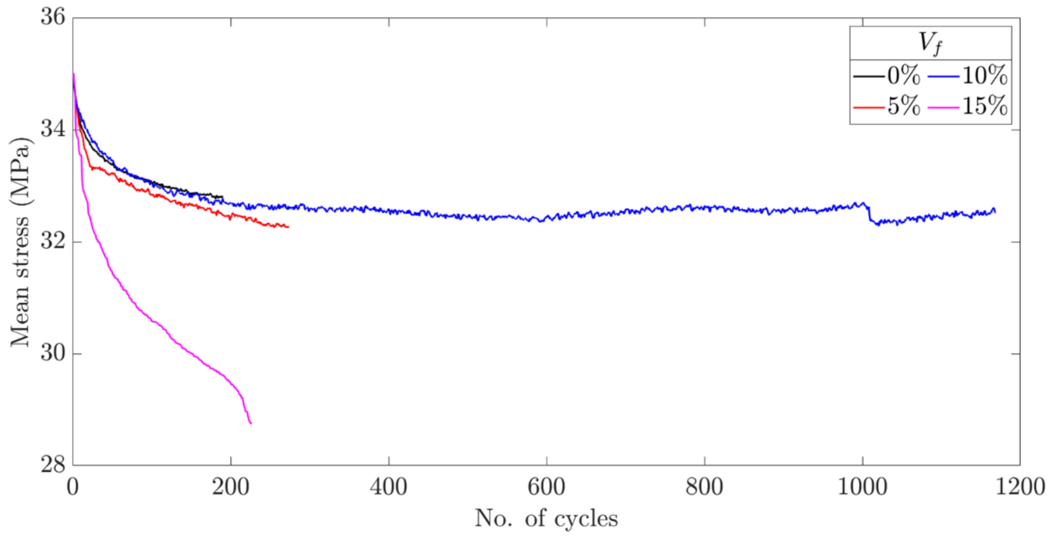

Figure 37 Variation of mean stress until fracture

5.3.2.1 Crack initiation, coalescence and propagation mechanism

Crack initiation in all the samples is observed at almost the same number of cycles except for the neat epoxy which is found to undergo a catastrophic failure without any indication of crack initiation. The reason for this failure is the inherent brittle nature of epoxy resin that offers lower fracture energy [122]. The SEM images taken during the LCF testing suggest that for different samples, crack initiates at different sites such as in the matrix, at the matrix-fiber interface and within the fiber itself.

During the cyclic loading, the neat epoxy samples failed catastrophically as the epoxy matrix cracked after a certain number of cycles and no secondary phase was available to offer crack resistance. Further, in the case of samples with 5% V_f of glass fibers, most of the cracks are observed to initiate from the interface of the matrix and fiber, while in 10% V_f case, the dominant crack initiation sites are both, the matrix-fiber interface and the fiber itself (refer to Figure 38 and Figure 39) which eventually leads to the fiber breakage. The energy requirement for different crack initiation modes is different. As reported in our previous work, the fibre-matrix interface failure mode is associated with the least energy followed by the matrix cracking, and the maximum energy is associated with the fibre breakage [1] due to higher UTS of the fiber. As the consequence of this, in 10% V_f case, the crack is arrested within the fiber and prolongs the stage of crack initiation due to which crack propagation is delayed and the specimens endure more number of loading cycles. While, in the 5% V_f case, relatively lesser number of fibers are present to arrest the crack and hence the fiber-matrix interface is where the crack is arrested before eventually leading to failure.

Figure 38 (E) and Figure 39 (G) clearly show the distribution of cracks all over the RoI in the case of 5% V_f and 10% V_f. In the case of 15% V_f, the dominant crack initiation site is observed to be the matrix-fiber interface and all the cracks initiated within a very confined region as shown in Figure 40.

In the case of 15% V_f , owing to the fact that these specimens of PPC have more fibers embedded in the matrix compared to the other two, the stress distribution is such that it leads to a localized failure. Here the glass fibers in close proximity act as crack nucleation sites that result in coalescing the micro-cracks developed at the fiber-matrix interface. In this context, in 15% V_f, due to the densely packed reinforcement, nucleation of crack results in a close network for crack initiation causing faster crack coalescence throughout the entire RoI (refer to **Error! Reference source not found.**). This results in shorter crack initiation stage and faster transition to the crack propagation stage, and thus resulting in a shorter fatigue life.

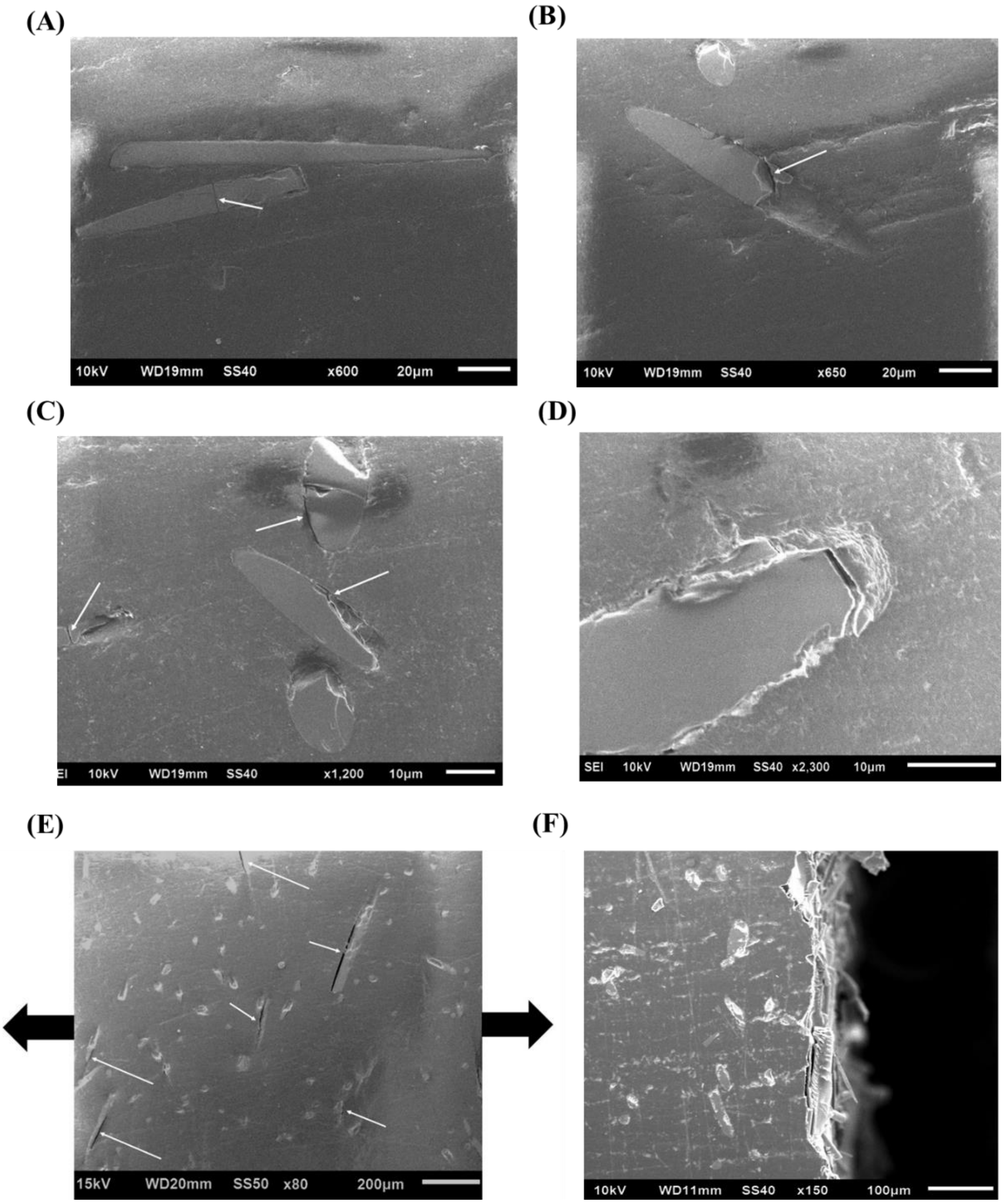

Figure 38 Crack initiation sites observed in 5% V_f specimens are indicated by white arrows. Crack initiation in the **(A), (B)** glass fiber **(C)**, **(D)** at the fiber-matrix interface and **(E)** crack distribution in the RoI with black arrows depicting the loading direction **(F)** fractured specimen showing separation through crack coalescence in matrix and the fiber-matrix interface only

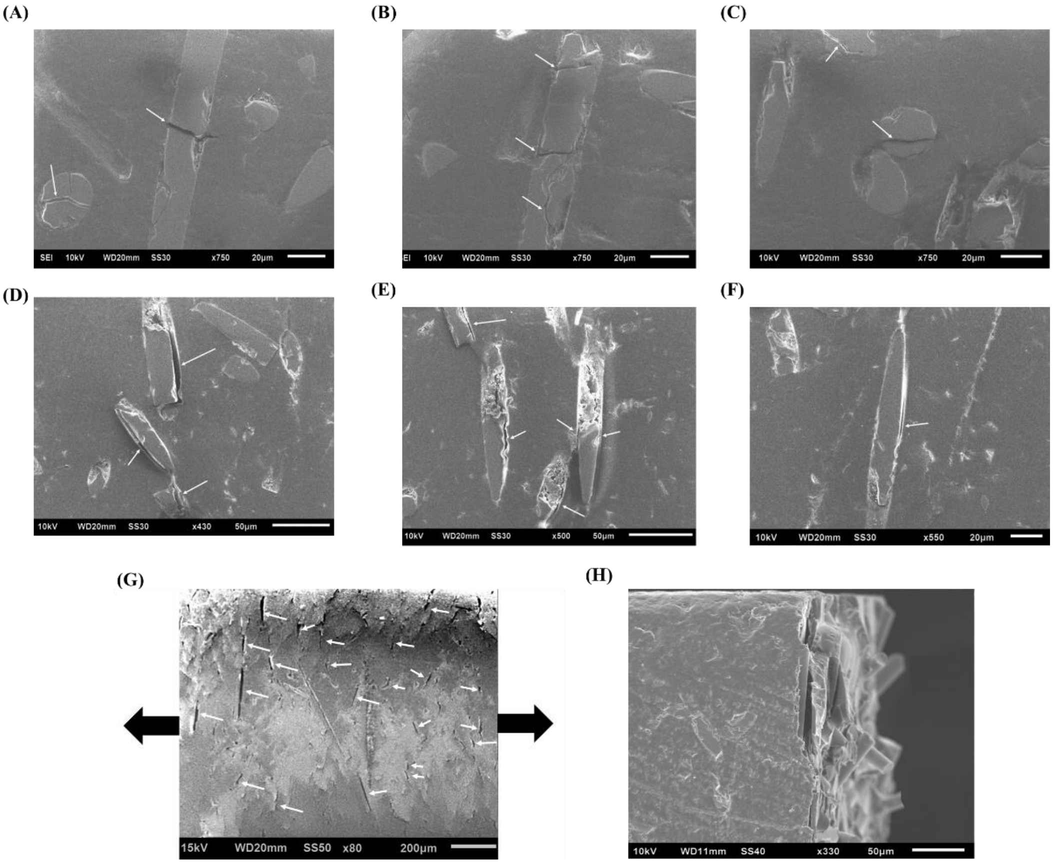

Figure 39 Crack initiation sites in 10% V_f are indicated by white arrows. Crack initiation in the **(A), (B), (C)** glass fiber **(D)**, **(E), (F)** at the fiber-matrix interface and **(G)** crack distribution in the RoI with black arrows depicting the loading direction **(H)** fractured specimen showing separation through crack coalescence in matrix and at the fiber-matrix interface

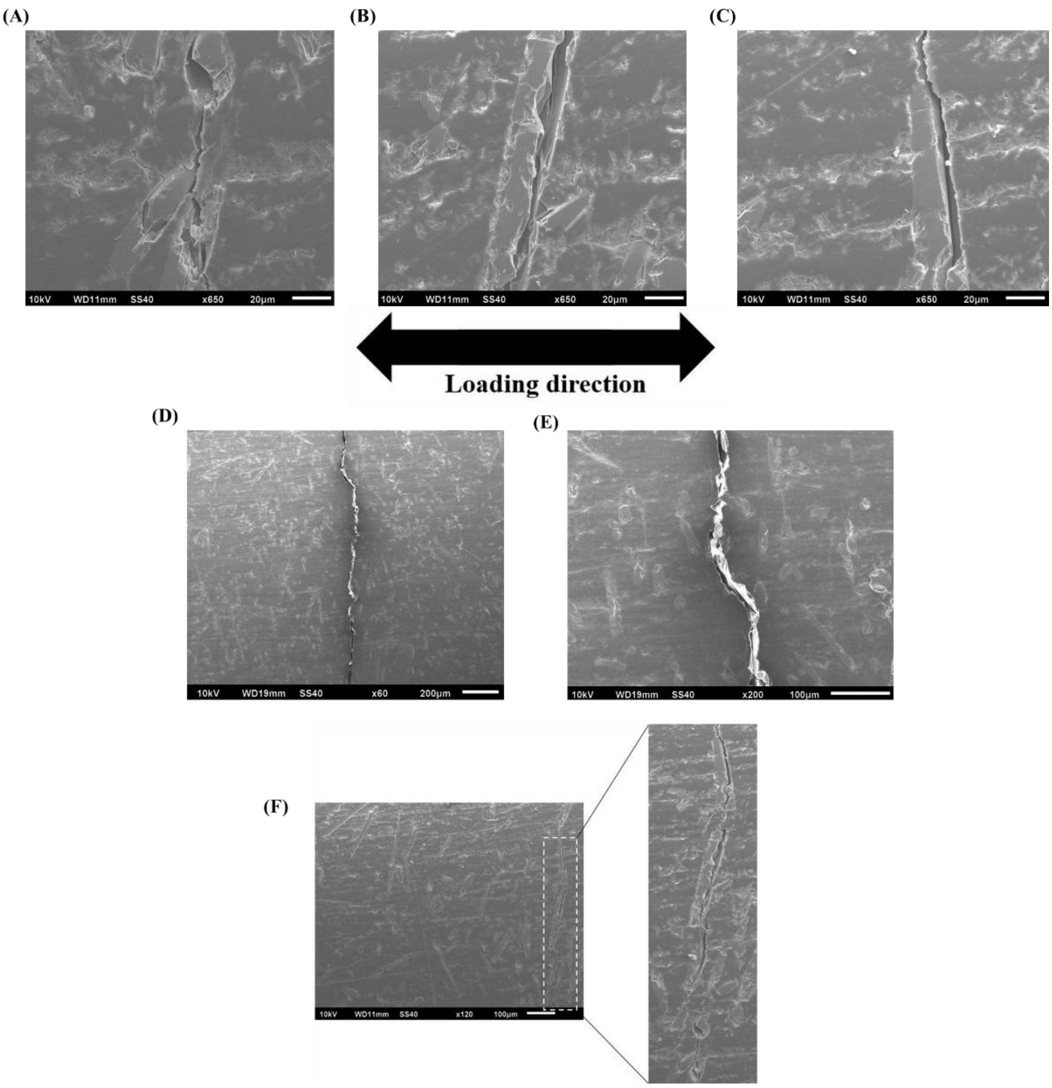

Figure 40 Crack initiation sites in 15% V_f are indicated by white arrows. Crack initiation at the **(A), (B), (C)** matrix-fiber interface**.** Propagation of crack **(D), (E)** by making a network through the cracks initiated at the interfaces due to high fiber volume fraction in 15% V_f just before the fractureare indicated by white arrows, **(F)** magnified view of the RoI

Crack propagation analysis in different specimens confirm the role of different crack initiation sites on the crack coalescence. In all the reinforced specimens, it is observed that fiber cracking does not contribute to further crack propagation as shown in **Figure *38*** Crack initiation sites observed in 5% V_f specimens are indicated by white arrows. Crack initiation in the **(A), (B)** glass fiber **(C)**, **(D)** at the fiber-matrix interface and **(E)** crack distribution in the RoI with black arrows depicting the loading direction **(F)** fractured specimen showing separation through crack coalescence in matrix and the fiber-matrix interface onlyFigure 38 (F), Figure 39 (H) and Figure 40 (F). The interfacial cracks are the ones that are majorly responsible for the crack coalescence and further propagation through the entire RoI. Similar observation is made in the case of interfacial cracks when the longitudinal length of the glass fibre reinforcement is short and aligned with the loading direction. Therefore, in Figure 41, a combined data from all the specimens tested corresponding to the angle of longitudinal axis of glass fibre with respect to the loading direction versus the length of glass fibre observed at the surface (in the ROI) for interfacial cracks is plotted. The range of fiber length observed in RoI is 10 - 310 μm. For most of the initiated cracks, the longitudinal axis of the fibers make an angle between 60º to 90º with the loading direction. Based on these observations, Figure 41 shows a probabilistic distinction between the safe zone and the crack initiation zone (encircled in red) that can affect the fatigue life of the polymer composites used in this study.

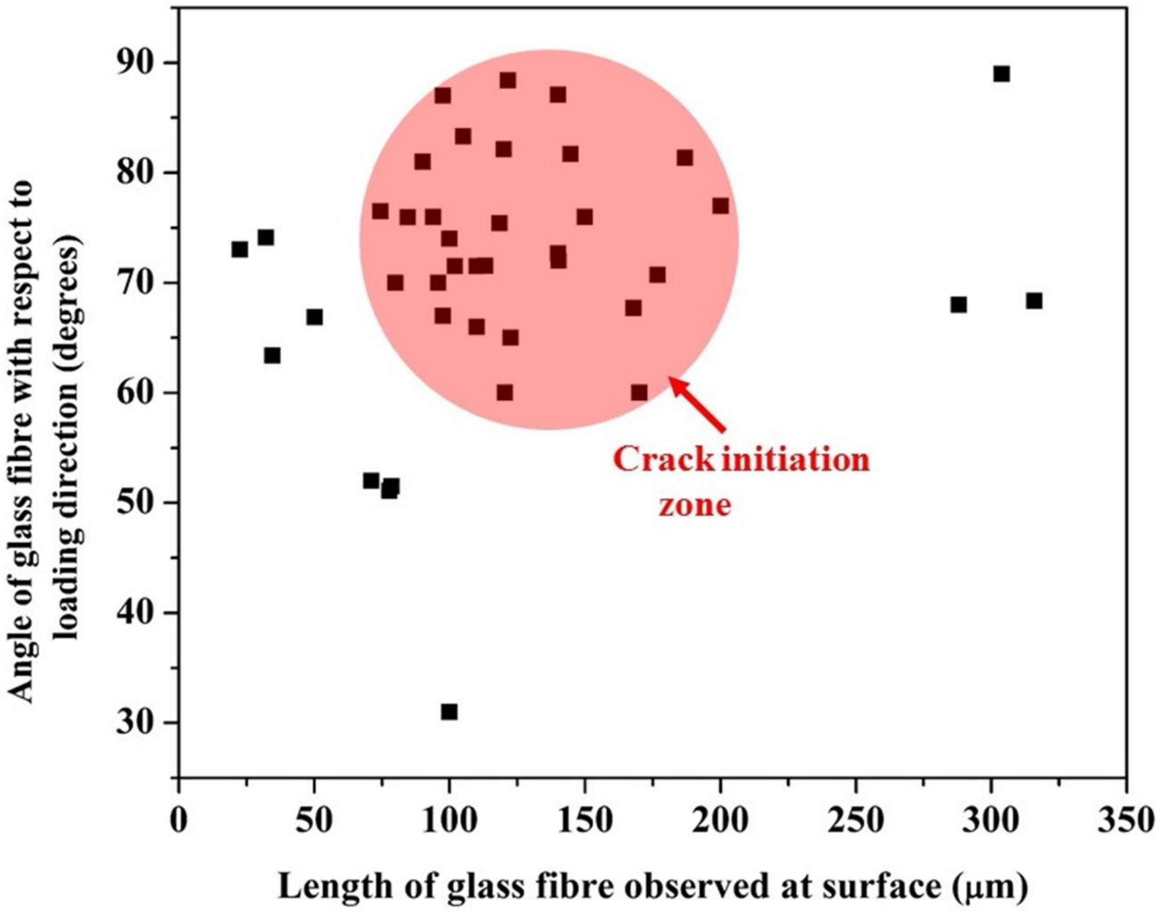

Figure 41 Variation of orientation of glass fibre reinforcement with the length of glass fibre observed at the surface for the interfacial crack initiation where the red zone is depicting the zone with higher probability of failure

Further, a detailed fractographic analysis is done to investigate the crack propagation stage and the undergoing mechanisms that resulted in initiation, coalescence and propagation of cracks at different sites. Figure 42 shows the SEM images of the fractured surfaces of the neat epoxy specimens. In Figure 42 (A), the entire cross section of 0% V_f fractured surface is shown and Figure 42 (B) shows that the crack initiates from the surface of RoI, rapidly propagates a little and results in a catastrophic failure. Figure 43 (A) shows the entire cross-section of the fractured surface of 5% V_f samples in which glass fibres are clearly visible. In Figure 43 (B) origin of crack initiation from RoI is shown and the morphology of the fractured surface clearly indicates the crack propagation direction and the region of catastrophic failure. Figure 43 (C) shows the brittle cleavage failure in 5% V_f specimen which is somewhat similar to the failure observed in case of neat epoxy.

Further, fractographs of 10% V_f (refer to Figure 44 (A), (B), (C)) and 15% V_f (refer to Figure 45 (A), (B), (C)), clearly show that the crack initiated from the surface of RoI. Figure 46 shows that in addition to fiber breakages, only a few fibers are pulled out in 10% V_f specimens. However, in 15% V_f specimens, relatively more fiber pull-out are observed along with fiber breakages (refer to Figure 46). The dominant mode of failure in case of 15% V_f specimens is observed to be the fiber-matrix interface separation. Owing to the larger volume fraction of fibers in this case, crack coalescing that occurs at the interface results in a catastrophic failure. Thus, resulting in a sharp drop in the mean stress and a shorter fatigue life. Despite all the reinforced specimens have shown same crack initiation life, the mentioned undergoing mechanisms observed during the microscopic investigations contribute to the highest fatigue life of 10% V_f specimens.

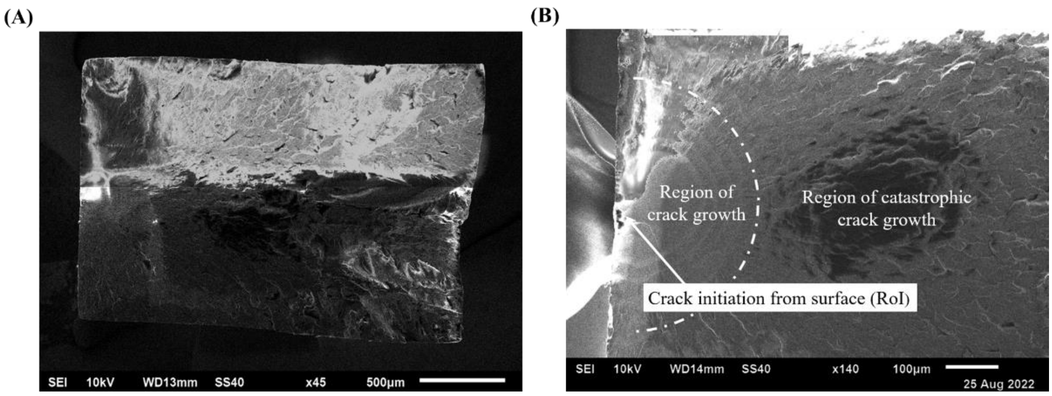

Figure 42 Fractographs of fatigue specimens of **(A)**, **(B)** 0% V_f

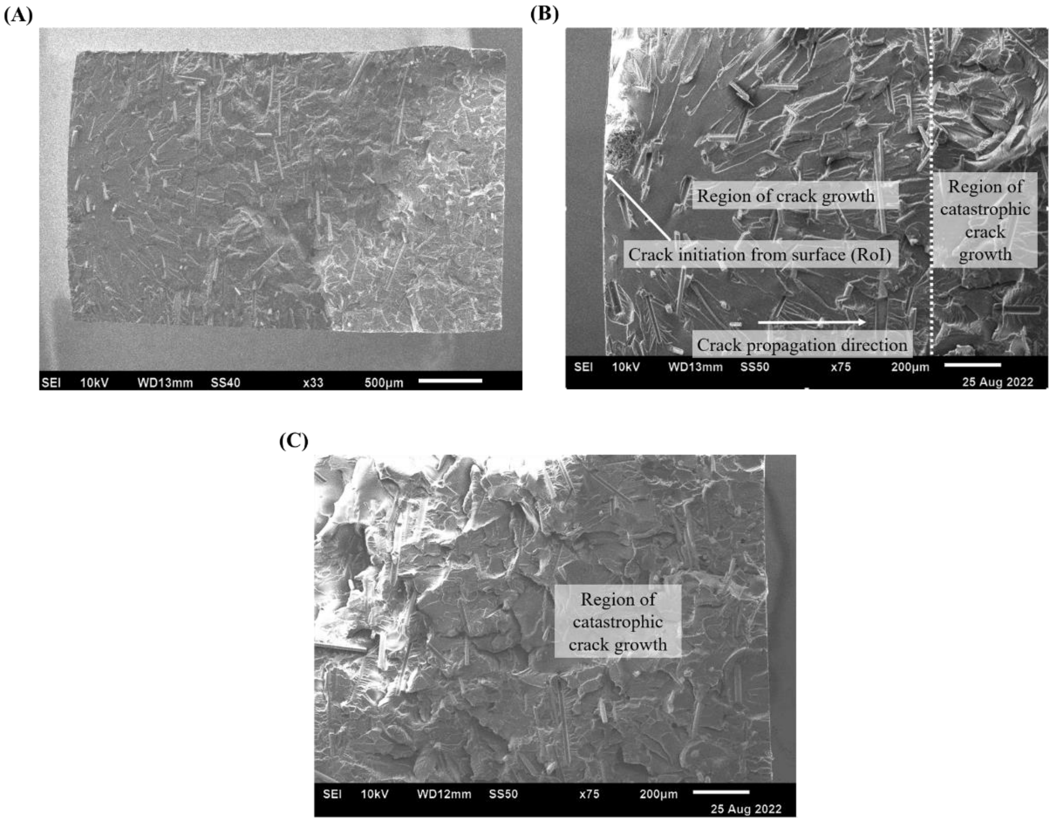

Figure 43 Fractographs of fatigue specimens of **(A)**, **(B)**, **(C)** 5% V_f

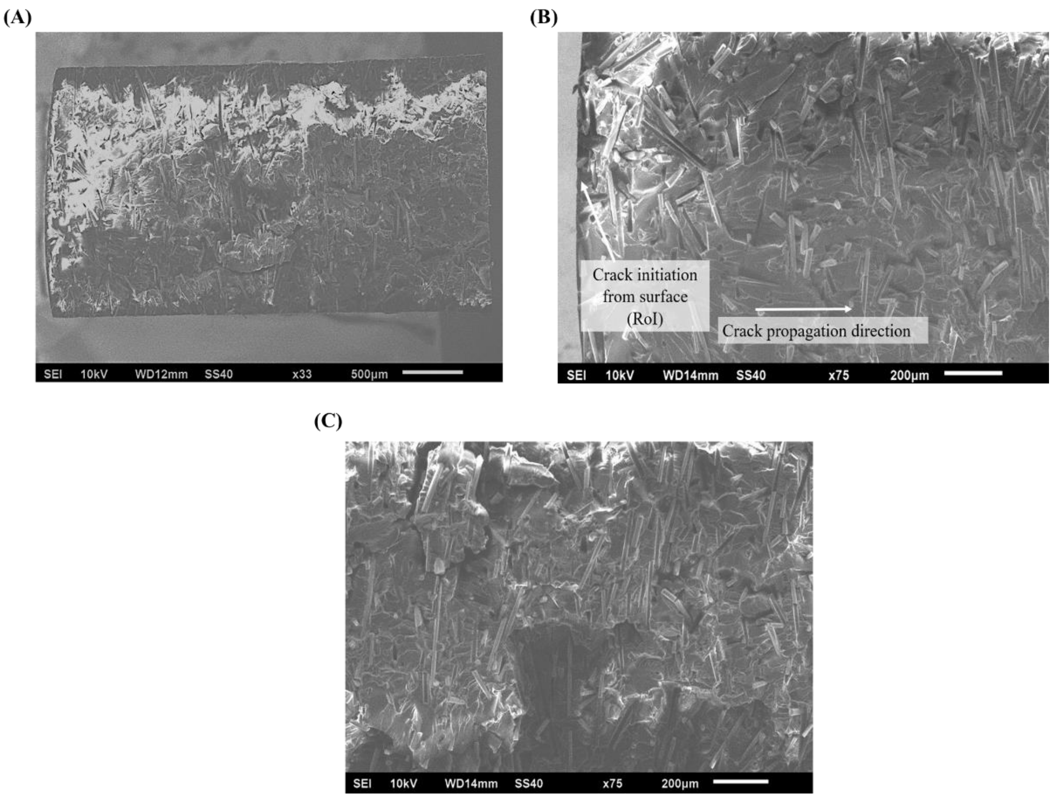

Figure 44 Fractographs of fatigue specimens of **(A)**, **(B)**, **(C)** 10% V_f

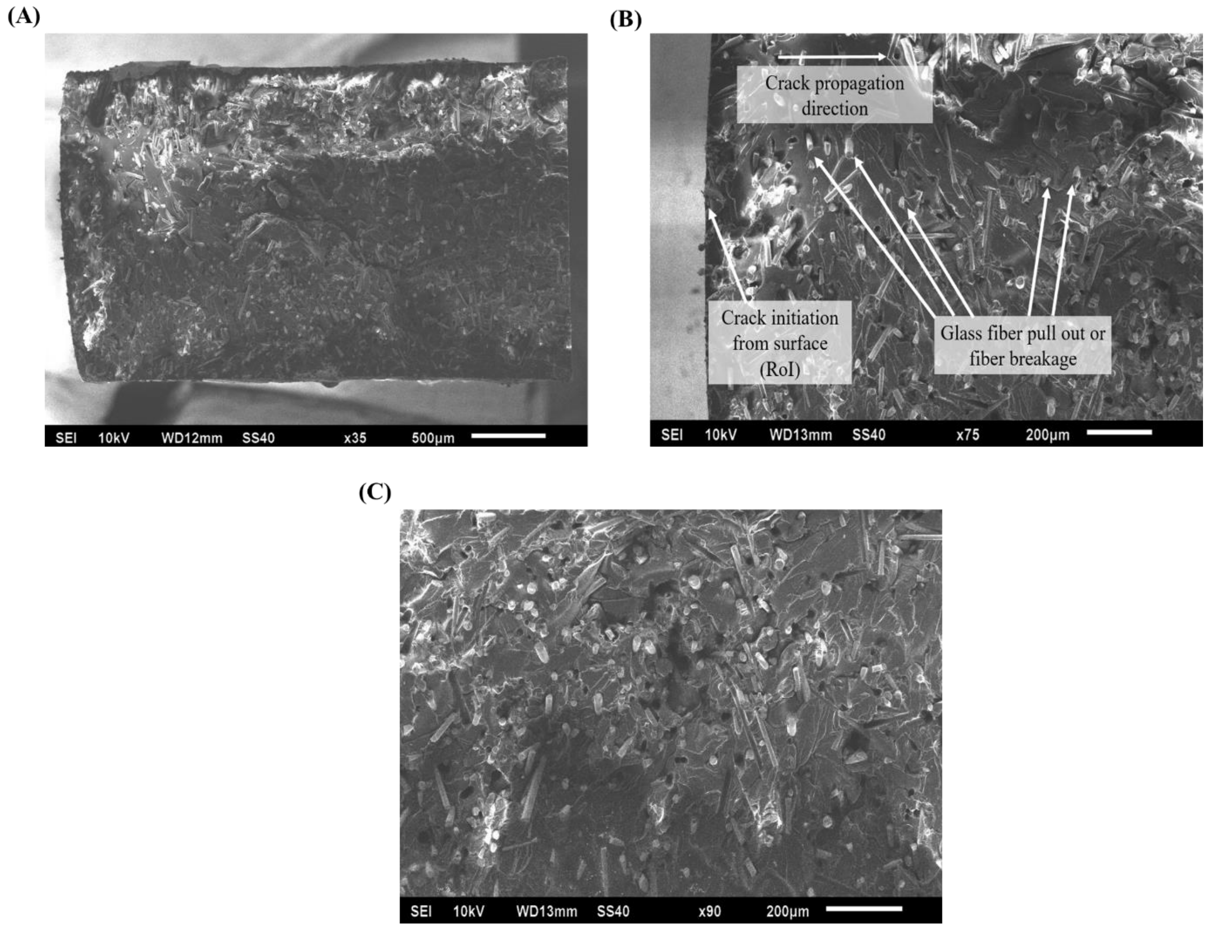

Figure 45 Fractographs of fatigue specimens of (A), (B), (C) 15% V_f

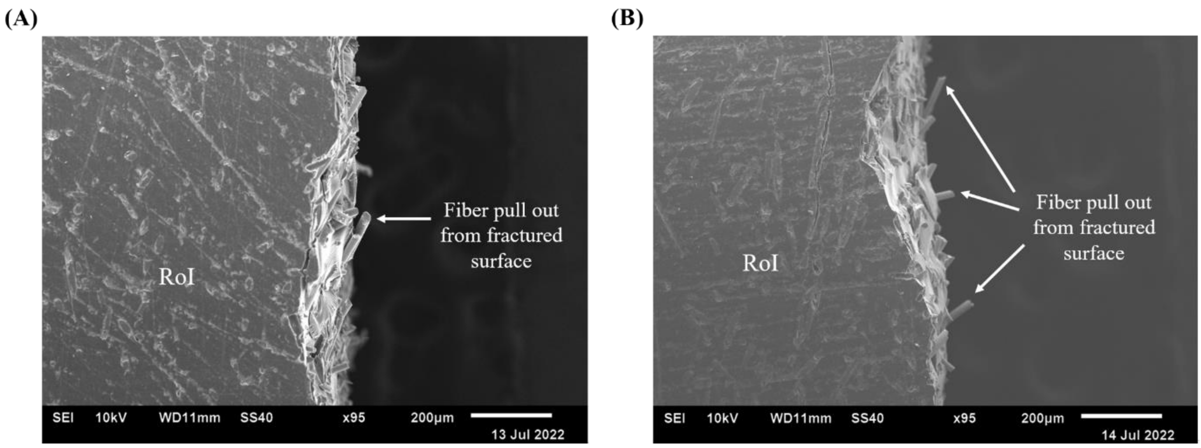

Figure 46 Fractured surface of RoI for **(A)** 10% V_f , **(B)** 15% V_f. The number of fiber pullout is higher in 15% V_f specimen due to catastrophic failure

Chapter 6

Conclusions and future scope

With a comprehensive understanding of the importance of the mechanical behaviour of particulate polymer composites under dynamic loading conditions, the current dissertation presents a robust and reliable predictive modeling framework for the investigation of the dynamic fracture toughness and an experimental study on fatigue behaviour of glass-filled epoxy composites. The proposed predictive model is developed based on a supervised machine learning algorithm, artificial neural network to successfully predict the dynamic fracture toughness corresponding to two different sets of predictor variables. Furthermore, in the interest of assessing the effect of inherent parametric stochasticity on the ultimate response of glass-filled epoxy composites, a computationally efficient framework of uncertainty quantification is presented. In addition to the investigation of fracture behavior, a crack initiation study under cyclic loading conditions indicating the fatigue response of these composites is also presented.

Conclusions stemming from these investigations are as follows:

- The first ANN model used for predicting the SIF history of the considered PPCs corresponding to the material properties is validated with the experimental results and the accuracy of the model is found to be ~91%. The normalized importance analysis results in the parameter importance order as follows: time > aspect ratio > dynamic elastic modulus > volume fraction. Also, using the same ANN architecture, predictions made for the crack initiation toughness of different aspect ratio of fillers are found to be in close agreement with the empirical results which indicate the reliability of the proposed framework.
- The second predictive model which utilized the dataset corresponding to the loading conditions has shown a prediction accuracy of ~86%. As a result of the normalized importance analysis that reflects the contribution of each input parameter in deciding the neural netwotk as per the calculated synaptic weights to predict the SIF history, the order of importance is obtained as: time > loading rate > shear wave speed > longitudinal wave speed > volume fraction.
- Results from the predictive model-I indicated that out of the three considered glass particles, spherical, flake and rod-shaped, rod-shaped particles reinforced epoxy

composite exhibited the highest dynamic fracture toughness. This finding is inline with the previously reported experimental investigation.

- Fractographic investigation has shown that the composite undergoes different failure modes in response to the applied dynamic loading. The observed failure modes are matrix cracking, filler-matrix interfacial separation, filler pull-out and filler breakages. In case of spherical glass fillers, matrix cracking and filler-matrix interfacial separation are found to be the dominating failure modes that contributed to the energy dissipation and improved the fracture toughness of the resulting composite compared to the neat epoxy counterpart. While, in the case of flake-shaped fillers, a few of the filler breakages are also observed along with the two modes mentioned in the case of spherical fillers which resulted in even more energy dissipation. In the case of rod-shaped fillers, due to the ~800 μm length of these fillers, more number of filler breakages are observed in addition to other failure modes which resulted in highest energy dissipation and hence the highest fracture toughness.
- At higher loading rate, the fillers tend to behave stiffer which results in breakage of fillers as the crack continues to grow. This results in higher energy dissipation and hence an overall increase in the crack initiation toughness is observed.

Further, a computational bridging is created between the limited experimental observations and large-scale data-driven Monte Carlo simulation to quantify the effect of inevitable uncertainties in the dynamic fracture toughness of particulate composites. This is achieved by exploiting artificial neural network as a surrogate of the original physical experiments based on advanced techniques like digital image correlation and scanning electron microscopy. The source uncertainty in critical geometric and material parameters such as aspect ratio, dynamic elastic modulus and volume fraction are captured at different time regimes and subsequently the ANN model is coupled with Monte Carlo simulation for efficient propagation and quantification of uncertainty in dynamic fracture toughness. The conclusions drawn from this experimental data-driven uncertainty quantification for dynamic fracture toughness of particulate glass-filled epoxy composites are as follows:

- The ANN model used to extract the benchmark solution for the SIF history without any stochaticity in the predictor variables has shown a prediction accuracy of ~96%.

- The effect of uncertainty in the input space has the most pronounced effect on the stress intensity factor in the pre-crack initiation regime for all the considered stochastic cases.
- Stochasticity in aspect ratio in combination with the dynamic elastic modulus have more pronounced effect on crack initiation toughness compared to the other possible individual and compound scenarios of uncertainty.
- The rod-shaped glass fillers have shown the most prominent effect of uncertainty on fracture toughness in all the considered stochastic cases.
- Aspect ratio is found to be the most sensitive input parameter in response to the inevitable stochasticity.

The experimental investigation of the fatigue response of the epoxy composites reinforced with rod-shaped glass fillers is carried out and the ultimate tensile strength of the resulting composites along with the fatigue life in terms of number of load cycles to initiate the crack and number of cycles to fracture are reported. Special attention is given to identifying the crack initiation sites and the underlying mechanisms that promote the crack growth. The major findings of this study are as follows:

- The uniaxial tensile test results reveal that the neat epoxy samples exhibit the maximum ultimate tensile strength of 70.8 MPa. In the reinforced cases, a marginal increase in the UTS is observed with the increasing volume fraction of the glass-particles, following an order of 5% (UTS = 61.4 MPa) < 10% (UTS = 63.8 MPa) < 15% (UTS = 66.2 MPa).
- With increasing volume fraction of the particles in the epoxy matrix, an increase in the elastic modulus is observed.
- Crack initiation is observed at almost the same number of cycles except for the neat epoxy samples wherein a catastrophic failure is observed. In the case, wherein 5% V_f of fillers is used, the crack initiation is observed at the matrix-filler interface. But in the case of 10% V_f, the cracks are observed within the filler as well. Moving to the 15% filler case, the crack is initiated within a confined region and due to the densely packed reinforcement the close network for crack initiation caused faster crack propagation and thus resulting in a shorter fatigue life.
- The particulate fillers are found to act as crack nucleation sites that result in coalescing the micro-cracks developed at the filler-matrix interface and within the filler itself.

- The interfacial cracks where the longitudinal length of glass fibres is nearly normal to loading axis or angle of the longitudinal axis of glass fibres with respect to loading direction is high (60º - 90º) has the highest probability of coalescence and further propagation.
- PPC with 10% volume fraction of rod-shaped glass fillers is found to exhibit the maximum fatigue life under the applied cyclic loading.

Future scope

With the above comprehensive investigations on fracture and fatigue behaviour of glass-filled epoxy composites, this research can be taken further in the following directions:

- Through independent investigation of two datasets for the importance of several input parameters, aspect ratio and loading rate are found to be the most influential ones. Thus, it is crucial to investigate the combined effect on the dynamic fracture toughness while considering both the parameters simultaneously. Another logical progression to this would be to develop a predictive modeling framework that considers the combined effect and investigate the effect of parametric uncertainty on the fracture toughness of the composite.
- Since rod-shaped fillers have shown the highest resistance to crack, effect of same shape but different aspect ratio can be further investigated.
- The current framework of uncertainty quantification addresses the parametric uncertainties efficiently and the same can be extended to investigate the effect of model uncertainties.
- Another interesting perspective would be to transform the current framework into an optimization problem where given a specific value of fracture toughness, right combination of parameters could be predicted.
- Since the fatigue response is investigated with only the rod-shaped fillers, additional experimental investigation considering the other two shapes can also be done.

Bibliography

[1] Kushvaha V. Synthesis, Processing and Dynamic Fracture Behavior of Particulate Epoxy Composites with Conventional and Hierarchical Micro-/Nano-fillers 2016.

[2] Kushvaha V, Branch A, Tippur H. Effect of Loading Rate on Dynamic Fracture Behavior of Glass and Carbon Fiber Modified Epoxy. In: Song B, Casem D, Kimberley J, editors. Dynamic Behavior of Materials, Volume 1, Springer International Publishing; 2014, p. 169–76.

[3] Tyson WR, Davies GJ. A photoelastic study of the shear stresses associated with the transfer of stress during fibre reinforcement. Br J Appl Phys 1965;16:199–205. https://doi.org/10.1088/0508-3443/16/2/313.

[4] Haque A, Ramasetty A. Theoretical study of stress transfer in carbon nanotube reinforced polymer matrix composites. Composite Structures 2005;71:68–77. https://doi.org/10.1016/j.compstruct.2004.09.029.

[5] Cowley KD, Beaumont PWR. The interlaminar and intralaminar fracture toughness of carbon-fibre/polymer composites: The effect of temperature. Composites Science and Technology 1997;57:1433–44. https://doi.org/10.1016/S0266-3538(97)00047-X.

[6] Balaganesan G, Velmurugan R, Srinivasan M, Gupta NK, Kanny K. Energy absorption and ballistic limit of nanocomposite laminates subjected to impact loading. International Journal of Impact Engineering 2014;74:57–66. https://doi.org/10.1016/j.ijimpeng.2014.02.017.

[7] Sun CT, Han C. A method for testing interlaminar dynamic fracture toughness of polymeric composites. Composites Part B: Engineering 2004;35:647–55. https://doi.org/10.1016/j.compositesb.2004.04.006.

[8] Gao J, Kedir N, Hernandez JA, Gao J, Horn T, Kim G, et al. Dynamic fracture of glass fiber-reinforced ductile polymer matrix composites and loading rate effect. Composites Part B: Engineering 2022;235:109754. https://doi.org/10.1016/j.compositesb.2022.109754.

[9] Sadowski T, Golewski P, Craciun E. Internal structure influence on the impact strength and dynamic fracture toughness of hybrid polymer matrix composites with integrated elastomer interlayers. Composite Structures 2021;258:113375. https://doi.org/10.1016/j.compstruct.2020.113375.

[10] Prasad MSS, Venkatesha CS, Jayaraju T. Experimental Methods of Determining Fracture Toughness of Fiber Reinforced Polymer Composites under Various Loading Conditions. Journal of Minerals and Materials Characterization and Engineering 2011;10:1263.

[11] Priya IIM, Vinayagam B. Enhancement of bi-axial glass fibre reinforced polymer composite with graphene platelet nanopowder modifies epoxy resin. Advances in Mechanical Engineering 2018;10:1687814018793261. https://doi.org/10.1177/1687814018793261.

[12] Argatov I. Artificial Neural Networks (ANNs) as a Novel Modeling Technique in Tribology. Front Mech Eng 2019;5. https://doi.org/10.3389/fmech.2019.00030.

[13] Altarazi S, Allaf R, Alhindawi F. Machine Learning Models for Predicting and Classifying the Tensile Strength of Polymeric Films Fabricated via Different Production Processes. Materials 2019;12:1475. https://doi.org/10.3390/ma12091475.

[14] Abueidda DW, Almasri M, Ammourah R, Ravaioli U, Jasiuk IM, Sobh NA. Prediction and optimization of mechanical properties of composites using convolutional neural networks. Composite Structures 2019;227:111264. https://doi.org/10.1016/j.compstruct.2019.111264.

[15] Bacigalupo A, Gnecco G, Lepidi M, Gambarotta L. Machine-Learning Techniques for the Optimal Design of Acoustic Metamaterials. J Optim Theory Appl 2020;187:630–53. https://doi.org/10.1007/s10957-019-01614-8.

[16] Dittanet P, Pearson RA. Effect of silica nanoparticle size on toughening mechanisms of filled epoxy. Polymer 2012;53:1890–905. https://doi.org/10.1016/j.polymer.2012.02.052.

[17] Wang F, Zhang K, Liang W, Wang Z, Tay TE, Lu S, et al. Epoxy/CNT@X nanocomposite: Improved quasi-static, dynamic fracture toughness, and conductive functionalities by non-ionic surfactant treatment. Polymer Testing 2020;81:106256. https://doi.org/10.1016/j.polymertesting.2019.106256.

[18] Sandeep B, Suresha B, Divakar HN. Fracture toughness of alumina filler filled glass fabric reinforced epoxy composites. Materials Today: Proceedings 2021;43:1792–7. https://doi.org/10.1016/j.matpr.2020.10.489.

[19] Kawaguchi T, Pearson RA. The effect of particle–matrix adhesion on the mechanical behavior of glass filled epoxies. Part 2. A study on fracture toughness. Polymer 2003;44:4239–47. https://doi.org/10.1016/S0032-3861(03)00372-0.

[20] Liang J-Z. Impact fracture toughness of hollow glass bead-filled polypropylene composites. J Mater Sci 2007;42:841–6. https://doi.org/10.1007/s10853-006-0074-z.

[21] Lauke B. On the effect of particle size on fracture toughness of polymer composites. Composites Science and Technology 2008;68:3365–72. https://doi.org/10.1016/j.compscitech.2008.09.011.

[22] Piggott MR. The effect of aspect ratio on toughness in composites. J Mater Sci 1974;9:494–502. https://doi.org/10.1007/BF00737854.

[23] Fu S-Y, Feng X-Q, Lauke B, Mai Y-W. Effects of particle size, particle/matrix interface adhesion and particle loading on mechanical properties of particulate–polymer composites. Composites Part B: Engineering 2008;39:933–61. https://doi.org/10.1016/j.compositesb.2008.01.002.

[24] Hulugappa B, Achutha MV, Suresha B. Effect of Fillers on Mechanical Properties and Fracture Toughness of Glass Fabric Reinforced Epoxy Composites. Journal of Minerals and Materials Characterization and Engineering 2016;04:1. https://doi.org/10.4236/jmmce.2016.41001.

[25] Jiang F, Vecchio KS. Hopkinson Bar Loaded Fracture Experimental Technique: A Critical Review of Dynamic Fracture Toughness Tests. Applied Mechanics Reviews 2009;62. https://doi.org/10.1115/1.3124647.

[26] Jajam KC, Tippur HV. Quasi-static and dynamic fracture behavior of particulate polymer composites: A study of nano- vs. micro-size filler and loading-rate effects. Composites Part B: Engineering 2012;43:3467–81. https://doi.org/10.1016/j.compositesb.2012.01.042.

[27] Fengchun J, Ruitang L, Xiaoxin Z, Vecchio KS, Rohatgi A. Evaluation of dynamic fracture toughness KId by Hopkinson pressure bar loaded instrumented Charpy impact test. Engineering Fracture Mechanics 2004;71:279–87. https://doi.org/10.1016/S0013-7944(03)00139-5.

[28] Kushvaha V, Tippur H. Effect of Filler Particle Shape on Dynamic Fracture Behavior of Glass-Filled Epoxy. In: Chalivendra V, Song B, Casem D, editors. Dynamic Behavior of Materials, Volume 1, Springer New York; 2013, p. 513–22.

[29] Klepaczko JR, Petrov YV, Atroshenko SA, Chevrier P, Fedorovsky GD, Krivosheev SI, et al. Behavior of particle-filled polymer composite under static and dynamic loading. Engineering Fracture Mechanics 2008;75:136–52. https://doi.org/10.1016/j.engfracmech.2007.02.016.

[30] Kitey R, Tippur HV. Role of particle size and filler–matrix adhesion on dynamic fracture of glass-filled epoxy. I. Macromeasurements. Acta Materialia 2005;53:1153–65. https://doi.org/10.1016/j.actamat.2004.11.012.

[31] Kitey R, Tippur HV. Role of particle size and filler–matrix adhesion on dynamic fracture of glass-filled epoxy. II. Linkage between macro- and micro-measurements. Acta Materialia 2005;53:1167–78. https://doi.org/10.1016/j.actamat.2004.11.011.

[32] Duan Z, He H, Liang W, Wang Z, He L, Zhang X. Tensile, Quasistatic and Dynamic Fracture Properties of Nano-Al2O3-Modified Epoxy Resin. Materials 2018;11:905. https://doi.org/10.3390/ma11060905.

[33] Lebar A, Aguiar R, Oddy A, Petel OE. Particle surface effects on the spall strength of particle-reinforced polymer matrix composites. International Journal of Impact Engineering 2021;150:103801. https://doi.org/10.1016/j.ijimpeng.2020.103801.

[34] Yesgat AL, Kitey R. Effect of filler geometry on fracture mechanisms in glass particle filled epoxy composites. Engineering Fracture Mechanics 2016;160:22–41. https://doi.org/10.1016/j.engfracmech.2016.03.034.

[35] Vu-Khanh T. Toughness of Flake-Reinforced Polypropylene: Journal of Thermoplastic Composite Materials 2016. https://doi.org/10.1177/089270579100400103.

[36] Katoueizadeh E, Zebarjad SM, Janghorban K. Mechanical properties of epoxy composites embedded with functionalized urea-formaldehyde microcapsules containing an oxidizable oil. Materials Chemistry and Physics 2021;260:124106. https://doi.org/10.1016/j.matchemphys.2020.124106.

[37] Jajam KC, Tippur HV. Role of inclusion stiffness and interfacial strength on dynamic matrix crack growth: An experimental study. International Journal of Solids and Structures 2012;49:1127–46. https://doi.org/10.1016/j.ijsolstr.2012.01.009.

[38] Majer Z, majer@fme.vutbr.cz E, Hutař P, Náhlík L. Determination of the Effect of Interphase on the Fracture Toughness and Stiffness of a Particulate Polymer Composite. Mech Compos Mater 2013;49:475–82. https://doi.org/10.1007/s11029-013-9364-0.

[39] Bie BX, Han JH, Lu L, Zhou XM, Qi ML, Zhang Z, et al. Dynamic fracture of carbon nanotube/epoxy composites under high strain-rate loading. Composites Part A: Applied Science and Manufacturing 2015;68:282–8. https://doi.org/10.1016/j.compositesa.2014.10.001.

[40] Owens AT, Tippur HV. A Tensile Split Hopkinson Bar for Testing Particulate Polymer Composites Under Elevated Rates of Loading. Exp Mech 2008;49:799. https://doi.org/10.1007/s11340-008-9192-7.

[41] Lee D, Tippur H, Bogert P. Quasi-static and dynamic fracture of graphite/epoxy composites: An optical study of loading-rate effects. Composites Part B: Engineering 2010;41:462–74. https://doi.org/10.1016/j.compositesb.2010.05.007.

[42] Lee D, Tippur HV, Jensen BJ, Bogert PB. Tensile and Fracture Characterization of PETI-5 and IM7/PETI-5 Graphite/Epoxy Composites Under Quasi-Static and Dynamic Loading Conditions. Journal of Engineering Materials and Technology 2011;133. https://doi.org/10.1115/1.4003487.

[43] Kushvaha V, Tippur H. Effect of filler shape, volume fraction and loading rate on dynamic fracture behavior of glass-filled epoxy. Composites Part B: Engineering 2014;64:126–37. https://doi.org/10.1016/j.compositesb.2014.04.016.

[44] Hutař P, Náhlík L, Majer Z, Knésl Z. The Effect of an Interphase on Micro-Crack Behaviour in Polymer Composites. In: Murín J, Kompiš V, Kutiš V, editors. Computational Modeling and Advanced Simulations, Dordrecht: Springer Netherlands; 2011, p. 83–97. https://doi.org/10.1007/978-94-007-0317-9_5.

[45] Tanimoto Y, Kitagawa T, Aida M, Nishiyama N. Experimental and computational approach for evaluating the mechanical characteristics of dental composite resins with various filler sizes. Acta Biomaterialia 2006;2:633–9. https://doi.org/10.1016/j.actbio.2006.06.006.

[46] Cho J, Joshi MS, Sun CT. Effect of inclusion size on mechanical properties of polymeric composites with micro and nano particles. Composites Science and Technology 2006;66:1941–52. https://doi.org/10.1016/j.compscitech.2005.12.028.

[47] Zhang MH, Chen JK. Analysis of interfacial fracture strength of an inclusion in a polymeric composite considering cohesive force. Computational Materials Science 2012;61:6–11. https://doi.org/10.1016/j.commatsci.2012.03.017.

[48] Pazhouheshgar A, Vanini SAS, Moghanian A. The experimental and numerical study of fracture behavior of 58s bioactive glass/polysulfone composite using the extended finite elements method. Mater Res Express 2019;6:095208. https://doi.org/10.1088/2053-1591/ab3495.

[49] Yang Z, Kang G, Liu R, Chen P. Predicting the mechanical behaviour of highly particle-filled polymer composites using the nonlinear finite element method. Composite Structures 2022;286:115275. https://doi.org/10.1016/j.compstruct.2022.115275.

[50] Ghassemieh E, Naseehi V. Prediction of failure and fracture mechanisms of polymeric composites using finite element analysis. Part 1: Particulate filled composites. Polymer Composites 2001;22:528–41. https://doi.org/10.1002/pc.10557.

[51] Ponnusami SA, Turteltaub S, van der Zwaag S. Cohesive-zone modeling of crack nucleation and propagation in particulate composites. Engineering Fracture Mechanics 2015;149:170–90. https://doi.org/10.1016/j.engfracmech.2015.09.050.

[52] Ju JW, Lee HK. A micromechanical damage model for effective elastoplastic behavior of ductile matrix composites considering evolutionary complete particle debonding. Computer Methods in Applied Mechanics and Engineering 2000;183:201–22. https://doi.org/10.1016/S0045-7825(99)00219-4.

[53] Lee K, Moorthy S, Ghosh S. Multiple scale computational model for damage in composite materials. Computer Methods in Applied Mechanics and Engineering 1999;172:175–201. https://doi.org/10.1016/S0045-7825(98)00229-1.

[54] Tavarez FA, Plesha ME. Discrete element method for modeling solid and particulate materials. International Journal for Numerical Methods in Engineering 2007;70:379–404. https://doi.org/10.1002/nme.1881.

[55] Wolff MFH, Salikov V, Antonyuk S, Heinrich S, Schneider GA. Three-dimensional discrete element modeling of micromechanical bending tests of ceramic–polymer composite materials. Powder Technology 2013;248:77–83. https://doi.org/10.1016/j.powtec.2013.07.009.

[56] Dai G, Mishnaevsky L. Damage evolution in nanoclay-reinforced polymers: A three-dimensional computational study. Composites Science and Technology 2013;74:67–77. https://doi.org/10.1016/j.compscitech.2012.10.003.

[57] Kakavas PA, Kontoni D-PN. Numerical investigation of the stress field of particulate reinforced polymeric composites subjected to tension. International Journal for Numerical Methods in Engineering 2006;65:1145–64. https://doi.org/10.1002/nme.1483.

[58] Ghajari M, Iannucci L, Curtis P. A peridynamic material model for the analysis of dynamic crack propagation in orthotropic media. Computer Methods in Applied Mechanics and Engineering 2014;276:431–52. https://doi.org/10.1016/j.cma.2014.04.002.

[59] Nafar Dastgerdi J, Anbarlooie B, Marzban S, Marquis G. Mechanical and real microstructure behavior analysis of particulate-reinforced nanocomposite considering debonding damage based on cohesive finite element method. Composite Structures 2015;122:518–25. https://doi.org/10.1016/j.compstruct.2014.12.009.

[60] Cannillo V, Bondioli F, Lusvarghi L, Montorsi M, Avella M, Errico ME, et al. Modeling of ceramic particles filled polymer–matrix nanocomposites. Composites Science and Technology 2006;66:1030–7. https://doi.org/10.1016/j.compscitech.2005.07.030.

[61] Wang Y-F, Yang Z-G. Finite element model of erosive wear on ductile and brittle materials. Wear 2008;265:871–8. https://doi.org/10.1016/j.wear.2008.01.014.

[62] Bansal M, Singh IV, Mishra BK, Bordas SPA. A parallel and efficient multi-split XFEM for 3-D analysis of heterogeneous materials. Computer Methods in Applied Mechanics and Engineering 2019;347:365–401. https://doi.org/10.1016/j.cma.2018.12.023.

[63] Msekh MA, Silani M, Jamshidian M, Areias P, Zhuang X, Zi G, et al. Predictions of J integral and tensile strength of clay/epoxy nanocomposites material using phase field model. Composites Part B: Engineering 2016;93:97–114. https://doi.org/10.1016/j.compositesb.2016.02.022.

[64] Hamdia KM, Msekh MA, Silani M, Vu-Bac N, Zhuang X, Nguyen-Thoi T, et al. Uncertainty quantification of the fracture properties of polymeric nanocomposites based on phase field modeling. Composite Structures 2015;133:1177–90. https://doi.org/10.1016/j.compstruct.2015.08.051.

[65] Rizzi E, Papa E, Corigliano A. Mechanical behavior of a syntactic foam: experiments and modeling. International Journal of Solids and Structures 2000;37:5773–94. https://doi.org/10.1016/S0020-7683(99)00264-4.

[66] Arencón D, Velasco JI. Fracture Toughness of Polypropylene-Based Particulate Composites. Materials 2009;2:2046–94. https://doi.org/10.3390/ma2042046.

[67] Lauke B, Fu S-Y. Aspects of fracture toughness modeling of particle filled polymer composites. Composites Part B: Engineering 2013;45:1569–74. https://doi.org/10.1016/j.compositesb.2012.07.021.

[68] Meng Q, Wang T. An improved crack-bridging model for rigid particle-polymer composites. Engineering Fracture Mechanics 2019;211:291–302. https://doi.org/10.1016/j.engfracmech.2019.02.028.

[69] Ayyar A, Chawla N. Microstructure-based modeling of the influence of particle spatial distribution and fracture on crack growth in particle-reinforced composites. Acta Materialia 2007;55:6064–73. https://doi.org/10.1016/j.actamat.2007.06.044.

[70] Mishnaevsky L. Nanostructured interfaces for enhancing mechanical properties of composites: Computational micromechanical studies. Composites Part B: Engineering 2015;68:75–84. https://doi.org/10.1016/j.compositesb.2014.08.029.

[71] Segurado J, LLorca J. Computational micromechanics of composites: The effect of particle spatial distribution. Mechanics of Materials 2006;38:873–83. https://doi.org/10.1016/j.mechmat.2005.06.026.

[72] Arash B, Exner W, Rolfes R. A finite deformation phase-field fracture model for the thermo-viscoelastic analysis of polymer nanocomposites. Computer Methods in Applied Mechanics and Engineering 2021;381:113821. https://doi.org/10.1016/j.cma.2021.113821.

[73] Raffaelli C, Bose A, Vrusch CHMP, Ciarella S, Davris T, Tito NB, et al. Rheology, Rupture, Reinforcement and Reversibility: Computational Approaches for Dynamic Network Materials. In: Creton C, Okay O, editors. Self-Healing and Self-Recovering Hydrogels, Cham: Springer International Publishing; 2020, p. 63–126. https://doi.org/10.1007/12_2020_61.

[74] Nayak R, Tarkes DP, Satapathy A. A computational and experimental investigation on thermal conductivity of particle reinforced epoxy composites. Computational Materials Science 2010;48:576–81. https://doi.org/10.1016/j.commatsci.2010.02.025.

[75] Mital SK, Murthy PLN, Goldberg RK. Micromechanics for Particulate-Reinforced Composites. Mechanics of Composite Materials and Structures 1997;4:251–66. https://doi.org/10.1080/10759419708945883.

[76] Patnaik A, Satapathy A, Chand N, Barkoula NM, Biswas S. Solid particle erosion wear characteristics of fiber and particulate filled polymer composites: A review. Wear 2010;268:249–63. https://doi.org/10.1016/j.wear.2009.07.021.

[77] Mishnaevsky L, Dai G. Hybrid and hierarchical nanoreinforced polymer composites: Computational modeling of structure–properties relationships. Composite Structures 2014;117:156–68. https://doi.org/10.1016/j.compstruct.2014.06.027.

[78] Tzetzis D, Tsongas K, Mansour G. Determination of the Mechanical Properties of Epoxy Silica Nanocomposites through FEA-Supported Evaluation of Ball Indentation Test Results. Mat Res 2017;20:1571–8. https://doi.org/10.1590/1980-5373-MR-2017-0454.

[79] Wiangkham A, Ariyarit A, Aengchuan P. Prediction of the mixed mode I/II fracture toughness of PMMA by an artificial intelligence approach. Theoretical and Applied Fracture Mechanics 2021;112:102910. https://doi.org/10.1016/j.tafmec.2021.102910.

[80] Daghigh V, Lacy TE, Daghigh H, Gu G, Baghaei KT, Horstemeyer MF, et al. Machine learning predictions on fracture toughness of multiscale bio-nano-composites. Journal of Reinforced Plastics and Composites 2020;39:587–98. https://doi.org/10.1177/0731684420915984.

[81] Cidade RA, Castro DSV, Castrodeza EM, Kuhn P, Catalanotti G, Xavier J, et al. Determination of mode I dynamic fracture toughness of IM7-8552 composites by digital image correlation and machine learning. Composite Structures 2019;210:707–14. https://doi.org/10.1016/j.compstruct.2018.11.089.

[82] Hamdia KM, Silani M, Zhuang X, He P, Rabczuk T. Stochastic analysis of the fracture toughness of polymeric nanoparticle composites using polynomial chaos expansions. Int J Fract 2017;206:215–27. https://doi.org/10.1007/s10704-017-0210-6.

[83] Pruksawan S, Wang F. Modeling of toughening effect in rigid particulate-filled polymer composites by artificial intelligence: a review. Advanced Composite Materials 2022;0:1–18. https://doi.org/10.1080/09243046.2022.2083304.

[84] Hamdia KM, Lahmer T, Nguyen-Thoi T, Rabczuk T. Predicting the fracture toughness of PNCs: A stochastic approach based on ANN and ANFIS. Computational Materials Science 2015;102:304–13. https://doi.org/10.1016/j.commatsci.2015.02.045.

[85] Jin K, Luo H, Wang Z, Wang H, Tao J. Composition optimization of a high-performance epoxy resin based on molecular dynamics and machine learning. Materials & Design 2020;194:108932. https://doi.org/10.1016/j.matdes.2020.108932.

[86] Blackman BRK, Kinloch AJ, Sohn Lee J, Taylor AC, Agarwal R, Schueneman G, et al. The fracture and fatigue behaviour of nano-modified epoxy polymers. J Mater Sci 2007;42:7049–51. https://doi.org/10.1007/s10853-007-1768-6.

[87] Boonyapookana A, Nagata K, Mutoh Y. Fatigue crack growth behavior of silica particulate reinforced epoxy resin composite. Composites Science and Technology 2011;71:1124–31. https://doi.org/10.1016/j.compscitech.2011.02.015.

[88] Verma V, Sharma C. Fatigue behavior of epoxy alumina nanocomposite – role of particle morphology. Theoretical and Applied Fracture Mechanics 2020;110:102807. https://doi.org/10.1016/j.tafmec.2020.102807.

[89] Basaran C, Nie S, Hutchins CS, Ergün H. Influence of Interfacial Bond Strength on Fatigue Life and Thermo-Mechanical Behavior of a Particulate Composite: An Experimental Study. International Journal of Damage Mechanics 2008;17:123–47. https://doi.org/10.1177/1056789507077437.

[90] Bellemare SC, Bureau MN, Denault J, Dickson JI. Fatigue crack initiation and propagation in polyamide-6 and in polyamide-6 nanocomposites. Polymer Composites 2004;25:433–41. https://doi.org/10.1002/pc.20036.

[91] Bortz DR, Merino C, Martin-Gullon I. Carbon nanofibers enhance the fracture toughness and fatigue performance of a structural epoxy system. Composites Science and Technology 2011;71:31–8. https://doi.org/10.1016/j.compscitech.2010.09.015.

[92] Moloney AC, Kausch HH, Kaiser T, Beer HR. Parameters determining the strength and toughness of particulate filled epoxide resins. J Mater Sci 1987;22:381–93. https://doi.org/10.1007/BF01160743.

[93] Zhao S, Schadler LS, Hillborg H, Auletta T. Improvements and mechanisms of fracture and fatigue properties of well-dispersed alumina/epoxy nanocomposites. Composites Science and Technology 2008;68:2976–82. https://doi.org/10.1016/j.compscitech.2008.07.010.

[94] Gadaree KP, Salee G. Fatigue crack propagation in composites with spherical fillers—part 1. Polymer Composites 1983;4:19–25. https://doi.org/10.1002/pc.750040104.

[95] Brown EN, White SR, Sottos NR. Retardation and repair of fatigue cracks in a microcapsule toughened epoxy composite – Part I: Manual infiltration. Composites Science and Technology 2005;65:2466–73. https://doi.org/10.1016/j.compscitech.2005.04.020.

[96] Antunes FV, Ferreira JM, Costa JD, Capela C. Fatigue life predictions in polymer particle composites. International Journal of Fatigue 2002;24:1095–105. https://doi.org/10.1016/S0142-1123(02)00016-6.

[97] Nishioka T, Atluri SN. Path-independent integrals, energy release rates, and general solutions of near-tip fields in mixed-mode dynamic fracture mechanics. Engineering Fracture Mechanics 1983;18:1–22. https://doi.org/10.1016/0013-7944(83)90091-7.

[98] Fracture Mechanics: Fundamentals and Applications. Routledge & CRC Press n.d. https://www.routledge.com/Fracture-Mechanics-Fundamentals-and-Applications/Janssen-Zuidema-Wanhill/p/book/9780415346221 (accessed August 25, 2022).

[99] Zhang Z, Friedrich K. Artificial neural networks applied to polymer composites: a review. Composites Science and Technology 2003;63:2029–44. https://doi.org/10.1016/S0266-3538(03)00106-4.

[100] Tang H, Lin Y, Andrews C, Sodano HA. Nanocomposites with increased energy density through high aspect ratio PZT nanowires. Nanotechnology 2010;22:015702. https://doi.org/10.1088/0957-4484/22/1/015702.

[101] Guth E. Theory of Filler Reinforcement. Journal of Applied Physics 1945;16:20–5. https://doi.org/10.1063/1.1707495.

[102] Zhu Y, Bakis CE, Adair JH. Effects of carbon nanofiller functionalization and distribution on interlaminar fracture toughness of multi-scale reinforced polymer composites. Carbon 2012;50:1316–31. https://doi.org/10.1016/j.carbon.2011.11.001.

[103] Trinchero R, Larbi M, Torun HM, Canavero FG, Swaminathan M. Machine Learning and Uncertainty Quantification for Surrogate Models of Integrated Devices With a Large Number of Parameters. IEEE Access 2019;7:4056–66. https://doi.org/10.1109/ACCESS.2018.2888903.

[104] Sharma A, Mukhopadhyay T, Rangappa SM, Siengchin S, Kushvaha V. Advances in Computational Intelligence of Polymer Composite Materials: Machine Learning Assisted Modeling, Analysis and Design. Arch Computat Methods Eng 2022. https://doi.org/10.1007/s11831-021-09700-9.

[105] Scarth C, Cooper JE, Weaver PM, Silva GHC. Uncertainty quantification of aeroelastic stability of composite plate wings using lamination parameters. Composite Structures 2014;116:84–93. https://doi.org/10.1016/j.compstruct.2014.05.007.

[106] Sampaio L (Luiz). Eigenvector perturbation methodology for uncertainty quantification of turbulence models n.d.

[107] Najm HN. Uncertainty Quantification and Polynomial Chaos Techniques in Computational Fluid Dynamics. Annual Review of Fluid Mechanics 2009;41:35–52. https://doi.org/10.1146/annurev.fluid.010908.165248.

[108] Karsh PK, Kumar RR, Dey S. Radial Basis Function-Based Stochastic Natural Frequencies Analysis of Functionally Graded Plates. Int J Comput Methods 2020;17:1950061. https://doi.org/10.1142/S0219876219500610.

[109] Dey S, Naskar S, Mukhopadhyay T, Gohs U, Spickenheuer A, Bittrich L, et al. Uncertain natural frequency analysis of composite plates including effect of noise – A polynomial neural network approach. Compos Struct 2016;143:130–42. https://doi.org/10.1016/j.compstruct.2016.02.007.

[110] Dey S, Mukhopadhyay T, Khodaparast HH, Adhikari S. Fuzzy uncertainty propagation in composites using Gram–Schmidt polynomial chaos expansion. Applied Mathematical Modeling 2016;40:4412–28. https://doi.org/10.1016/j.apm.2015.11.038.

[111] Cunha A, Nasser R, Sampaio R, Lopes H, Breitman K. Uncertainty quantification through the Monte Carlo method in a cloud computing setting. Computer Physics Communications 2014;185:1355–63. https://doi.org/10.1016/j.cpc.2014.01.006.

[112] Mukhopadhyay T, Chakraborty S, Dey S, Adhikari S, Chowdhury R. A Critical Assessment of Kriging Model Variants for High-Fidelity Uncertainty Quantification in Dynamics of composite Shells. Arch Computat Methods Eng 2017;24:495–518. https://doi.org/10.1007/s11831-016-9178-z.

[113] Dey S, Mukhopadhyay T, Adhikari S. Stochastic free vibration analysis of angle-ply composite plates – A RS-HDMR approach. Composite Structures 2015;122:526–36. https://doi.org/10.1016/j.compstruct.2014.09.057.

[114] Zhang J. Modern Monte Carlo methods for efficient uncertainty quantification and propagation: A survey. Wiley Interdisciplinary Reviews: Computational Statistics 2021;13:e1539. https://doi.org/10.1002/wics.1539.

[115] Li X, Gong C, Gu L, Jing Z, Fang H, Gao R. A reliability-based optimization method using sequential surrogate model and Monte Carlo simulation. Struct Multidisc Optim 2019;59:439–60. https://doi.org/10.1007/s00158-018-2075-3.

[116] Mukhopadhyay T, Naskar S, Dey S, Adhikari S. On quantifying the effect of noise in surrogate based stochastic free vibration analysis of laminated composite shallow shells. Compos Struct 2016;140. https://doi.org/10.1016/j.compstruct.2015.12.037.

[117] Mukhopadhyay T. A multivariate adaptive regression splines based damage identification methodology for web core composite bridges including the effect of noise. Jnl of Sandwich Structures & Materials 2018;20:885–903. https://doi.org/10.1177/1099636216682533.

[118] Rothon R. Particulate-filled Polymer Composites. iSmithers Rapra Publishing; 2003.

[119] Saltelli A, Annoni P, Azzini I, Campolongo F, Ratto M, Tarantola S. Variance based sensitivity analysis of model output. Design and estimator for the total sensitivity index. Computer Physics Communications 2010;181:259–70. https://doi.org/10.1016/j.cpc.2009.09.018.

[120] Herman J, Usher W. SALib: An open-source Python library for Sensitivity Analysis. Journal of Open Source Software 2017;2:97. https://doi.org/10.21105/joss.00097.

[121] Arora A, Kumar R, Mahajan DK. In-situ Study of the Effect of Hydrogen on Fatigue Crack Initiation in Polycrystalline Nickel. Procedia Structural Integrity 2019;14:790–7. https://doi.org/10.1016/j.prostr.2019.07.057.

[122] Garg AC, Mai Y-W. Failure mechanisms in toughened epoxy resins—A review. Composites Science and Technology 1988;31:179–223. https://doi.org/10.1016/0266-3538(88)90009-7.

List of publications

Journal publications:

- **Sharma, Aanchna**, S. Kumar, Anand and Kushvaha, Vinod. "Effect of aspect ratio on dynamic fracture toughness of particulate polymer composite using artificial neural network." *Engineering Fracture Mechanics* 228 (2020): 106907. doi.org/10.1016/j.engfracmech.2020.106907.
- **Sharma, Aanchna** and Kushvaha, Vinod. "Predictive modeling of fracture behaviour in silica-filled polymer composite subjected to impact with varying loading rates using artificial neural network." Engineering Fracture Mechanics 239 (2020): 107328. doi.org/10.1016/j.engfracmech.2020.107328.
- **Sharma, Aanchna**, Mukhopadhyay, Tanmoy Sanjay Mavinkere Rangappa, Siengchin, Suchart and Kushvaha, Vinod. "Advances in computational intelligence of polymer composite materials: machine learning assisted modeling, analysis and design." *Archives of Computational Methods in Engineering* 29 (2022): 3341-3385. doi.org/10.1007/s11831-021-09700-9.
- **Sharma, Aanchna**, Mukhopadhyay, Tanmoy, Kushvaha, Vinod. “Experimental data-driven uncertainty quantification for the dynamic fracture toughness of particulate polymer composites.” *Engineering Fracture Mechanics* (2022): 108724. doi.org/10.1016/j.engfracmech.2022.108724
- **Sharma, Aanchna,** Arora, Aman, Kushvaha, Vinod, Mahajan, Dhiraj. “Fatigue response of glass-filled epoxy composites: A crack initiation and propagation study.” (Under preparation).

Conference publications:

- **Sharma, Aanchna,** Madhushri, Priyanka, Kushvaha, Vinod, and S. Kumar, Anand, “Prediction of the Fracture Toughness of Polymer Composites using K-Nearest Neighbor (KNN) Method,” IEEE Xplore, 20th International Conference on Computational Performance Evaluation (ComPE 2020).
- **Sharma, Aanchna,** Kushvaha, Vinod. “Uncertainty Quantification Of The Dynamic Fracture Toughness Of Particulate Polymer Composites Using A Surrogate Based Methodology”, Proceedings of the 20th European Conference on Composite Materials, 2022, Lausanne, Switzerland.